

Aus der I. Medizinischen Klinik (Institut für Kardiologie, Angiologie,
Pneumologie, Hämostaseologie und internistische Intensivmedizin)
der Medizinischen Fakultät Mannheim
(Direktor: Prof. Dr. med. M. Borggrefe)

Effects of Gastrointestinal Cancer Cell Secretion on Ion Channel Functions of Human-Induced Pluripotent Stem Cell-Derived Cardiomyocytes

Inauguraldissertation
zur Erlangung des medizinischen Doktorgrades
der
Medizinischen Fakultät Mannheim
der Ruprecht-Karls-Universität
zu
Heidelberg

vorgelegt von
Rujia Zhong
aus
Liaoning, China
2020

Dekan: Prof. Dr. med. Sergij Goerd

Referent: Prof. Dr. med. M. Borggreffe

CONTENTS

1. ABBREVIATIONS.....	1
2. ABSTRACT	3
3. INTRODUCTION.....	5
4. MATERIALS AND METHODS	14
4.1 The main reagents and instruments	14
4.2 Experimental methods	19
4.2.1 Study design.....	19
4.2.2 Cancer cell culture.....	21
4.2.3 Differentiation and culture of hiPSCs.....	21
4.2.4 Manual cell counting and MTT assay.....	23
4.2.5 Polymerase chain reaction assays	24
4.2.6 Patch-clamp.....	24
4.2.7 Western blotting.....	27
4.2.8 Immunofluorescence	29
4.2.9 Genomic DNA extraction	30
4.2.10 Dot blotting	30
4.2.11 Bisulfite sequence	31
4.2.12 Sequencing polymerase chain reaction.....	33
4.2.13 PCR products purification.....	33
4.2.14 Plasmid ligation and amplification	34
4.2.15 Plasmid extraction	35
4.2.16 Overexpression of the ten-eleven translocation family enzymes	36
4.2.17 Statistics	37
4.2.18 Ethics statements	37
5. RESULTS	38
5.1 Culture medium for cancer cells had no effect on the growth of hiPSC-CMs.....	38
5.2 Effects of cancer cell secretion on action potentials of hiPSC-CMs.....	39
5.3 Effects of cancer cell secretion on ion channel currents in hiPSC-CMs	41
5.4 Effects of cancer cell secretion on ion channel expression in hiPSC-CMs ...	47
5.5 Cancer cell secretion enhanced the DNA methylation of genome and ion channel genes.....	54
5.6 The expression of DNA methylation enzymes was elevated by cancer cell secretion.....	56

5.7 Overexpression of TET1 attenuated the enhancement of DNA methylation by cancer cell secretion	58
5.8 Reduction of DNA methylation reversed the effects of cancer cell secretion on expression levels of ion channels.....	61
5.9 Overexpression of TET1 changed ion channel currents	63
6. DISCUSSION.....	67
7. SUMMARY	75
8. REFERENCES	76
9. CURRICULUM VITAE.....	87
10. PUBLICATIONS	88
11. ACKNOWLEDGEMENT	90

1. ABBREVIATIONS

AP: Action potential

APA: Amplitude of action potential

AP1: Activator protein -1

APD10: Action potential duration at 10% repolarization

APD50: Action potential duration at 50% repolarization

APD90: Action potential duration at 90% repolarization

BSA: Bovine serum albumin

Cm: Membrane capacitance

CVD: Cardiovascular disease

DNMTs: DNA methyltransferases

EBV: Epstein-Barr virus

E. coli: *Escherichia coli*

ER: Estrogen receptor

GI: Gastrointestinal

Gm: Membrane conductance

hiPSC-CM: human-induced pluripotent stem cell-derived cardiomyocytes

iNOS: Inducible nitric oxide synthase

iPSCs: Induced pluripotent stem cells

I_{Ca-L}: L-Type calcium channel current

I_{Ca-T}: T-Type calcium channel current

I_{K1}: Inward rectifier potassium current

I_{Kr}: Rapidly activating delayed rectifier potassium channel current

I_{Ks}: Slowly activating delayed rectifier potassium channel current

I_{Na}: Sodium current

I_{NCX}: Na⁺/Ca²⁺ exchanger current

I_{to}: Transient outward potassium current

IL-1β: Interleukin-1β

JNK: c-Jun N-terminal kinase

LMP1: Latent membrane protein 1

LMP2A: Latent membrane protein 2A

LV: Left ventricle

mRNA: messenger RNA

miRNA: microRNA

Myh7: Myosin heavy chain 7

Myl4: Myosin light chain 4

NF- κ B: Nuclear factor- κ B

PCR: Polymerase chain reaction

RP: Resting potential

TET: Ten-eleven translocation

V_{max}: The maximal depolarization velocity of action potential

VTE: Venous thromboembolism

4-AP: 4-Aminopyridine

5-mC: 5-methylcytosine

5-hmC: 5-hydroxymethylcytosine

5-fC: 5-formylcytosine

5-caC: 5-carboxylcytosine

2. ABSTRACT

Background - Cardiovascular disease (CVD) and cancer remain the two most common causes of mortality in developed countries. It is believed that cancer may interact with the host organs both in the microenvironment and at a distant anatomic site. Gastrointestinal (GI) cancers are a group of highly aggressive malignancies with heavy cancer-related mortalities. More and more evidences suggest a correlation between cancer and arrhythmias. However, there are no experimental studies investigating the effects of cancer cell secretion on ion channel function in human cardiomyocytes. DNA methylation, which is mainly established and maintained by DNA methyltransferases (DNMTs) by adding methyl groups to DNA molecules, is one of the mechanisms of epigenetic regulations. Recent researches suggest that DNA methylation can respond to external stimuli and is related to the functional status of cells in cardiovascular disease. Human-induced pluripotent stem cell-derived cardiomyocytes (hiPSC-CMs) have been demonstrated to recapitulate the physiological and pathological features of human cardiomyocytes and therefore are useful for studies on human cardiac diseases.

Purposes - The study was designed to assess the possible effects of gastrointestinal cancer cell secretion on cardiac ion channel functions and explore the underlying epigenetic mechanism by using hiPSC-CMs.

Methods - The hiPSC-CMs generated from human skin fibroblasts of a healthy donor were treated by GI cancer cell (AGS or SW480 cells, cultured for 8 days) medium in different concentrations (the cancer cell secretion groups) or the same medium without cancer cell culture (medium control) for 48 hours, and hiPSC-CMs without any treatment were taken as control group. Then qPCR, patch-clamp, western blotting, immunostaining, dot blotting, bisulfite sequence and overexpression of the ten-eleven translocation (TET) family enzymes were used for the study.

Results - Patch clamp recordings of action potentials (AP) exhibited that the maximum depolarization velocity (V_{max}) and the action potential amplitude (APA) were reduced in cancer cell secretion groups compared with control. The action potential duration at 10% repolarization (APD10) prolonged in cancer cell secretion groups. In ion channel current measurements, peak Na^+ current (I_{Na}) was significantly reduced in cancer cell secretion groups, in agreement with the V_{max} and APA reduction. The transient outward current (I_{to}) was decreased in presence of cancer cell secretion compared with control group, consistent with the APD10 prolongation. Both the late Na^+ and the slowly activating delayed rectifier K^+ current (I_{Ks}) were significantly increased. qPCR results showed that the expression of SCN5A (Na^+ channel, $Na_v1.5$) and KCND3 (I_{to} , $K_v4.3$) were decreased, while SCN10A (Na^+ channel, $Na_v1.8$) and KCNQ1 (I_{Ks} , $K_v7.1$) were increased by cancer cell secretion. Furthermore, the changes of protein expression level of ion channels determined by western blotting and immunofluorescence, respectively, were in consistent with the results of qPCR and current measurements. The whole genome DNA methylation level detected by 5-mC antibody was increased in cancer cell secretion groups, along with increased protein levels of DNMT3A and DNMT3B, but no differences of 5-hmC level were observed. After overexpression of TET1 enzyme that is responsible for DNA demethylation, DNA methylation level of 5-mC of the cancer cell secretion groups was decreased and both the current and protein expression level of I_{to} and I_{Ks} channels were rescued.

Conclusions - Gastrointestinal cancer cell secretion can induce ion channel dysfunctions and subsequently abnormal action potentials, which may contribute to occurrence of arrhythmias in cancer patients. The ion channel dysfunctions might result from DNA methylation of ion channel genes.

Key words - Gastrointestinal cancer cell secretion; hiPSC; cardiomyocyte; electrophysiology; ion channel; DNA methylation.

3. INTRODUCTION

Cardiovascular disease (CVD) and cancer are the two most common causes of mortality worldwide.^{1, 2} Data from World Health Organization in 2018 show that worldwide about 18 millions of people die from CVD annually,³ while about 18 million patients suffer from and about 10 million die of cancer.⁴ Due to the success of basic and therapeutic researches, cancer treatments have become more effective. Also improved diagnostic and therapeutic modalities achieve remarkable progress in improving the survival rates of cancer patients. It has been reported by the American Cancer Society that there were more than 15.5 million cancer survivors in the USA in 2016, and this number was projected to reach more than 20 million by year 2024.⁵ However, the improvement of survival rate in cancer patients may be limited by adverse effects associated with anti-cancer treatment. A survey conducted by the US National Health and Nutrition Examination showed that 51% of 1807 cancer survivors died of cancer and 33% died of heart disease in 7 years follow-up,⁶ including the development of newly diagnosed cardiovascular problems, or the exacerbation of previously identified cardiovascular disease.¹ Among the anti-cancer therapy related adverse effects, cardiotoxicity is the second most common cause of morbidity and mortality.⁷ The cardiovascular toxicity of cancer treatment, which manifests as cardiac dysfunctions, remains a major obstacle for cancer survival. It may compromise the effectiveness of the anticancer therapy and can negatively affect the survival or life quality of oncological patients.^{7, 8} The rise in the incidence of CVD among patients affected by cancers has drawn attention. Even worse, in some cancer patients, cardiovascular deaths are more common than cancer deaths.⁹ The risk of atrial fibrillation, which is one of the most common arrhythmias in cancer patients, may be higher than that in patients without cancer.^{10, 11} The newly-onset of atrial fibrillation in cancer patients may reflect a more advanced cancer stage and herald a poorer oncological prognosis. It is estimated that during the subsequent initiation of anticoagulation

therapy, cancer could increase the risk of venous thromboembolism (VTE) 4 to 7 times and the risk of bleeding 2 times.^{12, 13} The cardiovascular problems are involved in primary or secondary malignancies, as well as the result of cardiotoxicity in cancer treatments (including chemotherapy, radiation, and adjuvant therapies) with adverse effects on heart function and structure.⁹ The potential cardiovascular toxicity of anti-cancer agents includes QT prolongation, arrhythmias, myocardial ischemia, stroke, hypertension, thromboembolism, left ventricular dysfunction, and heart failure.¹⁴ In order to alleviate the cardiotoxicity of cancer treatment, methods have been applied, such as the introduction of highly sensitive diagnostics, coadministration of dexrazoxane, and application of new forms and less toxic chemotherapy analogs. However, there is no recommendation for cardiovascular drugs used to protect the heart function for cancer patients. Only the “2016 European Guidelines on cardiovascular disease prevention in clinical practice” announced that prophylactic treatment should be performed as early as possible to minimize the cardiotoxicity of anthracyclines in high-risk patients.¹⁵

Most researches focus on the cardiotoxicity of anti-cancer therapy, but cancer itself could affect cardiovascular system. Tumors are believed to influence the microenvironment to promote their proliferation, migration, invasion, metastasis, and also therapy resistance.¹⁶ However, evidences have revealed that tumor could interact with the host beyond the local tissue microenvironment and actively perturb host organs at distant anatomic sites.¹⁷ It has been reported that the incidence of CVD is 10-fold higher in cancer survivors than that in controls, along with higher rates of congestive heart failure and stroke, and higher incidence of cardiovascular risk factors.^{18, 19} Tumors can cause arrhythmia in cancer patients through direct infiltration, systematic inflammation, metabolic derangements, impaired oxygenation, and electrolyte or endocrine abnormalities.²⁰ A study demonstrated that heart rate variability and cardiorespiratory coordination were changed in patients with breast

cancer.²¹ Another study on acute leukemia patients found that cardiac autonomic functions were changed with a decrease in heart rate variability.²² In addition, one epidemiologic analysis from health insurance research database including 24,125 newly diagnosed patients with malignant disease identified during the study period revealed that patients with cancer had a higher risk of developing atrial fibrillation, with 1.8% who experienced newly onset atrial fibrillation after cancer diagnosis, and 2.4% who had pre-existing atrial fibrillation.²³ Another study suggested that cancer patients with a preserved ejection fraction, irrespective of cancer drug therapies, had evidence of subclinical myocardial dysfunction, manifested by a decrease in circumferential and radial tension.²⁴ These findings further demonstrate that a tumor may itself have a deleterious effect on myocardial function of heart. Animal study also reported that mice injected with lung carcinoma cells showed degenerative structural cardiac lesions and a significant reduction in myocardial innervation²⁵. Overall, the aforementioned evidences indicate that cancer may affect the electrophysiology of cardiomyocytes, independent of cancer therapy.

Gastrointestinal cancers are a group of highly aggressive malignancies with heavy cancer-related mortalities.¹⁶ It has been reported that patients with GI cancers showed lower heart rate variability.²⁶ Atrial fibrillation is the most common form of cardiac arrhythmia, and it becomes an epidemic as population ages. Recently, the association between the incidence of atrial fibrillation and colorectal cancer has drawn much attention. A study found that patients with colorectal cancer have a 2-fold higher incidence of atrial fibrillation than patients with non-neoplastic diseases.²⁷ However, there are no experimental studies investigating the potential role of GI cancers on cardio electrophysiology. In the present study, we aim to assess the possible cardiac effects induced by gastrointestinal cancer cell secretion and explore their electrophysiological and molecular mechanisms.

Epigenetic modification represents all genetic changes in meiosis and mitosis inheritance that do not involve a change in the DNA nucleotide sequence itself, but will affect the tight packaging of DNA and the ability to be accessed by transcription factors.²⁸ It is an important and heritable mechanism of gene expression regulation. Epigenetic mechanisms such as histone tail modification and DNA methylation may contribute to differential gene regulation. Among epigenetic changes, DNA methylation is one of the earliest and most thoroughly studied mechanisms of epigenetic modifications.^{29, 30} Generally, DNA methylation is consistently high throughout the genome, with 60-80% of CpG methylating.³¹ It occurs at the cytosine residue of CG doublet sequences, which form clusters known as CpG islands and trend to be located at 5' gene promoter regions. Methylation of CpG islands at promoters may physically impede the binding of transcriptional proteins to the gene, which is correlated with strong repressive effect of transcription.³² The DNA methylation process is primarily regulated by DNA methyltransferases (DNMTs) and ten-eleven translocation (TET) family enzymes.³³ Three DNMTs (DNMT1, DNMT3a and DNMT3b) are required for establishment and maintenance of DNA methylation patterns. Two additional enzymes (DNMT2 and DNMT3L) may also have more specialized but related functions.^{34, 35} DNMT1 appears to be responsible for the maintenance of established patterns of DNA methylation, while DNMT3a and 3b seem to mediate establishment of new DNA methylation patterns.³⁶ DNA demethylation is the removal of a methyl group from DNA. This mechanism is equally as important as and coupled with DNA methylation. The TET family of 5-methylcytosine (5-mC) hydroxylases includes TET1, TET2 and TET3. These proteins may promote DNA demethylation by binding to CpG rich regions to prevent unwanted DNA methyltransferase activity, and by converting 5-mC to 5-hydroxymethylcytosine (5-hmC), 5-hmC to 5-formylcytosine (5-fC), and 5-fC to 5-carboxylcytosine (5-caC) through hydroxylase activity.³⁷ TET1 and TET2 both play important roles in embryonic development, and TET3 is

essential for oocyte reprogramming. DNMT3a and TET1 cooperate to regulate promoter epigenetic landscapes in mouse embryonic stem cells.³¹ Whole genome examination of the cardiomyocytes from embryos, newborns, adults and hypertrophic mice found that TET-mediated DNA methylation can regulate the expression of key cardiac genes such as myosin heavy chain 7 (Myh7), indicating that this epigenetic mechanism plays an important role in the development and disease of the heart.³⁸

DNA methylation is crucial to regulate the functioning of the genome and has an important impact on normal cell physiology, including development, differentiation and DNA protein interactions. Increasing evidence suggests that external stimuli, like environmental and lifestyle factors, may affect gene expression by disrupting DNA methylation patterns. Lifestyle factors such as nutrition and exercise could change epigenetics. Abnormal patterns of DNA methylation can induce many diseases, such as cancer, autoimmune diseases, inflammatory disease, and atherosclerosis. Other chronic diseases, including metabolic diseases like obesity, metabolic syndrome and diabetes, are also prone to epigenetic modifications.³⁹ Recent researches also suggest that DNA methylation can respond to external stimuli and is related to the functional status of cells in cardiovascular disease. Some results imply that reduced genomic methylation indicates disease risk or progression and aberrant DNA methylation of specific genes takes part in cardiovascular diseases. One research found that the methylation of estrogen receptor (ER)- α promoter could increase the severity of atherosclerotic lesions.⁴⁰ Another article provided evidence for dynamic DNA methylation in cardiac hypertrophy, which indicated that neonatal rat cardiomyocytes after 7 days of phenylephrine intervention exhibited contractile dysfunction and significant inhibition of promoter methylation of up-regulated genes associated with hypertrophy.⁴¹ One study found that DNA methylation-mediated gene expression regulation might play an important role in the pathogenesis of atrial fibrillation.⁴² Lower level of global

5-mC was also reported to be associated with higher mortality in hypertension, ischemic heart disease or stroke.⁴³⁻⁴⁵ Numerous studies have demonstrated that tumor-suppressor genes are silenced by hypermethylation of DNA in the promoter region in different cancer types.⁴⁶ Hypermethylation of the promoter regions also plays an important role in the development of colorectal tumors.^{47, 48} Other molecules, such as microRNA (miRNA) and inflammatory factors, could also be regulated by DNA methylation in cancers.^{49, 50} Hypermethylation in cancer can often be found in genes with tumor suppressive properties, and this epigenetic change has also been observed to affect potential cancer-promoting gene. While, whether the mechanism of cardiovascular toxicity of cancer is associated with DNA methylation is an area worthy of further research and discussion.

The heart pump function, which is critical for blood circulation in the whole body, bases on the regular contraction of cardiomyocytes. The cell contraction is coupled to the cellular electrical activity. When a myocyte is excited, the membrane potential depolarizes from a negative to a positive potential initiating the cell contraction and then repolarizes to resting potential leading to cell relaxation. The periodical change of membrane potential forms the cardiac action potential (AP), which is important for both the rhythm and force of cardiomyocyte contraction. The action potential can be divided into five phases, which involve contributions of different ion channel currents (Figure1). Phase 0 is a rapid change in voltage across the cell membrane from a negative resting potential to a positive potential, also called a depolarization, lasting less than 2ms in ventricular cells.⁵¹ This change results predominantly from the activation of Na⁺ channel, specifically Na_v1.5 channels.⁵² Phase 1 begins with the rapid inactivation of the Na⁺ channels, which could reduce the Na⁺ entry. At the same time, a rapidly activating K⁺ channel, the transient outward current (I_{to}) channel, opens shortly, allowing for a brief flow of K⁺ ions out of the cell, and repolarizing the membrane potential slightly, which mainly leads to the notch of the action

potential waveform.⁵³ Phase 2 is also known as plateau period, during which the inward currents, mainly the L-type calcium channel current, and outward currents, mainly the rapidly activating delayed rectifier K⁺ current (I_{Kr}), are similar in strength but in opposite direction. Therefore, the potential change only slowly and slightly. During the phase 3 of the action potential, also called the “rapid repolarization” phase, the outward K⁺ channel currents including I_{Kr} and I_{Ks} (the slowly activating delayed rectifier K⁺ current), largely increased, setting the membrane potential back to resting potential. During phase 4 (the resting time), the Na⁺ and Ca²⁺ ions flowed into cells, and the K⁺ ions flowed out of cells are transported by ion pumps (ATPases) back to their original site. The movement of all these ions causes the membrane potential to remain relatively constant.⁵⁴ Furthermore, the inward rectifier potassium current (I_{K1}), which activates late in phase 3 and remains conducting throughout phase 4, plays also a role in maintaining the resting membrane potential.⁵⁵ In addition, the Na⁺/Ca²⁺ exchanger can be activated during the repolarization phase. The depolarization velocity (V_{max}) of APs predominantly determines the speed of excitation conduction. The repolarization velocity mainly determines the duration of APs (APD). Dysfunctions of ion channels that contribute to cardiac APs may lead to cardiac disorders. For example, loss-of-function of Na⁺ channels cause reduced peak Na⁺ currents (I_{Na}) and V_{max} , leading to conduction defect, which may cause arrhythmias such as that in Brugada syndrome. A loss-of-function of HERG channels causes reduced I_{Kr} and prolonged APD that is reflected as a long-QT interval in ECG. The long-QT interval may result in arrhythmias and therefore is named as long-QT syndrome. On the contrary, a gain-of-function of HERG channels enhances I_{Kr} and APD shortening and hence the short-QT syndrome.

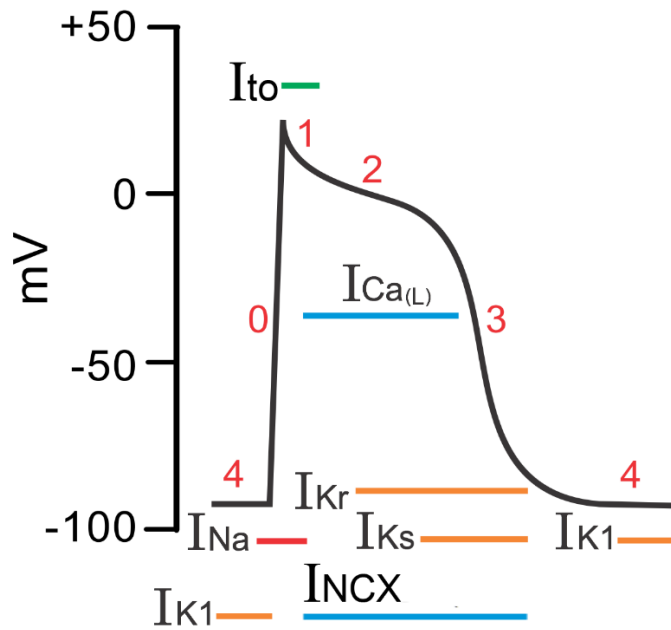


Figure 1. Schematic diagram of typical action potentials and related currents

For experimental studies on ion channel functions or their roles for human cardiac disorders, human cardiomyocytes are an ideal source. However, it is very difficult to obtain enough human cardiomyocytes, especially, the ventricular cardiomyocytes for experimental studies. As alternatives, animal models or animal cells have been employed for studies. Due to the differences between animal and human being, animals or animal cells are not ideal for mimicking the human cardiac diseases. Besides animal cells, some human cell lines, like HEK293 and HeLa cells have been used for some studies investigating ion channel functions.^{56, 57} These non-cardiac cells are not ideal for functional studies because they cannot generate action potential and contraction. Since the successful reprogramming of adult somatic cells to induced pluripotent stem (iPS) cells and generation of functional cardiomyocytes from human iPS cells (hiPSC-CM),⁵⁸⁻⁶¹ hiPSC-CMs have been demonstrated to have the electrophysiological properties including action potentials which are similar to those of native cardiomyocytes.^{62, 63} Therefore, hiPSC-CMs provide a platform to investigate cardiac ion channel functions.

In summary, more and more evidences suggest a correlation between cancer and arrhythmias. However, the effect of cancer cells on the electrophysiology of cardiomyocytes is rarely studied. It is unknown whether GI cancer cell secretion influences ion channel function of human cardiomyocytes. Here, we hypothesize that GI cancer cell secretion may change the electrophysiology of human cardiac cells through epigenetic modifications. The aim of the study is to use the iPSC-CM platform to examine the possible effects of cancer cell secretion on cardiac ion channel functions and investigate the mechanisms of effects, mainly focusing on the epigenetic regulation of ion channel gene. The results of this study may give insight into mechanisms behind arrhythmias in cancer patients and provide novel therapeutic targets for treatment of arrhythmias.

4. MATERIALS AND METHODS

4.1 The main reagents and instruments

4.1.1 The main reagents for the experiments

Table1. Name and company of the reagents.

Name	Company	Item number
DMEM, high glucose, pyruvate	Gibco	41966029
Penicillin-Streptomycin	Thermo Fisher Scientific	15140122
Fetal Bovine Serum	Gibco	10500-056
L-Glutamine	Thermo Fisher Scientific	25030024
0.4% Trypan Blue	Sigma-Aldrich	T8154
Dimethyl Sulfoxide	Sigma-Aldrich	D2650
MTT reduction product Synonym	Sigma-Aldrich	88417
TeSR™-E8™	StemCell Technologies	5900
Matrigel Growth Factor Reduced (GFR)	Corning	354230
Basement Membrane Matrix		
0.5 M EDTA Solution	AppliChem	A4892.0500
ROCK Inhibitor (Y27632)	Miltenyi Biotec	130-095-563
RPMI Medium 1640 (1X) + GlutaMAX	Gibco	61870044
RPMI 1640 Medium, no glucose, no glutamine	Biological Industries	01-101-1A
B-27® Supplement (50X), serum free	Gibco	17504001
Ascorbic Acid 2-Phosphate	Sigma-Aldrich	A8960
Sesquimagnesium Salt Hydrate		
Sodium Pyruvate 100mM	Gibco	11360039
Dimethyl Sulfoxide	Sigma-Aldrich	D2650
Recombinant Human/Mouse/rat Activin A	R&D Systems	338-AC-010
Recombinant Human BMP-4	R&D Systems	314-BP-010
Human FGF-2 Premium Grade	Miltenyi Biotec	130-093-841
StemMACS CHIR99021	StemMACS	130-103-926

Name	Company	Item number
IWP-2	StemCell Technologies	72122
Collagenase I	Worthington	LS004196
Trypsin-EDTA 0.05%	Gibco	25300054
Sodium Lactate Solution	Sigma-Aldrich	71723
Hepes 1M Solution	Thermo Fisher Scientific	15630080
2-Mercaptoethanol (50 mM)	Gibco	31350010
DPBS, no calcium, no magnesium	Thermo Fisher Scientific	14190250
75cm ² Cell Culture Flask with Vented Cap	Falcon	353136
24 Well Cell Culture Plate	Falcon	353047
15mL High Clarity PP Centrifuge Tube	Falcon	352096
50mL High Clarity PP Centrifuge Tube	Falcon	352070
35mm Cell Culture Dish	Ibidi	81151
Cell Scrapers	Thermo Fisher Scientific	353085
EMD Millipore Stericup Sterile Vacuum Filter	Thermo Fisher Scientific	SCVPU11RE
Fast Optical 96-Well Reaction Plate,	Thermo Fisher Scientific	4346907
4 Chamber Polystyrene Vessel Tissue Culture Treated Glass Slides	Falcon	354114
Ethanol Absolut	Merck Millipore	107017
Methanol Absolut	Merck Millipore	106009
Total RNA extraction reagent	Qiagen	338112
High-Capacity cDNA Reverse Transcription Kit	Thermo Fisher Scientific	4368814
SibirRoxHot Master Mix, ROX 0.1µM	Bioron	119405
RIPA Puffer	Sigma-Aldrich	R0278
Protease Inhibitor Cocktail	Sigma-Aldrich	P8340
BCA Protein Assay Kit	Thermo Fisher Scientific	23227
Glycine	Merck Millipore	3570

Name	Company	Item number
Tris	Carl Roth	5429.1
Sodium dodecyl sulfate, SDS pellets	Serva	20765
Ammonium Persulfate	Bio-Rad	1610700
30 % Acrylamide	Carl Roth	3029.1
TEMED	Bio-Rad	1610800
PVDF Transfer Membrane	Merck Millipore	GE1060009
Milchpulver	Carl Roth	T145.3
ECL Western Blotting Substrate	Thermo Fisher Scientific	32209
BSA	Thermo Fisher Scientific	10270106
Nitrocellulose Blotting-Membrane	PeQlab	39-1010
Paraformaldehyde 4%	Roth	P087.4
Triton X-100	Sigma-Aldrich	T-9284
Proteinase K	Qiagen	19131
Yeast Extract	Sigma-Aldrich	Y1625
Tryptone	Sigma-Aldrich	T9410
Agarose	Sigma-Aldrich	A5030
Ampicillin, sodium salt	Thermo Fisher Scientific	11593027
EpiTect Bisulfite Kits	Qiagen	59104
TaKaRa EpiTaq HS (for bisulfite-treated DNA)	TAKARA	R110A
Wizard SV Gel and PCR Clean-Up System	Promega	A9281
DNA Ligation Kit, Mighty Mix	TAKARA	6023
T-Vector	TAKARA	3270
X-Gal	Invitrogen	B1690
Phenol:Chloroform:IAA, 25:24:1	Invitrogen	AM9730
<i>E. coli</i> HST08 Premium Competent Cells	TAKARA	9128
Quick Plasmid Miniprep Kit	Thermo Fisher Scientific	K210010
Sodium Chloride	Sigma-Aldrich	S9625

Name	Company	Item number
Potassium chloride	Sigma-Aldrich	P3911
Calcium chloride	Sigma-Aldrich	C3881
Magnesium chloride hexahydrate	Sigma-Aldrich	MD250
Glucose	Sigma-Aldrich	G7528
HEPEs	Sigma-Aldrich	H-3375
EGTA	Sigma-Aldrich	E4378
MyATP	Sigma-Aldrich	A9187
Sodium hydroxide	Sigma-Aldrich	S-5881
Cesium hydroxide solution	Sigma-Aldrich	232068
Hydrochloric acid	Sigma-Aldrich	H1758
Cesium chloride	Sigma-Aldrich	289329
Barium chloride	Sigma-Aldrich	449644
Nickel chloride	Sigma-Aldrich	339350
TEA-Cl	Sigma-Aldrich	T2265
Nifedipine	Sigma-Aldrich	N7634
Tetrodotoxin	Roth	6973.1
E-4031	Sigma-Aldrich	M5060
4-Aminopyridine	Sigma-Aldrich	275875
Chromanol 293B	Sigma-Aldrich	C2615
Niflumic acid	Sigma-Aldrich	N0630
Lidocaine	Sigma-Aldrich	L7757
Dihydroouabain	Sigma-Aldrich	D0670
Aspartic acid	Sigma-Aldrich	1043819

Table2. Primer sequences for real-time polymerase chain reaction (PCR).

Gene	Gene description	Assay ID
GADPH	Glyceraldehyde-3-phosphate dehydrogenase	Hs99999905_m1
SCN5A	Nav1.5	Hs00165693_m1
SCN10A	Nav1.8	Hs01045137_m1
CACNA1C	Ca _v 1.2	Hs01062258_m1
SLC8A1	NCX1	Hs00167681_m1
KCND3	K _v 4.3 (I _{to})	Hs00542597_m1
KCNH2	K _v 11.1 (hERG /I _{kr})	Hs04234270_m1
KCNQ1	K _v 7.1, α-subunit of I _{ks}	Hs00923522_m1
KCNJ2	Inward rectifier K ⁺ channel Kir2.1	Hs00265315_m1

4.1.2 The main instruments for the experiments

Table3. Name and company of the instruments

Name	Company
Cytometry plate	BRAND
Pipetus	Eppendorf
Centrifuge	M&S Laborgerate GMBH
Incubator	Thermo HeRacell 240
Thermostat	Memmert
Microscope	Leica DMIL
Fluorescence microscope	Leica DMRE DFC3000G
PCR Amplifier	PeQSTAR PeQlab
qPCR	Applied Biosystems stepone Plus
Microplate Readers	Tecan infinite m200
Electrophoresis Chambers	BIO-RAD
The ChemiDoc MP Imaging System	PeQlab
Patch electrodes	World Precision Instruments MTW 150F
DMZ-Universal Puller	Zeitz-InstrumenteVertriebs GmbH
ISO-3 multitasking patch-clamp program	MFK M. Friedrich

4.2 Experimental methods

4.2.1 Study design

To investigate the cardiac effects of cancer secretion in hiPSC-CMs, especially the GI cancers, the stomach and colon cancer cells were adopted. Considering the importance of cell numbers and cell growth time for the concentration of components secreted by cultured cancer cells, we tried to generate the growth curve by manual cell counting and MTT (3-(4,5-dimethylthiazol-2-yl)-2,5-diphenyltetrazolium bromide) assay. The number of seeding cancer cells was fixed (1×10^5) and the culture media (for studies investigating the effects of components secreted by cancer cells) were collected when the cancer cells grew to a plateau-phase. For the treatment of cardiomyocytes, conditioned cancer cell media were 10%, 20%, 40%, and 80% diluted in fresh cardio culture medium for cardiomyocytes. As conditional control groups, the fresh culture medium for cancer cells, which was not cultured with cancer cells and used as a medium control, was also added in cardiomyocyte culture medium at the same percentages (10%, 20%, 40%, and 80%). Then after 48h, the cardiomyocytes were collected for following experiments. The specific group information and experiment design are described in Figure 2.

To determine whether the cancer cell secretion changes action potential parameters and ion channels responsible for APs, action potentials and different ion channel currents including Na^+ , Ca^{2+} , K^+ , $\text{Na}^+/\text{Ca}^{2+}$ exchanger were recorded by patch clamp whole cell recording technique in hiPSC-CMs treated with cultured or non-cultured (medium control) cancer cell medium to examine effects of cancer cell secretion. Meanwhile, the expression of the respective ion channels was assessed by qPCR and western blotting at mRNA and protein level.

To identify possible mechanisms of cancer secretion on the electrophysiology of hiPSC-CMs, the possible epigenetic regulation of cancer secretion on the electrophysiology of hiPSC-CMs was investigated. First, the

whole genome methylation level was measured by dot blotting and the protein levels of DNMTs (for DNA methylation) and TET1 (for DNA demethylation) were detected by western blotting. Then the DNA methylation level of CpG sites in gene promoter was investigated by bisulfite sequencing polymerase chain reaction. Next, the effect was confirmed by overexpression of TET1. After overexpression of TET1, the ion channel currents were again assessed to further confirm the epigenetic regulation of ion channels by cancer secretions.

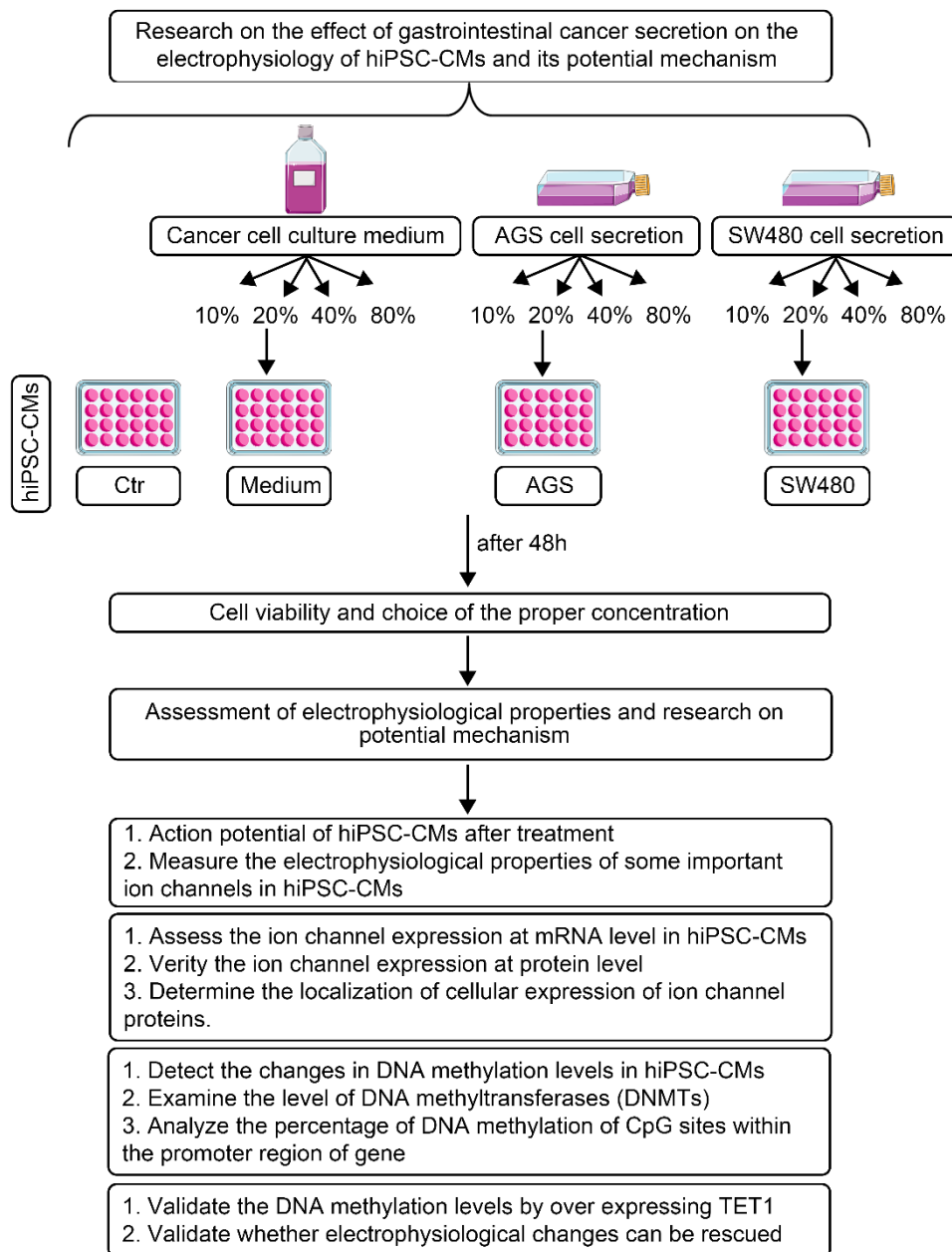


Figure 2. Study design. “Ctr” represents hiPSC-CMs without medium for cancer cells.

“Medium” represents hiPSC-CMs with addition of un-cultured medium for cancer cell

(medium control). “AGS” represents hiPSC-CMs with addition of cultured medium of AGS cancer cells. “SW480” represents hiPSC-CMs with addition of cultured medium of SW480 cancer cells.

4.2.2 Cancer cell culture

The two cancer cell lines AGS and SW480 were gifts from Dr. Isabel Hinsenkamp and Dr. Elke Burgermeister from Department of Internal Medicine II of the Medical Faculty Mannheim. The detailed information is listed as followed:

(1) AGS (ATCC® CRL-1739™) comes from stomach

<https://www.lgcstandards-atcc.org/Products/All/CRL-1739.aspx>

(2) SW480 [SW-480] (ATCC® CCL-228™) comes from colon

<https://www.lgcstandards-atcc.org/Products/All/CCL-228.aspx>

Cancer cells (1×10^5 cells) were seeded in T75 flasks, and then cultured in DMEM (10mL) supplemented with 10% FBS and 1% Pen/Strep. The medium was changed every 2 days until reaching the plateau-phase, at which the total number of AGS and SW480 cancer cells in a T75 flask increased to about 4.0×10^6 and 7.7×10^6 respectively.

4.2.3 Differentiation and culture of hiPSCs

The hiPSCs were generated from primary healthy donor fibroblasts derived from skin biopsies in the department of dermatology, university medical center Mannheim. The hiPSCs were maintained in E8 medium (StemCell Technologies) supplemented with human albumin and ascorbic acid. Then the directed differentiation of hiPSCs into cardiomyocytes (hiPSC-CMs) was initiated at 80–90% confluence in 24-well plates with Matrigel coated. The cardio differentiation medium composed of RPMI 1640 with Glutamax and HEPES (Thermo Fisher Scientific), 2% B27 (Thermo Fisher Scientific), 0.2mg/ml L-ascorbic acid 2-phosphate (Sigma-Aldrich), 1% Sodium Pyruvate (Gibco), and 1% Pen/Strep (Thermo Fisher Scientific). For cardio differentiation

the hiPSCs were sequentially treated with 1 μ M CHIR99021 (StemMACS), 5ng/ml BMP4 (R&D Systems), 9ng/ml activin A (R&D Systems), 5ng/ml FGF (Miltenyi Biotec) for 3 days and then 5 μ M IWP2 (StemCell Technologies) for about 8-10 days with the cardio differentiation medium. Differentiated cells were glucose-starved and supplemented with 5mM Sodium Lactate Solution (Sigma-Aldrich), 50mM 2-mercaptoethanol (Gibco) with RPMI 1640 without glucose nor glutamine to metabolically select hiPSC-CMs around day 13-15. The iPSC-CMs were cultured in maintenance media at least to day 50-60 for further maturation. The successful differentiation of hiPSC-CMs was confirmed by immunofluorescence of cardiac markers α -actinin and myosin light chain 4 (Myl4) (figure 3). Cardiomyocytes were dissociated from 24-well plates for biological studies or plated on Matrigel-coated 3.5cm petri dishes for patch-clamp measurements. For preparing the single cell from 24-well plate to dishes, the following steps were performed:

- (1) We put 300 μ l collagenase in PRMI1640 medium in every well, then the cells were incubated at 37 °C for 40min.
- (2) 1ml pipette was used to pipette un and down 10 times of cell suspension.
- (3) Then the cell suspension was centrifuged at 250g, at room temperature for 2min, and the supernatant aspirated.
- (4) The cell precipitation was washed with DPBS (no calcium, no magnesium), again centrifuged at 250g, at room temperature for 2min, and the supernatant was aspirated.
- (5) Then 300 μ l 0.05%trypsin was added to the tube, then pipetted up and down 10 times, incubated at 37 °C for 2min.
- (6) For stopping the reaction, we added 300 μ l PRMI 1640 medium and 10% FCS, centrifuged the cell suspension at 250g at room temperature for 2min, aspirated supernatant after centrifugation.

(7) To resuspend the cells, cardio differentiation medium was added, pipetted up and down 10 times with 10ml pipette, and then the cell suspension was added to dishes.

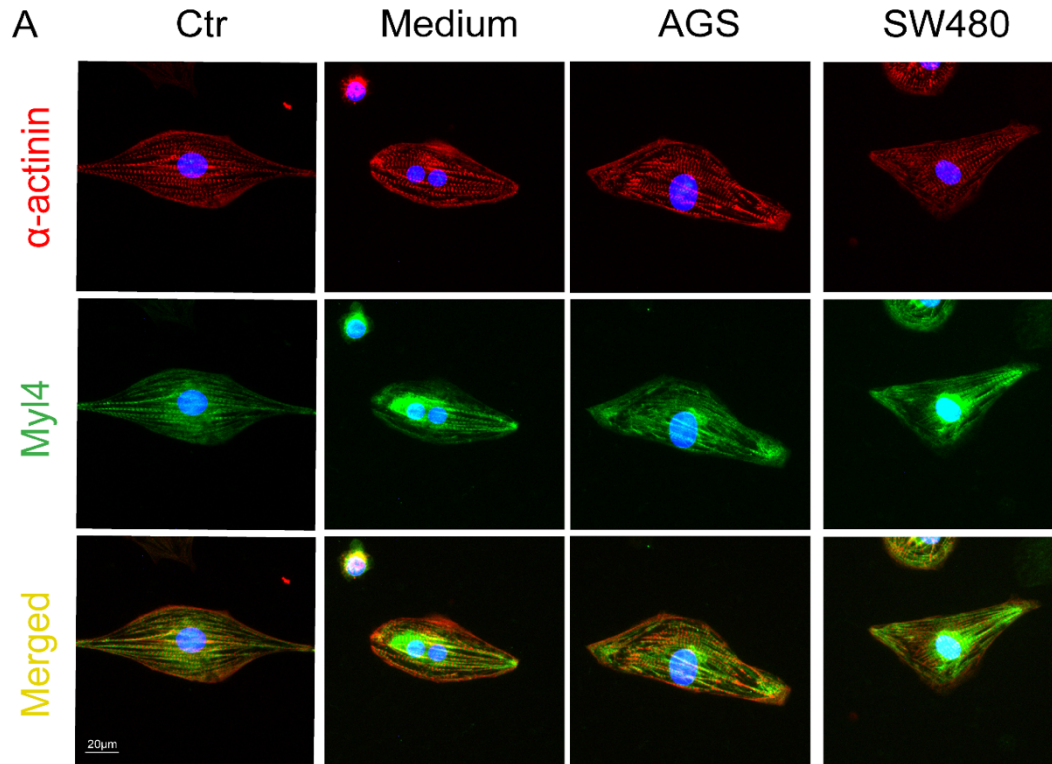


Figure.3 Immunostaining of human induced pluripotent stem cell-derived cardiomyocyte (hiPSC-CM) marker of different groups. Shown is the expression of α -actinin (red) and Myl4 (green) in hiPSC-CMs. “Ctr” represents hiPSC-CMs without medium for cancer cells. “Medium” represents hiPSC-CMs with addition of un-cultured medium for cancer cells. “AGS” represents hiPSC-CMs with addition of cultured medium of AGS cancer cells. “SW480” represents hiPSC-CMs with addition of cultured medium of SW480 cancer cells. Scale bars, 20 μ m.

4.2.4 Manual cell counting and MTT assay

Manual cell counting was carried out with a hemocytometer and a microscope, using 0.4% trypan blue-treated cell suspension. The number of cells in all 4 outer squares were counted and then divided by 4 (the mean number of cells per square). The number of cells per milliliter of suspension equaled to the number of the living cells per square multiplied by 10^4 .

MTT assay is a quantitative colorimetric method, which allows evaluation of cell viability and proliferation, and cytotoxicity of different compounds. The method is based on enzyme reduction of MTT tetrazolium salt (3-(4,5-dimethylthiazolyl)-2,5-diphenyltetrazolium bromide) to its dark blue insoluble formazan. The hiPSC-CMs around day 50-60 were seeded in 96-well plates (5×10^3 cells per well) and cultured for 12h in a cell incubator. Then different concentration of cancer cell media was added for another 48h. The hiPSC-CMs added with fresh cardio culture media were used as a negative control. Then 20 μ L MTT (5 mg/mL in PBS, Sigma-Aldrich) were added to each well. After 4h incubation, the supernatant was replaced with 150 μ L of DMSO solution (Sigma-Aldrich). Absorbance OD was measured at 490nm and cell viability is calculated.

4.2.5 Polymerase chain reaction assays

PCR-analyses were carried out to assess the ion channel expression at mRNA level in hiPSC-CMs. hiPSC-CMs were dissected and extracted for total RNA with RNAiso Plus (Total RNA extraction reagent) (Qiagen, Hilden, Germany). The cDNA synthesized from total RNA was amplified by qPCR on the Real-time PCR System (Applied Biosystems 7500 Real-Time PCR Systems) using a PCR mix with hot start Taq DNA polymerase and SYBR Green (Sibir Rox Hot Mastermix, Catnumber 119405, BIORON, Germany) in the presence of sense and antisense primers (400nM each). The relative expression levels of each mRNA were calculated as the gene of interest relative to GAPDH which was calculated by the $\Delta\Delta$ CT method, based on the threshold cycle (CT), as fold change = $2^{-\Delta(\Delta$ CT)}, where Δ CT = CT_{gene of interest} - CT_{GAPDH} and $\Delta(\Delta$ CT) = Δ CT_{cancer cell medium} - Δ CT_{control}.

4.2.6 Patch-clamp

The hiPSC-CMs plated on Matrigel-coated 3.5cm petri dishes were used for the following patch-clamp measurements. All the experiments of action potentials (APs) and different ion channel currents were measured by whole-

cell patch clamp recording techniques and carried out at room temperature (22-25° C). Patch electrodes we used were borosilicate glass capillaries (MTW 150F; world Precision Instruments, Inc., Sarasota, FL) and were pulled with DMZ-Universal Puller (Zeitz-InstrumenteVertriebs GmbH, Martinsried, Germany) and filled with pre-filtered pipette solution. The pipette resistance ranged from 1–2 MΩ for measurements. To isolate one type of ion channel current from other types of channels, a specific channel blocker or solution was used. Recording was started when the current stabilized (usually within 3 to 5 minutes). In order to examine the cell capacitance, a voltage pulse from -70 to -75mV was given for recording the capacitance transient current. Then the area under transient current curve was calculated and divided by 5 mV to get the whole cell capacitance in pF, which was used for calculating current density.

Resting and action potentials

With the current-clamp techniques without stimulation (CC-mode), the resting membrane (RP) potential was recorded. For measuring APs paced at a fixed frequency, if the RP was more positive than -70mV, negative currents (-10 to -50pA) was injected into the cell to keep the RP at -70 to -75mV. Then action potential (AP) was provoked to pulse stimulations (1nA for 5ms) at 0.5Hz, 1Hz, 2Hz, and 3Hz. The effects of cancer cell secretion on APS in different groups were assessed.

Membrane currents

By voltage-clamp techniques, membrane currents were measured at whole-cell level. Cardiomyocytes express many types of ion channels in plasma membrane, which are important for the normal functions of the cells. The electrophysiological properties of different ion channel currents in hiPSC-CMs cultured with cancer cell media were characterized and compared with those cultured without cancer cell medium. Recordings were started when the current became stable, usually within 3 to 5 minutes. To assess the effects of cancer cell secretion on ion channel functions, the channel currents or gating kinetics

including the activation, inactivation, and recovery from inactivation of the peak sodium current (I_{Na}), the L-type calcium channel current (I_{Ca-L}) and Na^+ - Ca^{2+} exchanger current (I_{NCX}), the transient outward K^+ current (I_{to}), the inward rectifier potassium current (I_{K1}), the slowly activating delayed rectifier potassium channel current (I_{Ks}) and the rapidly activating delayed rectifier potassium channel current (I_{Kr}) were analyzed. Currents were sampled and analyzed by an ISO-3 multitasking patch-clamp program (MFK M. Friedrich, Niedernhausen, Germany). The whole-cell currents were measured at the peak or end of each pulse and normalized to cell capacitance to obtain the current density (pA/pF). The density was plotted versus the respective voltages, yielding the activation (I/V) curves of channels in the cell. The membrane conductance (G_m) was calculated as $G_m = I / (E_m - E_{rev})$. I is macroscopic current, E_m is the test membrane potential, and E_{rev} is the reversal potential. G_m values were plotted against test voltages to obtain conductance-voltage (G/V) curves.

Solutions for patch clamp measurements

For AP measurements, the isotonic solution contained 130mmol/L NaCl, 5.9mmol/L KCl, 1.2mmol/L $MgCl_2$, 2.4mmol/L $CaCl_2$, 11mmol/L glucose, and 10 mmol/L HEPES (pH 7.4 (NaOH)). The pipette solution contained 20mmol/L KCl, 110mmol/L K-aspartate, 1mmol/L $MgCl_2$, 0.5mmol/L EGTA, 2mmol/L ATP, 0.5mmol/L GTP, and 10mmol/L HEPES (pH 7.2 (KOH)).

For peak sodium current (I_{Na}) measurements, the bath solution contained 20mmol/L NaCl, 110mmol/L CsCl, 1.8mmol/L $CaCl_2$, 1mmol/L $MgCl_2$, 10mmol/L HEPES, 10mmol/L glucose, and 0.001mmol/L nifedipine (pH 7.4 (CsOH)). Microelectrodes were filled with 10mmol/L NaCl, 135mmol/L CsCl, 2mmol/L $CaCl_2$, 3mmol/L MgATP, 2mmol/L TEA-Cl, 5mmol/L EGTA, and 10mmol/L HEPES (pH 7.2 (CsOH)).

The bath solution for L-type calcium channel current (I_{Ca-L}) recordings contained 140mmol/L TEA-Cl, 5mmol/L $CaCl_2$, 1mmol/L $MgCl_2$, 10mmol/L HEPES, 0.003mmol/L E-4031, 0.02mmol/L TTX, and 3mmol/L 4-AP (pH 7.4

(CsOH)). The pipette solution contained 10mmol/L NaCl, 135mmol/L CsCl, 2mmol/L CaCl₂, 3mmol/L MgATP, 2mmol/L TEA-Cl, 5mmol/L EGTA, and 10mmol/L HEPES (pH 7.2 (CsOH)).

The bath solution for Na⁺-Ca²⁺ exchanger current (I_{NCX}) measurements contained 135mmol/L NaCl, 10mmol/L CsCl, 2mmol/L CaCl₂, 1mmol/L MgCl₂, 10mmol/L HEPES, 10mmol/L glucose, 0.01mmol/L nifedipine, 0.1mmol/L niflumic acid, 0.05mmol/L lidocaine, and 0.02mmol/L dihydroouabain (pH 7.4 (CsOH)). Microelectrodes were filled with 10mmol/L NaOH, 150mmol/L CsOH, 2mmol/L CaCl₂, 1mmol/L MgCl₂, 75mmol/L aspartic acid, and 5mmol/L EGTA (pH 7.2 (CsOH)).

For measuring K⁺ channel currents, the bath solution contained 130mmol/L NaCl, 5.9mmol/L KCl, 2.4mmol/L CaCl₂, 1.2mmol/L MgCl₂, 11mmol/L glucose, and 10mmol/L HEPES (pH 7.4 (NaOH)). The pipette solution contained 126mM KCl, 6mM NaCl, 1.2mM MgCl₂, 5mM EGTA, 11mM glucose, 10mM HEPES, and 1mM MgATP (pH 7.4 (KOH)). For the transient outward K⁺ current (I_{to}) measurements, 10 μ M nifedipine, 10 μ M TTX, and 3 μ M E-4031 were added in the bath solution to block I_{Ca-L} , I_{Na} , and I_{Kr} , respectively. For the inward rectifier current (I_{K1}) measurement, 10 μ M nifedipine and 3 μ M E-4031 were added. For the slowly activating delayed rectifier K⁺ (I_{Ks}) measurements, 10 μ M nifedipine, 3mM 4-AP, and 10 μ M TTX were added.

To improve the measurement of the rapidly activating delayed rectifier channels (I_{Kr}), the Cs⁺ instead of K⁺ ions were used as the charge carrier. External solution for Cs⁺ current measurements contains 140mmol/L CsCl, 2mmol/L MgCl₂, 10mmol/L HEPES, and 10mmol/L glucose (pH 7.4 (CsOH)). Pipette solution contained 140mmol/L CsCl, 2mmol/L MgCl₂, 10mmol/L HEPES, and 10mmol/L EGTA (pH 7.2 (CsOH)).

4.2.7 Western blotting

The ion channel expression at protein level was assessed by western blotting analysis. hiPSC-CMs were dissected and sonicated in RIPA buffer (R0278;

Merck KGaA, Darmstadt, Germany). The lysate was centrifuged at 12,000 × g for 10min at 4 °C. Then the supernatant fraction was collected for Western blotting analysis. BCA Protein Assay Kit (23227; Thermo Fisher Scientific, Waltham, MA, USA) was used to detect the protein concentration and all the concentration of samples were diluted to 1µg/µl with RIPA buffer. The protein samples were loaded 10ug per sample for SDS-PAGE, and then transferred to the PVDF membrane (IPVH00010, Immobilon-p, Merck KGaA, Darmstadt, Germany). Then the membranes were blocked with 5% nonfat milk in tris-buffered salt solution with tween (TBST) for 1h at room temperature. After blocking, the membranes were incubated with the primary antibodies at 4°C overnight. The primary antibodies used in western blotting analysis were as follow: Glyceraldehyde 3-phosphate dehydrogenase (GAPDH) (14C10) antibody (2118S, 1:10000; Cell Signaling, Chicago, IL, USA); anti-Na_v1.5 (SCN5A)(493-511) antibody (ASC-005, 1:500; Alomone Labs, Israel); anti-Ca_v1.2 (CACNA1C) antibody (ASC003, 1:500; Alomone Labs, Israel); anti-NCX1 antibody (ab135735, 1:500; Abcam, Cambridge, UK); anti-K_v4.3 (KCND3) antibody (APC-017, 1:500; Alomone Labs, Israel); anti-hK_v11.1 antibody (P9497, 1:400; Sigma-Aldrich, Merck KGaA, Darmstadt, Germany); anti-KCNQ1 antibody (APC-022, 1:500; Alomone Labs, Israel); anti-Kir2.1/BIK antibody (ab109750, 1:1000; Abcam, Cambridge, UK); DNMT1 antibody (NB100-56519, 1:5000; Novus Biologicals, USA); DNMT2 antibody (19221-1-AP, 1:1000; ProteinTech, IL, USA); DNMT3A antibody (NB120-13888, 1:2000; Novus Biologicals, USA); DNMT3B antibody (NB300-516, 1:500; Novus Biologicals, USA); anti-TET1 antibody-C-terminal (ab101698, 1:1000; Abcam, Cambridge, UK). The secondary antibodies were anti-rabbit IgG-peroxidase produced in goat (A0545, 1:2000; Sigma-Aldrich, Merck KGaA, Darmstadt, Germany) or anti-mouse IgG-peroxidase produced in goat (A3682, 1:2000; Sigma-Aldrich, Merck KGaA, Darmstadt, Germany). The target protein bands were quantified by Fusion Solo system (Vilber, France) and measured with

software (AlphaView, Protein Simple, California, USA) for statistical analyses in all groups.

Table 4. The detail information of the gel involved in the western blotting.

Separating gel	8% /mL	10% /mL	12% /mL	Stacking gel	
ddH ₂ O	4.6	4	3.3	ddH ₂ O	2.8
1.5M Tris pH8.8	2.5	2.5	2.5	0.5M Tris pH6.8	1.25
10%SDS	0.1	0.1	0.1	10%SDS	0.05
10%APS	0.1	0.1	0.1	10%APS	0.05
Acrylamide	2.7	3.3	4	Acrylamide	0.85
TEMED	0.008	0.008	0.008	TEMED	0.005

4.2.8 Immunofluorescence

The localization of cellular expression of ion channel proteins was determined by immunofluorescence staining. Cardiomyocytes were dissociated from 24-well plates and plated onto the culture slides (354114; Thermo Fisher Scientific, Waltham, MA, USA). After incubated with cancer cell media or cardio culture medium for 48h, all slides were fixed with 4% paraformaldehyde at room temperature for 10min and permeabilized with 0.5% triton for 10min. After blocking with 5% bovine serum albumin (BSA, 10270106; Thermo Fisher Scientific, Waltham, MA, USA) for 30min, the slides were incubated with primary antibodies at 4°C, and then were incubated with the second antibodies anti-rabbit/mouse IgG (H+L), F(ab')₂ Fragment (1:2000; Cell Signaling, USA). The primary antibodies used on hiPSC-CMs were monoclonal anti- α -actinin (Sarcomeric) (A7811, 1:200; Sigma-Aldrich, Merck KGaA, Darmstadt, Germany); anti-Myl4 antibody (A20170301415, 1:200; Cloud-Clone corp, CCC, USA); anti-Nav1.5 (SCN5A)(493-511) antibody (ASC-005, 1:500; Alomone Labs, Israel); anti-Kv4.3 (KCND3) antibody (APC-017, 1:500; Alomone Labs, Israel); anti-KCNQ1 antibody (APC-022, 1:500; Alomone Labs, Israel). 3

random fields per wells (at least 10 cells) were photographed, and the immunofluorescence density of the positive staining per field was measured by Image-Pro Plus software (Media cybernetics, Acton, MA, USA).

4.2.9 Genomic DNA extraction

Extraction of DNA by phenol chloroform method:

- (1) First we put different groups of cells in 1.5ml Ep tubes, added 500 μ l of SNET solution (20mM Tris-HCl 0.121g, 5mM EDTA 0.093g, 400mM NaCl 1.17g, SDS 0.5g, add ddH₂O to 50ml), 10 μ l of proteinase K. Then we incubated the tubes in water bath at 55°C overnight.
- (2) Next day we added 500 μ l of PCI solution (phenol: chloroform: isoamyl alcohol = 25:24:1) to the lower layer of liquid and mixed gently until the mixture is homogeneous.
- (3) Then we centrifuged the tubes at 15000 rpm for 15 min at room temperature. The supernatant was loaded to a new Ep tube (about 400 μ l), an equal volume of isopropanol (400 μ l) was added. Then we mixed the liquid by inverting the tubes.
- (4) Again, centrifuged the tubes at 15000 rpm for 8 min at room temperature, discarded the supernatant, added 70% ethanol to wash and then centrifuged the tubes at 15000 rpm for 5-7 min at room temperature.
- (5) Then we discarded the supernatant. The DNA was dried for 5~10min. Then we added 30 μ l ddH₂O to every tube, to dissolve the genomic DNA.

4.2.10 Dot blotting

Dot blotting is a simple technique for immobilizing bulk unfractionated DNA on a nitrocellulose or nylon membrane. Hybridization analysis can then be carried out to determine the relative abundance of target sequences in the blotted DNA preparations. Genome DNA was extracted from hiPSC-CMs treated with or without cancer cell media by using phenol-chloroform extraction. The genome DNA was serially diluted and denatured in 0.1M NaOH/10 mM EDTA at 100°C for 10 minutes. The denatured DNA was spotted on membrane (0.2 μ m

nitrocellulose membrane) and air-dry. The membrane was washed with 20 × SSC buffer (175.3g NaCl, 88.2g trisodium citrate, pH 7.0 in 1L ddH₂O) and then soaked in denaturation solution (1.5M NaCl, 0.5M NaOH) for 10min, then in neutralization solution (1M NaCl, 0.5M Tris-HCl pH 7.0) for 5min. Then the membrane was baked for 2h at 80°C. After blocking the membrane with 5% nonfat milk in TBST for 1h at room temperature, the membrane was incubated with anti-5-methylcytidine antibody (ab10805, 1:5000; Abcam, UK) and recombinant anti-5-hydroxymethylcytosine (5-hmC) antibody [RM236] (ab214728, 1:1000; Abcam, UK) at 4°C overnight. The secondary antibodies are anti-mouse IgG, HRP-linked antibody (7074, 1:2000; Cell Signaling, Chicago, IL, USA). The dots were detected and quantified by Fusion Solo system (Vilber, France).

4.2.11 Bisulfite sequence

Genomic DNA bisulfite (BSP) conversion is to convert the unmethylated cytosines from cytosine (C) to uracil (U), while methylated cytosine cleavage is unchanged and remains C. The BSP primers are designed for PCR amplification in the target region. After expansion, U is converted to thymidine cleavage (T), while the CpG site of methylation in the extended sequence is still C, and the unmethylated CpG site is T. The PCR product is expanded, and after delivery, it is judged that some CpG sites are methylated. The bisulfite conversion of genome DNA from different groups was performed with EpiTect Bisulfite Kits (59104, QIAGEN, Germany). Specific steps were as follow:

- (1) The extracted genomic DNA was diluted. Then we added 800µl of RNase-free water to the required number of Bisulfite Mix powder tubes, and vortexed until the Bisulfite Mix was completely dissolved (concussive for 5min). If the dissolution was not homogeneous, it was heated to 60 ° C and then shook again.
- (2) Then the BSP reaction system was added to a 200µl PCR tube containing DNA solution (1ng to 2µg) and RNase-free water (total 20µl), dissolved

Bisulfite Mix 85µl, DNA Protect Buffer 35µl, total 140µl. They were mixed until DNA Protect Buffer changed from green to blue in the system.

- (3) The reaction was carried out under the following conditions: 95 ° C for 5min; 60 ° C for 25min; 95 ° C for 5min; 60 ° C for 85min; 95 ° C for 5min; 60 ° C for 175min; totally about 5h.
- (4) After the reaction was completed, we centrifuged the tubes, and transferred the reaction system into a 1.5ml Ep tube.
- (5) Then we added 560µl of configured Buffer BL to each reaction system (before using, we have already added carrier RNA at a final concentration of 10µg/ml to Buffer BL).
- (6) The EpiTect spin columns were put in the collection tube, and the system from step (5) was transferred into the EpiTect spin columns, centrifuged at maximum speed for 1min. Then we discarded the flowthrough in the collection tubes and placed the EpiTect spin columns in the collection tubes.
- (7) Then 500µl Buffer BW was added to each tube and centrifuged at maximum speed for 1min. Then we discarded the flowthrough in the collection tubes and placed the EpiTect spin columns back in the collection tubes.
- (8) Next, we added 500µl Buffer BD to each tube. The tubes were incubated for 15min at room temperature, then centrifuged at maximum speed for 1min. We discarded the flowthrough in the collection tubes and placed the EpiTect spin columns in the collection tubes.
- (9) Again, we added 500µl Buffer BW to each tube, centrifuged the tubes at maximum speed for 1min, discarded the flowthrough in the collection tubes, and placed the EpiTect spin column in the collection tube again, repeating this step again.
- (10) Next, we placed the EpiTect spin columns in new collection tubes and centrifuged them at maximum speed for 1min to remove residual liquid.

(11) Then we placed the EpiTect spin columns in new 1.5ml Ep tubes and placed 20µl Buffer EB into the center of the EpiTect spin columns. The BSP-DNA solution was collected by centrifugation at 15,000 x g for 1min.

4.2.12 Sequencing polymerase chain reaction

The promoter sequences were searched on UCSC Genome Browser (<https://genome.ucsc.edu/>). Bisulfite sequencing polymerase chain reaction (PCR) primers for CpG islands were designed by using Methyl Primer Express v1.0 software (Thermo Fisher Scientific, USA). PCR amplification was performed using TaKaRa EpiTaq HS (for bisulfite-treated DNA) kit (purchased from TAKARA, product number R110A) containing:

- (1) TaKaRa EpiTaq HS (5 U/µl) 0.25µl, 10× EpiTaq PCR Buffer (Mg²⁺ free) 5µl, 25mM MgCl 25µl, dNTP Mixture (2.5 mM each) 6µl, BSP-DNA <100 ng, 20 pmol each of the upstream and downstream primers, and ddH₂O to 50µl.
- (2) Reaction conditions: 98 ° C for 1min; (98 ° C for 10 s, 50 ° C for 30 s, 98 ° C for 30 s) × 40; 72 ° C for 10min. The BSP primer sequences of ion channels detected are shown in Table 5.

Table 5. Bisulfite sequencing PCR primers for CpG islands

	Primer 5' to 3'		Products
SCN5A CpG island	Forward	TGTGTTTTTAGGAAAGTGTGGT	364bp
	Reverse	ACTAACATACACACCAACACCC	
KCND3 CpG island	Forward	AGTAGTGGGGATTTATGGGTT	340bp
	Reverse	CAACACCTACTTAAAACCAAACC	
KCNQ1 CpG island	Forward	AGGTATTTGATAGTGGTGGTTT	393bp
	Reverse	TTACTCCTACCCTACCCTCA	

4.2.13 PCR products purification

After the reaction was completed, 1.5% agarose gel was adapted, and 120V electrophoresed for about 1 hour. The gel imager was exposed, and the gel was cut at the position of the strip. The PCR products were loaded for agarose

gel electrophoresis and purified using Wizard SV Gel and PCR Clean-Up System (A9281/2/5, Promega, USA):

- (1) First for dissolving the Gel slices, we excised DNA band from gel and placed gel slices in 1.5ml microcentrifuge tubes.
- (2) Then we added 10 μ l Membrane Binding Solution per 10mg of gel slice. The gel slices were vortexed and incubated at 50-65 °C until they were completely dissolved.
- (3) Next, we inserted SV Minicolumns into Collection Tubes.
- (4) Then we transferred the dissolved gel mixture or prepared PCR product to the Minicolumn assembly and incubated at room temperature for 1min.
- (5) The tubes were centrifuged at 16,000 X g for 1min. Then we discarded the flowthrough and reinserted Minicolumns into Collection Tubes.
- (6) All the tubes were added 700 μ l Membrane Wash Solution with ethanol. And centrifuged at 16,000 X g for 1min. Then we discarded the flowthrough and reinserted Minicolumns into Collection Tubes.
- (7) Again, we added 500 μ l Membrane Wash Solution with ethanol to the tubes and centrifuged them at 16,000 X g for 5min.
- (8) Next, we discarded the flowthrough and placed the columns back into the wash tubes and recentrifuged the column at 16,000 X g for 1min.
- (9) Then we transferred Minicolumns to clean 1.5ml microcentrifuge tubes. 30 μ l of Nuclease-Free Water was added to the Minicolumns and incubated at room temperature for 1min, and then centrifuged at 16,000 X g for 1min.
- (10) At last, we discarded the Minicolumns and tested the concentration of samples.

4.2.14 Plasmid ligation and amplification

The purified PCR products were inserted into pMD20-T vector with TaKaRa Mighty TA-cloning Kit (6028, Takara, Shiga, Japan) and transformed to *E. coli* HST08 Premium Competent Cells (9128, Takara, Shiga, Japan) for sequencing (Invitrogen, Thermo Fisher Scientific). The percentage of methylation of each

CpG site within the region amplified was determined by online software (<http://services.ibc.uni-stuttgart.de/BDPC/BISMA/>).

Plasmid ligation was performed as follows: 1µl of the above purified DNA, 1µl of pMD20-T vector, 3µl of ddH₂O, 5µl of Ligation Mighty Mix, reaction at 16 °C for 30 minutes. The whole amount of *E. coli* HST08 Premium Competent Cells (purchased from TAKARA, Cat. No. 9128) was added for conversion as follows:

- (1) *E. coli* HST08 Premium Competent Cells were thawed on ice before using, and 100µl of cells were added to a 15 ml round bottom Falcon tube.
- (2) Then we added DNA samples (≤10ng), placed them in ice for 30min, then at 42°C for 45s, then placed in ice for 1-2 minutes.
- (3) Next, we added 37°C pre-warmed SOC medium to 1ml, shook the culture at 37°C for 1h (160~225rpm).
- (4) An appropriate amount (100µl) was applied to the LB solid medium (the medium was added to the final concentration of 100µg/ml of ampicillin).
- (5) X-gal (20mg/ml) 40µl was applied to the plate 1 to 2 min before using.
- (6) Then we cultured them overnight at 37 °C.
- (7) After the colonies were grown, white colonies were picked, shaken overnight at 37 °C in LB liquid medium, then centrifugated at 220 rpm/min.

4.2.15 Plasmid extraction

To follow this procedure to purify plasmid DNA we used a centrifuge.

- (1) First, we centrifuged 1-5ml of the overnight LB-culture and removed all medium.
- (2) Then 250µl Resuspension Buffer with Rnase A was added to the cell pellets and the pellets were resuspended until they were homogeneous.
- (3) We added 250µl Lysis Buffer to the tubes, mixed them gently by inverting the capped tubes until the mixture was homogeneous, without vortex. Then the tubes were incubated for 5min at room temperature.

- (4) 350µl Precipitation Buffer was added per tube, mixed immediately by inverting the tube until the mixture was homogeneous, without vortex. Then the lysate was centrifuged at >12,000 X g for 10min.
- (5) We loaded the supernatant from step (4) onto a spin column in the 2ml wash tubes, again centrifuged the columns at 12,000 X g for 1min. Then we discarded the flowthrough and placed the column back into the wash tubes.
- (6) 500µl Wash Buffer with ethanol was added to every column. Then we incubated the columns for 1min at room temperature, centrifuged the columns at 12,000 X g for 1min. Then we discarded the flowthrough and placed the columns back into the wash tubes.
- (7) Next, we added 700µl Wash Buffer W9 with ethanol to every column, centrifuged the columns at 12,000 X g for 1min and discarded the flowthrough, emptied the columns and placed the columns back into the wash tubes, again centrifuged the column at 12,000 X g for 1min. Then discarded the wash tube with flowthrough.
- (8) Then we placed the Spin Column in the clean 1.5ml collection tubes. 50ul TE Buffer was added to the center of the columns. And we incubated the columns for 1min at room temperature.
- (9) Again, we centrifuged the columns at 12,000 X g for 2min. The collection tubes contained the purified plasmid DNA. So, we discarded the columns and detected the concentration of plasmid DNA.

4.2.16 Overexpression of the ten-eleven translocation family enzymes

The overexpression of TET1 gene was accomplished by transfection of TET1 plasmid FH-TET1-pEF. This plasmid expressed the full-length human TET1 gene. An empty backbone plasmid pEF1a-IRES-Neo was used as the empty control. FH-TET1-pEF was a gift from Anjana Rao (Addgene plasmid # 49792; <http://n2t.net/addgene:49792>; RRID:Addgene_49792) and pEF1a-IRES-Neo was a gift from Thomas Zwaka (Addgene plasmid # 28019; <http://n2t.net/addgene:28019>; RRID:Addgene_28019).^{64, 65} The transfection

was performed by using FuGENE® HD Transfection Reagent (E2311, Promega, WI, USA) according to the protocol provided by Promega. Briefly, we added for each well 1µg plasmid DNA to the Opti-MEM® medium and mixed well and added 3µl FuGENE® HD Transfection Reagent (3:1 FuGENE® HD Transfection Reagent: DNA) and mixed well immediately. The mixture was incubated for 5min in room temperature. Then added 25µl of the mixture was added to each well of 24-well plate and mixed by pipetting. The cells were incubated for 2 days.

4.2.17 Statistics

All data analyses were performed by an experienced technician who had no understanding of experimental grouping details and results. All statistical data were expressed as mean \pm standard error of the mean values (SEM). Statistical analyses were performed by GraphPad Prism 7 (GraphPad Software Inc., California, USA). Student's *t*-test, one-way analysis of variance (ANOVA), and two-way ANOVA with Dunnett's multiple comparisons post-test were applied. P values less than 0.05 are statistically significant. The n values in each figure legend reflect the number of cells used for the statistical analysis.

4.2.18 Ethics statements

This project was conducted in accordance with the ethical principles that have their origin in the Declaration of Helsinki. The generation and application of hiPSC-CMs have been approved by the Ethics Committee of Medical Faculty Mannheim, Heidelberg University (approval number: 2018-565N-MA).

5. RESULTS

5.1 Culture medium for cancer cells had no effect on the growth of hiPSC-CMs

Considering that the number of cancer cells in a flask was critical for the concentration of cell secretions in the culture medium that were taken for the study, cancer cell growth rate analyses of the two cancer cell lines (AGS and SW480) were performed by manual cell counting and MTT assay. The curves displayed that the growth of both cancer cell lines reached a maximum at day 8 of culture when AGS and SW480 cancer cells in a T75 flask increased to about 4.0×10^6 and 7.7×10^6 respectively. (Figure 4A, B). So, the cancer cell medium cultured for 8 days with same seeded number of cells was used for all experiments in this study.

Because different medium is required for culture of cancer cells and hiPSC-CMs, the cancer cell medium, when it was added into culture medium of hiPSC-CMs, may interfere the growth of hiPSC-CMs. Therefore, we checked the effect of non-cultured medium (for control) and different concentrations of medium cultured with same amount of cancer cells on the growth of hiPSC-CMs. The cancer cell medium was added into culture dishes with cardiomyocytes in four different concentrations, 10% (v/v), 20%, 40% and 80%, respectively. As shown in Figure 4C and D of the MTT assay, we found that different concentration of the medium with (AGS or SW480) or without (medium) cancer cells showed no effect on the cell viability of cardiomyocytes.

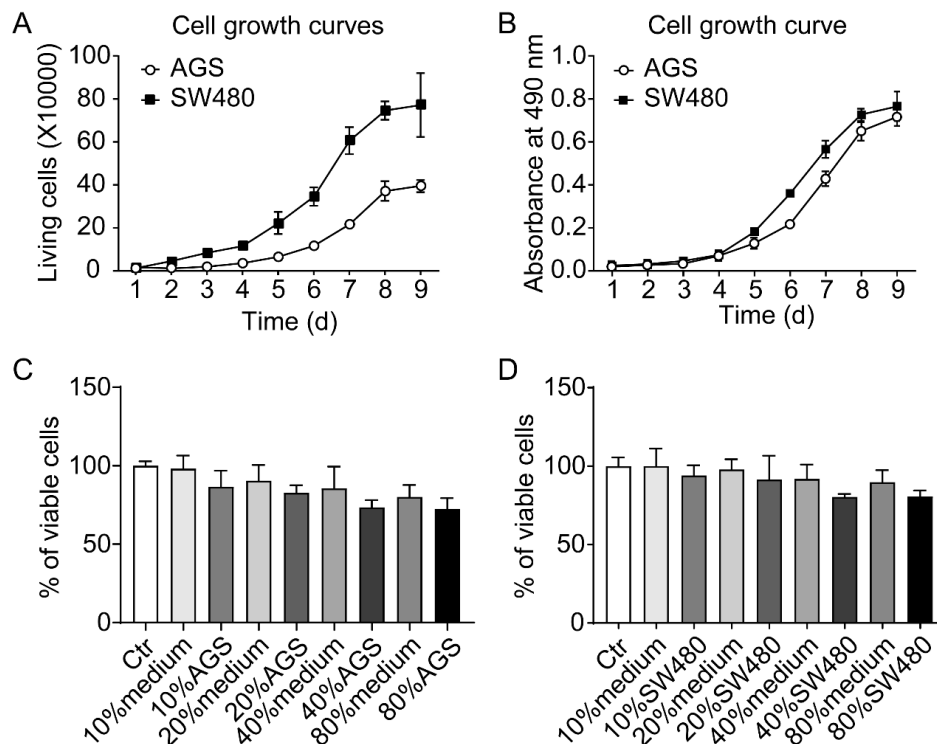
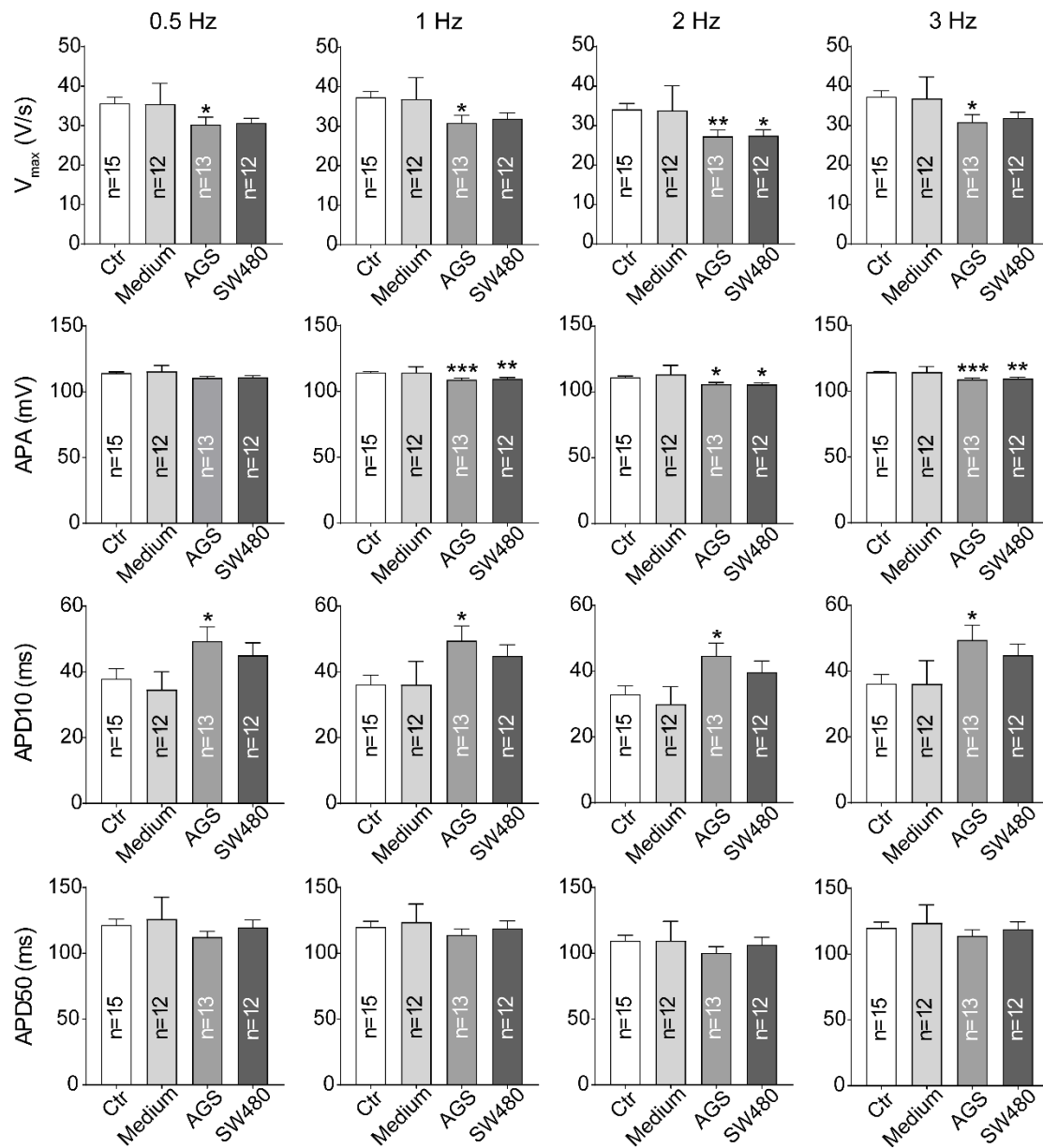


Figure 4. Cancer cell medium had no effect on cell growth of hiPSC-CMs. (A) Cell growth curve by cell counting. (B) Cell growth curve by MTT assay. (C, D) Cell viability of hiPSC-CMs under different concentrations of supernatant of AGS and SW480 cell culture and medium without cancer cells. “Ctr” represents data from hiPSC-CMs without medium for cancer cells. “Medium” represents data from hiPSC-CMs with addition of un-cultured medium for cancer cells. “AGS” represents data from hiPSC-CMs with addition of cultured medium of AGS cancer cells. “SW480” represents data from hiPSC-CMs with addition of cultured medium of SW480 cancer cells. Data are presented as mean \pm SEM and analyzed by one-way ANOVA.

5.2 Effects of cancer cell secretion on action potentials of hiPSC-CMs

To examine possible actions of cancer cells on the electrical characteristics of cardiomyocytes, the influence of cancer cell secretion on action potential (AP) of hiPSC-CMs were investigated (Figure 5). The results exhibited that the maximum depolarization velocity (V_{max}) and the action potential amplitude (APA) were reduced in AGS and SW480 groups compared with control (without cancer cell medium) and medium (without cancer cells) groups. The action

potential duration at 10% repolarization (APD 10) prolonged in the AGS and SW480 groups, while the action potential duration at 50% repolarization (APD 50) and 90% repolarization (APD 90) and the resting potential (RP) were similar in all groups. In addition, the effects of cancer cell secretion on AP paced at different frequencies were also examined. No frequency-dependence was detected.



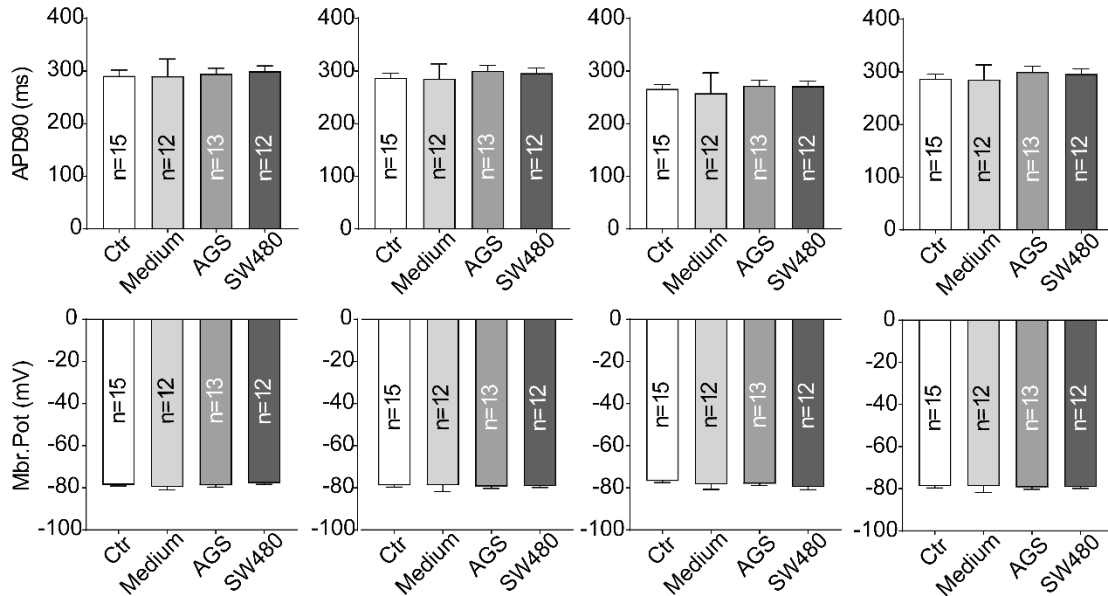


Figure 5. Action potential (AP) characteristics of hiPSC-CMs cultured with AGS and SW480 cancer cell media. “Ctr” represents data from hiPSC-CMs without medium for cancer cells. “Medium” represents data from hiPSC-CMs with addition of un-cultured medium for cancer cells. “AGS” represents data from hiPSC-CMs with addition of cultured medium of AGS cancer cells. “SW480” represents data from hiPSC-CMs with addition of cultured medium of SW480 cancer cells. Data are presented as mean \pm SEM and analyzed by one-way ANOVA. The cell number (n) of every experiment group is marketed on the column. *P<0.05, **P<0.01, ***P<0.001.

5.3 Effects of cancer cell secretion on ion channel currents in hiPSC-CMs

In order to uncover the ion channel current alterations responsible for the observed AP changes, voltage clamp recordings were performed. Different ion channel currents that contribute to APs were investigated. Specifically, the peak and late Na^+ current (I_{Na}), the L-type Ca^{2+} current ($I_{\text{Ca-L}}$), the $\text{Na}^+/\text{Ca}^{2+}$ exchanger current (I_{NCX}) and K^+ channel currents including the transient outward (I_{to}), the rapidly activating delayed rectifier (I_{Kr}), the slowly activating delayed rectifier (I_{Ks}) and the inward rectifier (I_{K1}) were assessed. The peak I_{Na} was significantly reduced in AGS and SW480 groups compared with control and medium groups (Figure 6A, B, and I), in agreement with the reduction of

V_{max} and APA of APs. The activation, inactivation and recovery curves of I_{Na} were not significantly changed (Figure 6C, D, E, F, G, H). The late sodium current increased in AGS and SW480 groups when compared with control and medium groups (Figure 6J).

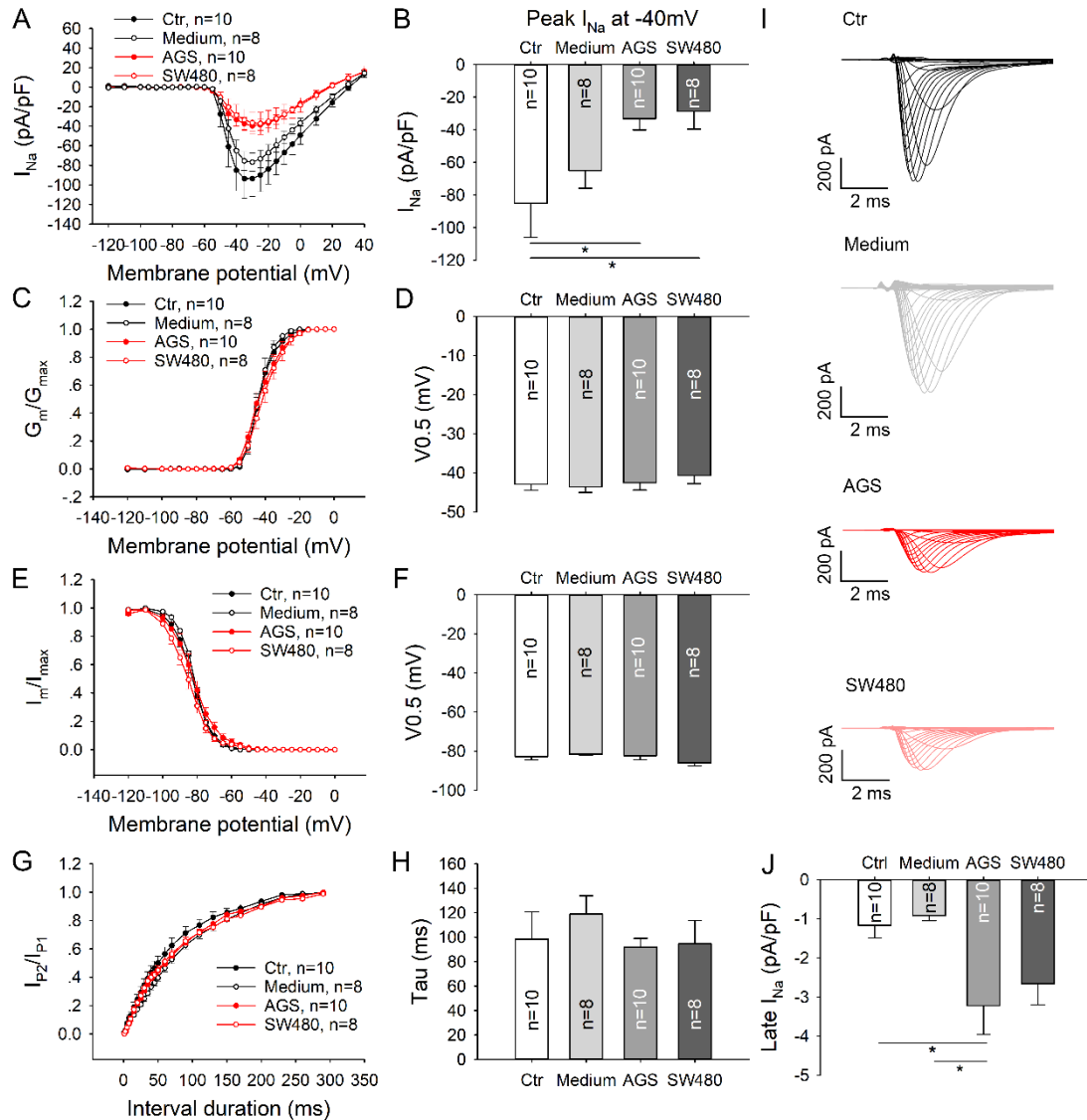


Figure 6. The sodium current was suppressed in hiPSC-CMs cultured with AGS and SW480 cancer cell media. (A) I-V curves of peak I_{Na} . (B) Mean values of peak I_{Na} at -40mV. (C) Activation curves of peak I_{Na} . (D) Mean values of $V_{0.5}$ (the voltage at half maximum) of activation. (E) Inactivation curves of peak I_{Na} . (F) Mean values of $V_{0.5}$ of inactivation. (G) Time course curves of recovery from inactivation of peak I_{Na} . (H) Mean values of time constants (tau) of tau recovery from inactivation (I) Representative traces of I_{Na} in Ctrl, medium, AGS, and SW480 groups. (J) Mean values of late I_{Na} at -40mV. “Ctr”

represents data from hiPSC-CMs without medium for cancer cells. “Medium” represents data from hiPSC-CMs with addition of un-cultured medium for cancer cells. “AGS” represents data from hiPSC-CMs with addition of cultured medium of AGS cancer cells. “SW480” represents data from hiPSC-CMs with addition of cultured medium of SW480 cancer cells. Data are presented as mean \pm SEM and analyzed by one-way ANOVA. The cell number of every experiment group is given as “n”. *P<0.05.

The sodium-calcium exchanger current, I_{NCX} , was similar in all the experimental groups (Figure 7). Neither the I-V curves of L-type Ca^{2+} current nor the channel gating kinetics (activation, inactivation and recovery from inactivation) were changed by the cancer cell secretion (Figure 8).

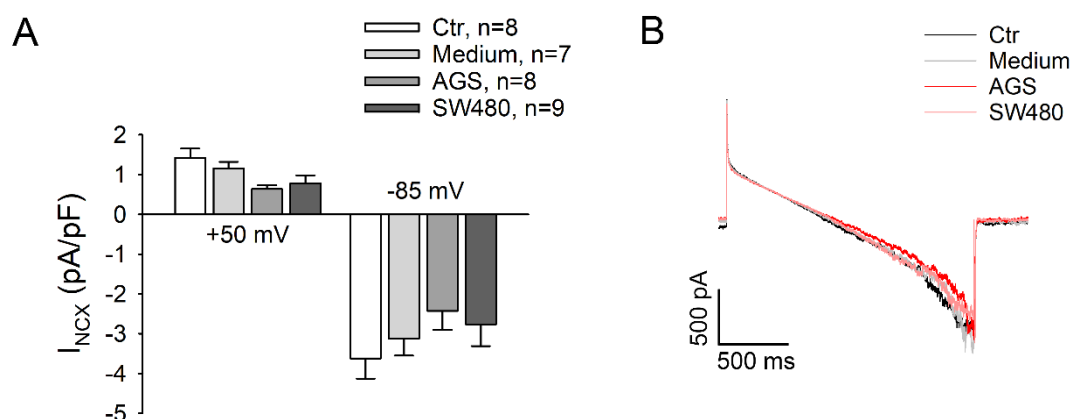


Figure 7. The sodium-calcium exchanger current (I_{NCX}) in hiPSC-CMs cultured with AGS and SW480 cancer cell media. (A) Mean values of I_{NCX} at 50mV and -85mV. (B) Representative traces of I_{NCX} in Ctrl, medium, AGS, and SW480 groups. “Ctr” represents data from hiPSC-CMs without medium for cancer cells. “Medium” represents data from hiPSC-CMs with addition of un-cultured medium for cancer cells. “AGS” represents data from hiPSC-CMs with addition of cultured medium of AGS cancer cells. “SW480” represents data from hiPSC-CMs with addition of cultured medium of SW480 cancer cells. Data are presented as mean \pm SEM and analyzed by one-way ANOVA. The cell number of every experiment group is marketed as “n”.

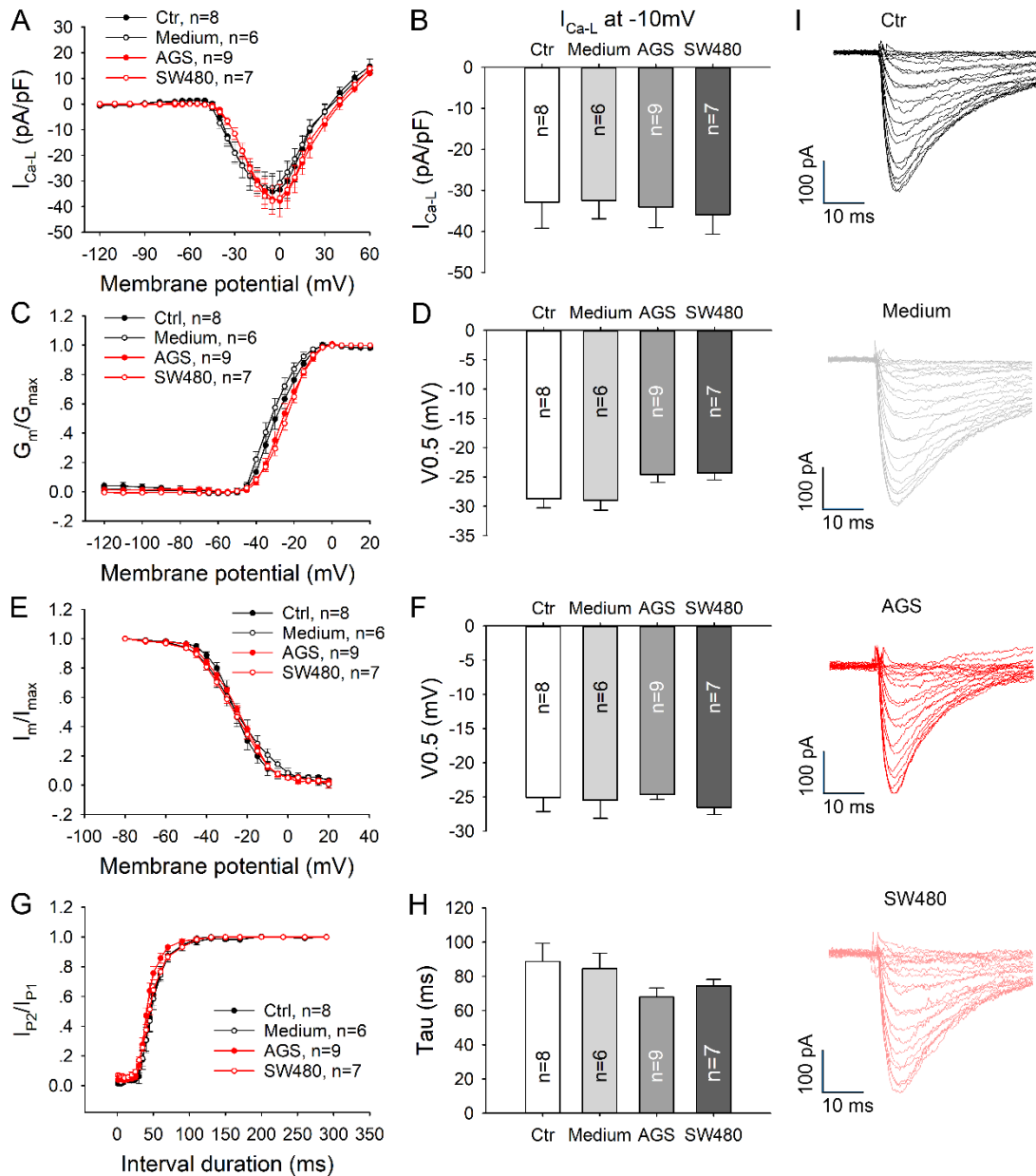


Figure 8. The L-type calcium current (I_{Ca-L}) in hiPSC-CMs cultured with AGS and SW480 cancer cell media. (A) I-V curves of I_{Ca-L} . (B) Mean values of peak I_{Ca-L} at -10mV. (C) Activation curves of I_{Ca-L} . (D) Mean values of $V_{0.5}$ (the voltage at half maximum) of activation. (E) Inactivation curves of peak I_{Ca-L} . (F) Mean values of $V_{0.5}$ of inactivation. (G) Time course curves of recovery from inactivation of I_{Ca-L} . (H) Mean values of time constants (τ) of recovery from inactivation. (I) Representative traces of I_{Ca-L} in Ctrl, medium, AGS, and SW480 groups. “Ctr” represents data from hiPSC-CMs without medium for cancer cells. “Medium” represents data from hiPSC-CMs with addition of un-cultured medium for cancer cells. “AGS” represents data from hiPSC-CMs with addition of cultured medium of

AGS cancer cells. “SW480” represents data from hiPSC-CMs with addition of cultured medium of SW480 cancer cells. Data are presented as mean \pm SEM and analyzed by one-way ANOVA. The cell number of every experiment group is shown as “n”.

The K^+ channel currents were differentially affected by the cancer cell secretion. I_{to} , the 4-AP (an I_{to} blocker) sensitive current, was declined in AGS and SW480 groups compared with control and medium groups (Figure 9), consistent with the prolongation of APD10.

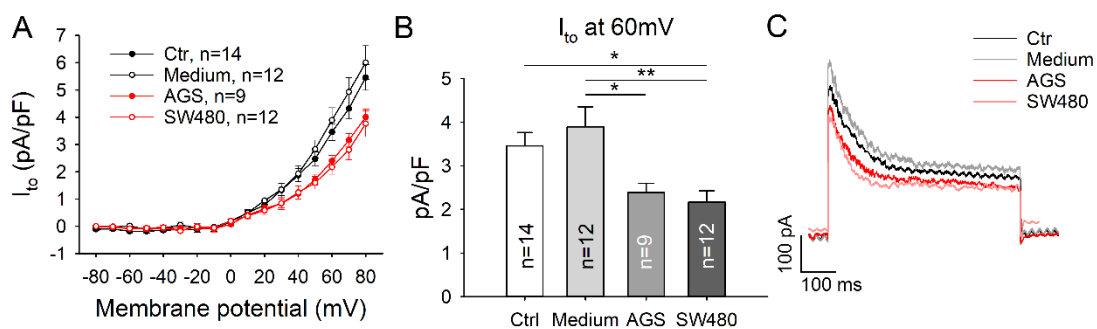


Figure 9. The transient outward current (I_{to}) decreased in hiPSC-CMs cultured with AGS and SW480 cancer cell media. (A) I-V curves of I_{to} . (B) Mean values of peak I_{to} at 60mV. (C) Representative traces of I_{to} in Ctrl, medium, AGS, and SW480 groups. “Ctr” represents data from hiPSC-CMs without medium for cancer cells. “Medium” represents data from hiPSC-CMs with addition of un-cultured medium for cancer cells. “AGS” represents data from hiPSC-CMs with addition of cultured medium of AGS cancer cells. “SW480” represents data from hiPSC-CMs with addition of cultured medium of SW480 cancer cells. Data are presented as mean \pm SEM and analyzed by one-way ANOVA. “n” represents the cell number of every group. * $P < 0.05$, ** $P < 0.01$.

The rapidly activating delayed rectifier potassium current (I_{Kr}) slightly increased (Figure 10), while the slowly activating delayed rectifier K^+ current, (I_{Ks}), was significantly higher in the cancer groups compared with control and medium groups (Figure11). The inward rectifier potassium current (I_{K1}) displayed no difference in all groups (Figure 12).

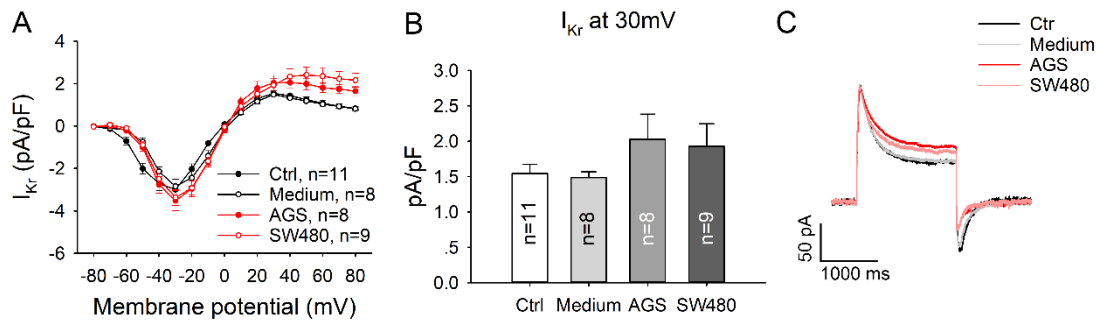


Figure 10. The rapidly activating delayed rectifier potassium current (I_{Kr}) in hiPSC-CMs cultured with AGS and SW480 cancer cell media. (A) I-V curves of I_{Kr} . (B) Mean values of I_{Kr} at 30mV. (C) Representative traces of I_{Kr} in Ctrl, medium, AGS, and SW480 groups. “Ctr” represents data from hiPSC-CMs without medium for cancer cells. “Medium” represents data from hiPSC-CMs with addition of un-cultured medium for cancer cells. “AGS” represents data from hiPSC-CMs with addition of cultured medium of AGS cancer cells. “SW480” represents data from hiPSC-CMs with addition of cultured medium of SW480 cancer cells. Data are presented as mean \pm SEM and analyzed by one-way ANOVA. The cell number of every experiment group is marketed as “n”.

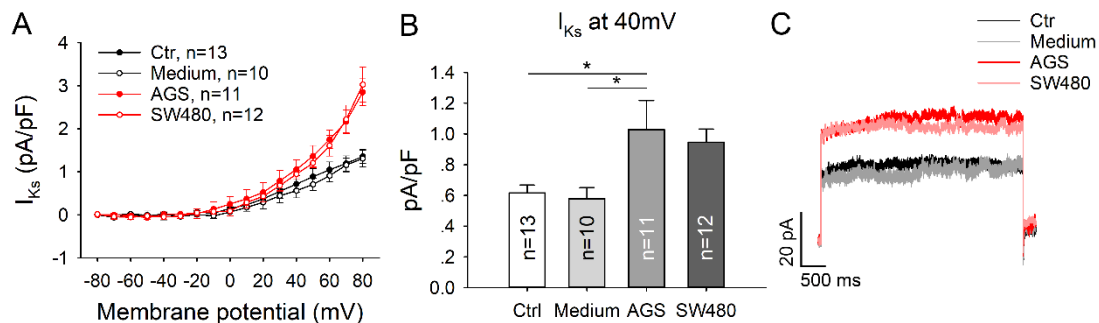


Figure 11. The slowly activating delayed rectifier K^+ current (I_{Ks}) in hiPSC-CMs cultured with AGS and SW480 cancer cell media. (A) I-V curves of I_{Ks} . (B) Mean values of peak I_{Ks} at 40mV. (C) Representative traces of I_{Ks} in Ctrl, medium, AGS, and SW480 groups. “Ctr” represents data from hiPSC-CMs without medium for cancer cells. “Medium” represents data from hiPSC-CMs with addition of un-cultured medium for cancer cells. “AGS” represents data from hiPSC-CMs with addition of cultured medium of AGS cancer cells. “SW480” represents data from hiPSC-CMs with addition of cultured medium of SW480 cancer cells. Data are presented as mean \pm SEM and analyzed by one-way ANOVA. The cell number of every experiment group is marketed as “n”. * $P < 0.05$.

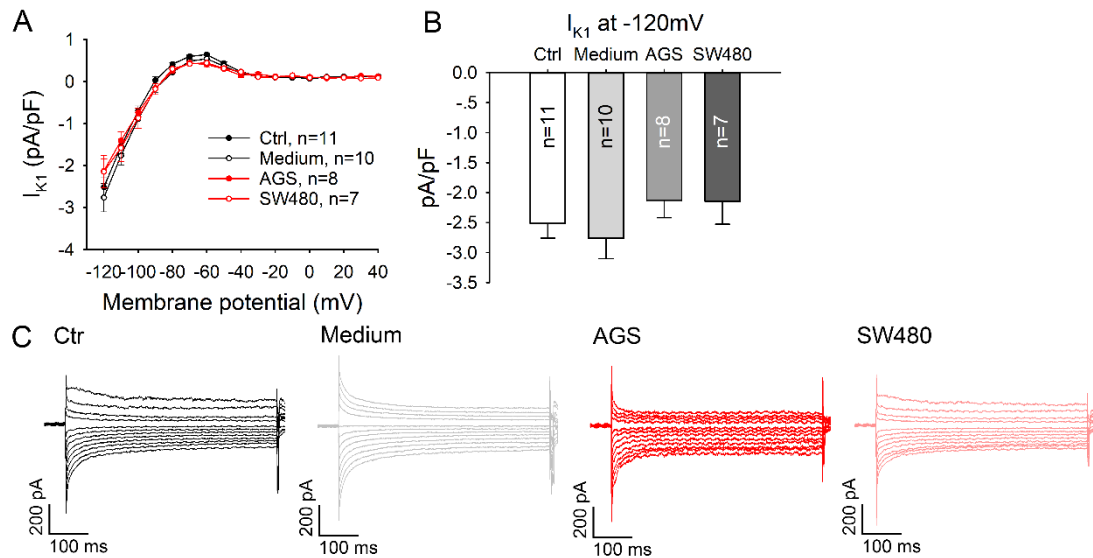


Figure 12. The inward rectifier potassium current (I_{K1}) in hiPSC-CMs cultured with AGS and SW480 cancer cell media. (A) I-V curves of I_{K1} . (B) Mean values of I_{K1} at -120mV. (C) Representative traces of I_{K1} in Ctrl, medium, AGS, and SW480 groups. “Ctr” represents data from hiPSC-CMs without medium for cancer cells. “Medium” represents data from hiPSC-CMs with addition of un-cultured medium for cancer cells. “AGS” represents data from hiPSC-CMs with addition of cultured medium of AGS cancer cells. “SW480” represents data from hiPSC-CMs with addition of cultured medium of SW480 cancer cells. Data are presented as mean \pm SEM and analyzed by one-way ANOVA. The cell number of every experiment group is marketed as “n”.

5.4 Effects of cancer cell secretion on ion channel expression in hiPSC-CMs

To investigate whether cancer secretions affect the expression of ion channels, PCR-analysis was carried out to assess the ion channel expression profile at mRNA level in hiPSC-CMs. PCR results showed that the expression of SCN5A (Na^+ channel, $\text{Na}_v1.5$), KCND3 (I_{to} , $\text{K}_{v4.3}$) and KCNJ2 ($\text{K}_{ir2.1}$, I_{K1}) was decreased in hiPSC-CMs with cancer cell medium (the AGS and SW480 groups) when compared with that in hiPSC-CMs treated with un-cultured cancer cell medium (the control group) (Figure 13). However, the level of SCN10A (Na^+ channel, $\text{Na}_v1.8$), KCNH2 (I_{Kr} , $\text{K}_{v11.1}$); KCNQ1 (I_{Ks} , $\text{K}_{v7.1}$) were increased. The expression

of CACNA1C (L-type Ca^{2+} channel), SLC8A1 (NCX, $\text{Na}^{+}\text{-Ca}^{2+}$ exchanger) showed no difference among AGS and SW480 and control groups.

Since the culture media for cancer cells and cardiomyocytes were different, the possible effects of different concentrations of un-cultured cancer cell medium on channel expression were also examined at the same time. It showed that the cancer cell medium without cancer cell secretion had no influence on the expression of ion channels in cardiomyocytes (Figure 14).

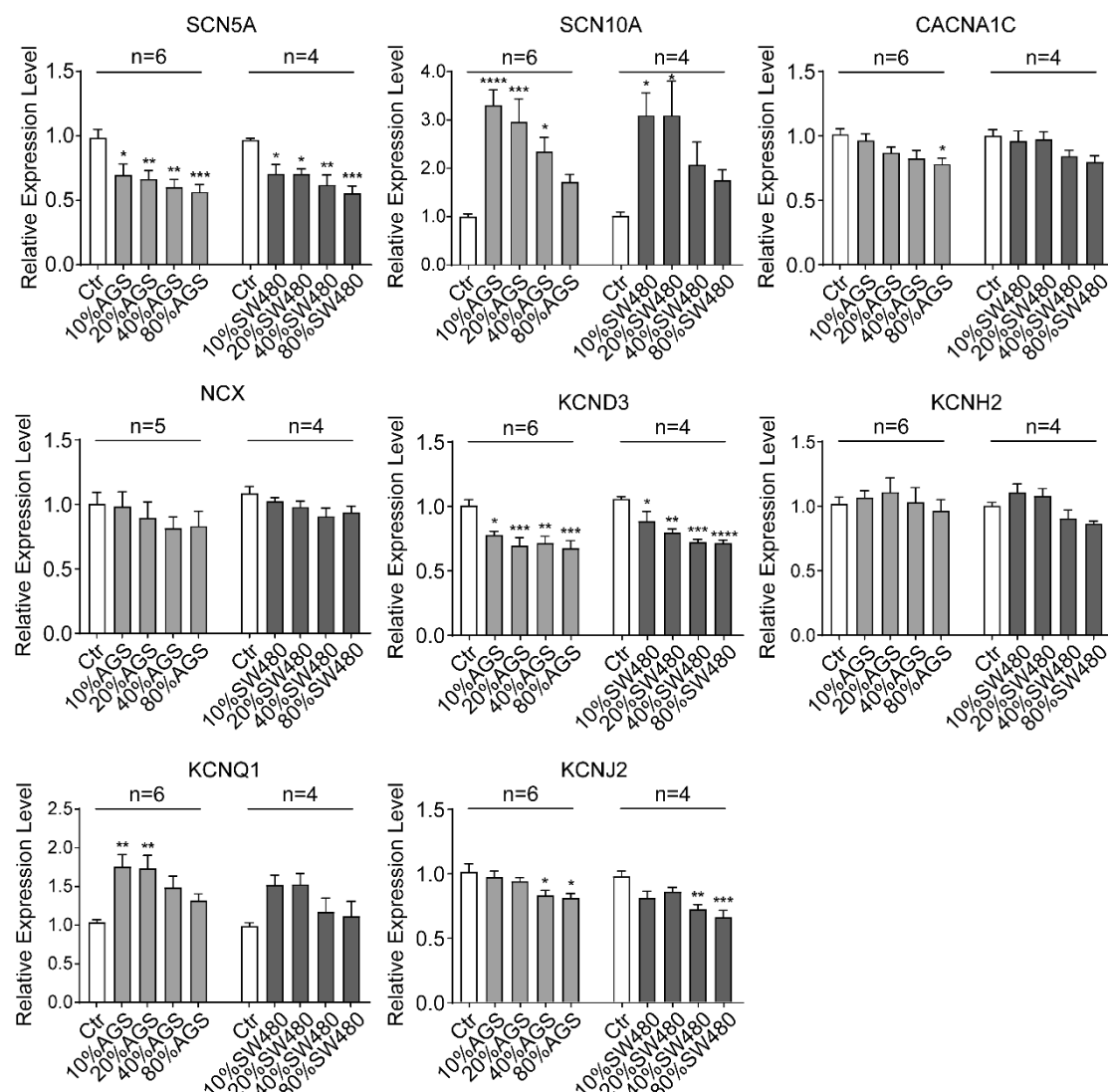


Figure 13. Ion channel expression profile at mRNA level in hiPSC-CMs cultured with different concentration of AGS and SW480 cancer cell media. Different concentration of cancer culture medium from flasks with cancer cells cultured for 8 days were added into flasks with hiPSC-CMs for 2 days. qPCR analysis was performed to evaluate expression

levels of different ion channels. “Ctr” represents data from hiPSC-CMs without medium for cancer cells. “AGS” represents data from hiPSC-CMs with addition of cultured medium of AGS cancer cells. “SW480” represents data from hiPSC-CMs with addition of cultured medium of SW480 cancer cells. Data are presented as mean ± SEM and analyzed by one-way ANOVA. The experimental (biological replicates) number of every experiment group is indicated as “n”. *P<0.05, **P<0.01, ***P<0.001, ****P<0.0001.

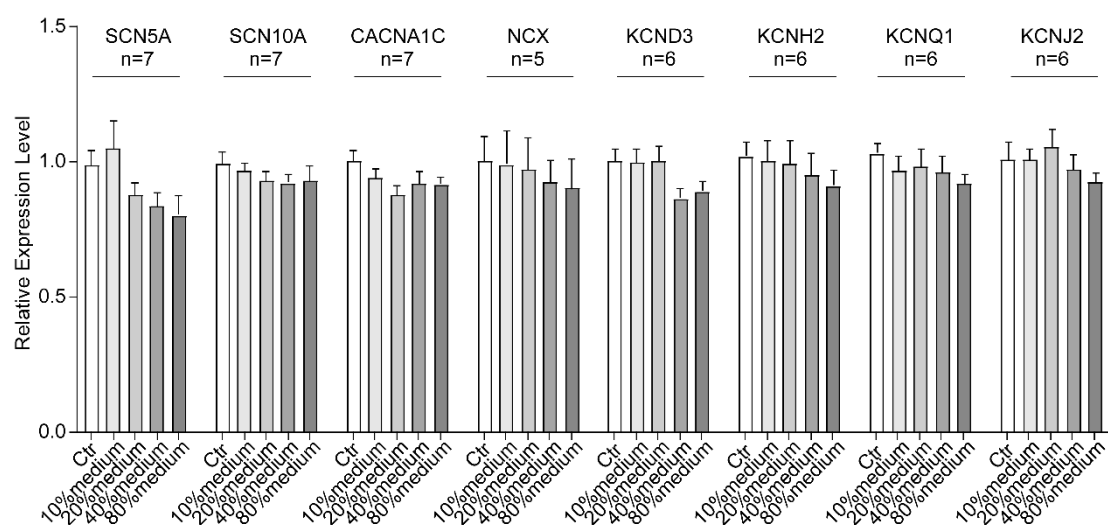


Figure 14. Ion channel expression profile at mRNA level in hiPSC-CMs cultured with different concentration of cancer culture medium without influence of cancer cells.

Different concentration of cancer culture medium from flasks without cancer cells were added into flasks with hiPSC-CMs for 2 days. qPCR analysis was performed to evaluate expression levels of ion channels. “Ctr” represents data from hiPSC-CMs without medium for cancer cells. “Medium” represents data from hiPSC-CMs with addition of uncultured medium for cancer cells. Data are presents as mean ± SEM and analyzed by one-way ANOVA. The experimental (biological replicates) number of every experiment group is indicated as “n”.

Then we checked the protein expression levels of channels. The western blotting analysis showed that SCN5A was decreased, whereas SCN10A was increased; CACNA1C and Na⁺/Ca²⁺ exchanger NCX were not changed (Figure 15); KCND3 and KCNQ1 were elevated, while HERG and KCNJ2 were

unchanged (Figure 16). All the results were in accordance with PCR assays and current measurements.

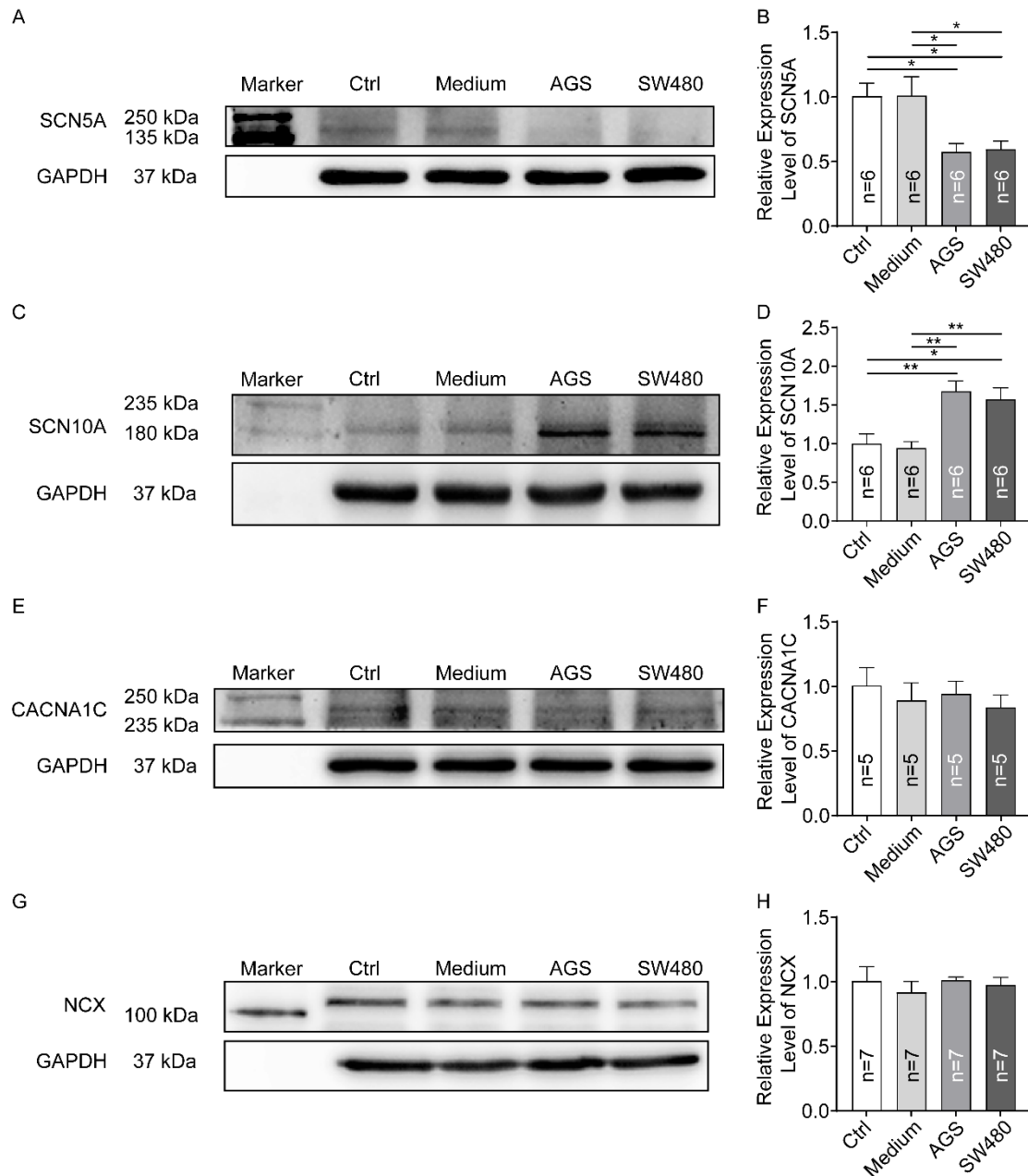


Figure 15. Protein expression levels of SCN5A, SCN10A, CACNA1C and NCX in hiPSC-CMs cultured with AGS and SW480 cancer cell media. (A) Protein bands detected with SCN5A antibody. (B) Statistical analyses of relative expression level of SCN5A. (C) Protein bands detected with SCN10A antibody. (D) Statistical analyses of relative expression level of SCN10A. (E) Protein bands detected with CACNA1C antibody. (F) Statistical analyses of relative expression level of CACNA1C. (G) Protein bands detected with NCX antibody. (H) Statistical analyses of relative expression level of NCX.

“Ctr” represents data from hiPSC-CMs without medium for cancer cells. “Medium” represents data from hiPSC-CMs with addition of un-cultured medium for cancer cells. “AGS” represents data from hiPSC-CMs with addition of cultured medium of AGS cancer cells. “SW480” represents data from hiPSC-CMs with addition of cultured medium of SW480 cancer cells. Data are presented as mean \pm SEM and analyzed by one-way ANOVA. The experimental number of every experiment group is marketed as “n”. * P <0.05, ** P <0.01.

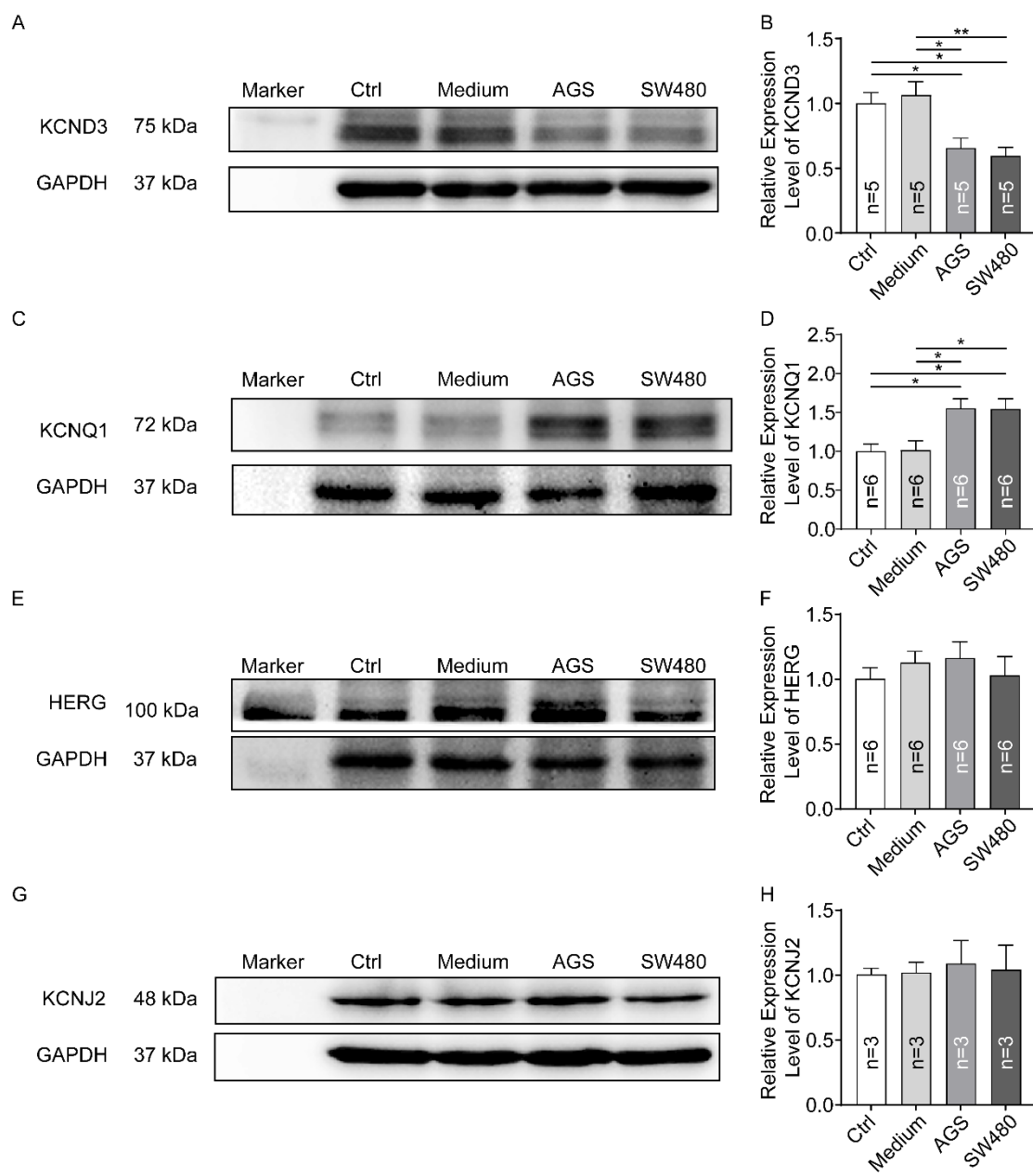


Figure 16. Protein expression levels of KCND3, KCNQ1, HERG and KCNJ2 in hiPSC-CMs cultured with AGS and SW480 cancer cell media. (A) Protein bands detected with KCND3 antibody. (B) Statistical analyses of relative expression level of KCND3. (C) Protein bands detected with KCNQ1 antibody. (D) Statistical analyses of relative expression level of KCNQ1. (E) Protein bands detected with HERG antibody. (F) Statistical analyses of relative expression level of HERG. (G) Protein bands detected with KCNJ2 antibody. (H) Statistical analyses of relative expression level of KCNJ2. “Ctr” represents data from hiPSC-CMs without medium for cancer cells. “Medium” represents data from hiPSC-CMs with addition of un-cultured medium for cancer cells. “AGS” represents data from hiPSC-CMs with addition of cultured medium of AGS cancer cells. “SW480” represents data from hiPSC-CMs with addition of cultured medium of SW480 cancer cells. Data are presented as mean \pm SEM and analyzed by one-way ANOVA. The experimental number of every experiment group is marketed as “n”. * P <0.05, ** P <0.01.

To further assess changes of channel proteins in sarcolemma membrane, the immunofluorescence technique was applied to assess the expression of ion channels on the membrane, focusing on the transient outward K^+ channel, the slowly activating delayed rectifier K^+ channel and the Na^+ channel. As shown in Figure 17, the expression levels of SCN5A and KCND3 in cell membrane were lower, but the KCNQ1 level was higher in cancer groups.

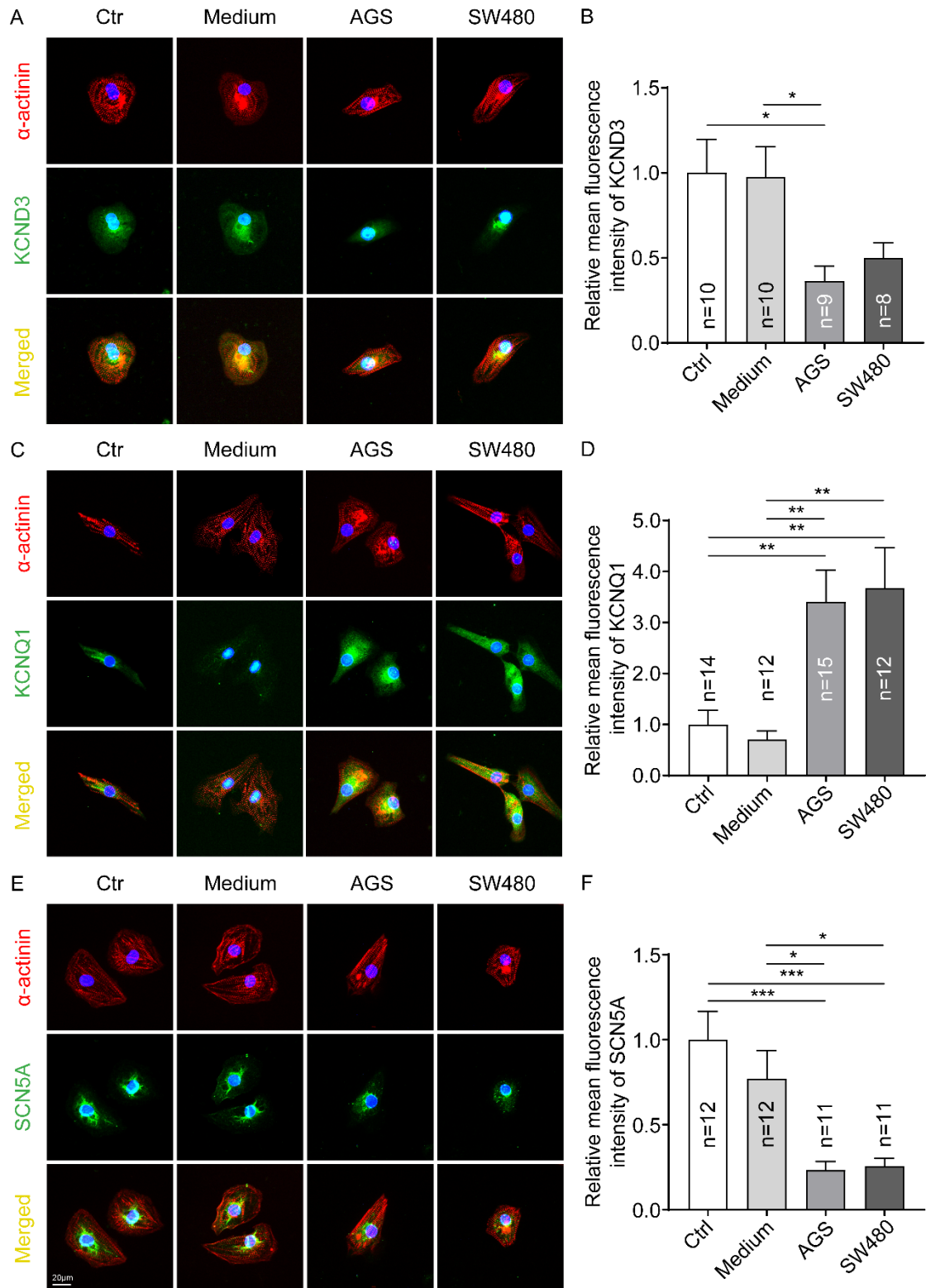


Figure 17. Immunofluorescence analysis of Na⁺ and K⁺ channels in human induced pluripotent stem cell–derived cardiomyocytes (hiPSC-CM). (A) Immunofluorescence detecting the expression of α -actinin (red) and KCND3 (green). (B) Statistical analyses of relative expression level of KCND3. (C) Immunofluorescence detecting the expression of

α -actinin (red) and KCNQ1 (green). (D) Statistical analyses of relative expression level of KCNQ1. (E) Immunofluorescence detecting the expression with α -actinin (red) and SCN5A (green). (F) Statistical analyses of relative expression level of SCN5A. “Ctr” represents data from hiPSC-CMs without medium for cancer cells. “Medium” represents data from hiPSC-CMs with addition of un-cultured medium for cancer cells. “AGS” represents data from hiPSC-CMs with addition of cultured medium of AGS cancer cells. “SW480” represents data from hiPSC-CMs with addition of cultured medium of SW480 cancer cells. Scale bars, 20 μ m. Data are presented as mean \pm SEM and analyzed by one-way ANOVA. The cell number of every experiment group is marketed as “n”. * P <0.05, ** P <0.01, *** P <0.001.

5.5 Cancer cell secretion enhanced the DNA methylation of genome and ion channel genes

To examine the potential epigenetic mechanism by which GI cancers cause ion channel dysfunctions and action potential prolongation, the levels of whole genome DNA methylation and DNA demethylation were both measured. The dot blotting results showed that the level of 5-methylcytosine (5-mC, indicating DNA methylation) but not 5-hydroxymethylcytosine (5-hmC, indicating DNA demethylation) was higher in AGS and SW480 groups compared with the control and medium groups (Figure 18). These data indicated that epigenetic modification of DNA methylation was enhanced in the cardiomyocytes treated with AGS and SW480 cancer cell media.

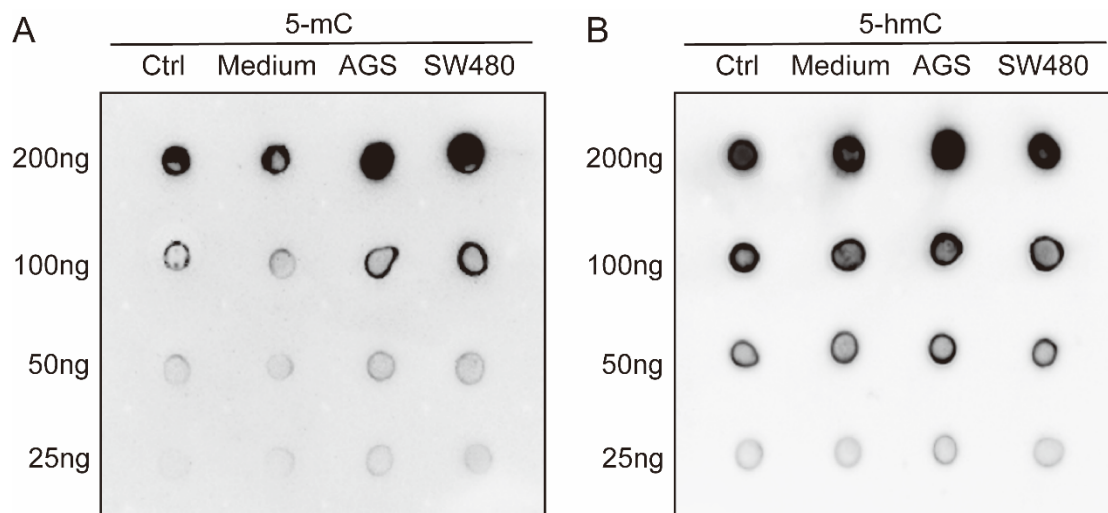


Figure 18. The level of whole genome DNA methylation in hiPSC-CMs cultured with AGS and SW480 cancer cell media. (A) 5-mC levels detected by dot blotting. (B) 5hmC levels detected by dot blotting. “Ctr” represents data from hiPSC-CMs without medium for cancer cells. “Medium” represents data from hiPSC-CMs with addition of un-cultured medium for cancer cells. “AGS” represents data from hiPSC-CMs with addition of cultured medium of AGS cancer cells. “SW480” represents data from hiPSC-CMs with addition of cultured medium of SW480 cancer cells.

To further investigate whether cancer secretion changes the DNA methylation in specific ion channel genes, we evaluated the methylation levels of CpG islands of promoters of I_{to} (KCND3), I_{Ks} (KCNQ1) and I_{Na} (SCN5A) channel genes (Figure 19). The methylation levels of CpG islands of KCND3 were higher in cancer secretion groups, while the methylation levels of KCNQ1 were lower than those in control and medium groups. No difference of methylation level of CpG islands in SCN5A gene was detected among all groups.

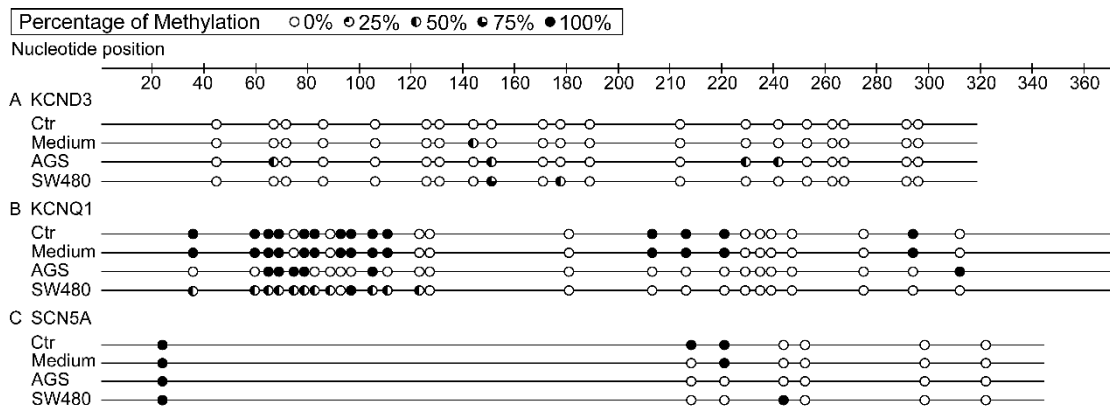


Figure 19. The methylation level of CpG islands of promoters. (A) The methylation level of CpG islands of promoters of KCND3. (B) The methylation level of CpG islands of promoters of KCNQ1. (C) The methylation level of CpG islands of promoters of SCN5A. “Ctr” represents data from hiPSC-CMs without medium for cancer cells. “Medium” represents data from hiPSC-CMs with addition of un-cultured medium for cancer cells. “AGS” represents data from hiPSC-CMs with addition of cultured medium of AGS cancer cells. “SW480” represents data from hiPSC-CMs with addition of cultured medium of SW480 cancer cells. The circles show different methylation sites. Different dark color in circles represents different percentage of methylation.

5.6 The expression of DNA methylation enzymes was elevated by cancer cell secretion

DNMTs are the main enzymes responsible for DNA methylation. We further checked the protein levels of DNMT1 (Figure 20 A, B), DNMT2 (Figure 20 C, D), DNMT3A (Figure 20 E, F) and DNMT3B (Figure 20 G, H). We found that DNMT3A and 3B levels were increased significantly in cancer cell secretion groups, in agreement with the elevated methylation in DNA. The TET enzyme family is responsible for DNA demethylation. Next, TET1 antibody was selected to detect the protein level of DNA demethylation enzymes. The level of TET1 enzyme was not changed by cancer cell secretion (Figure 20 I, J).

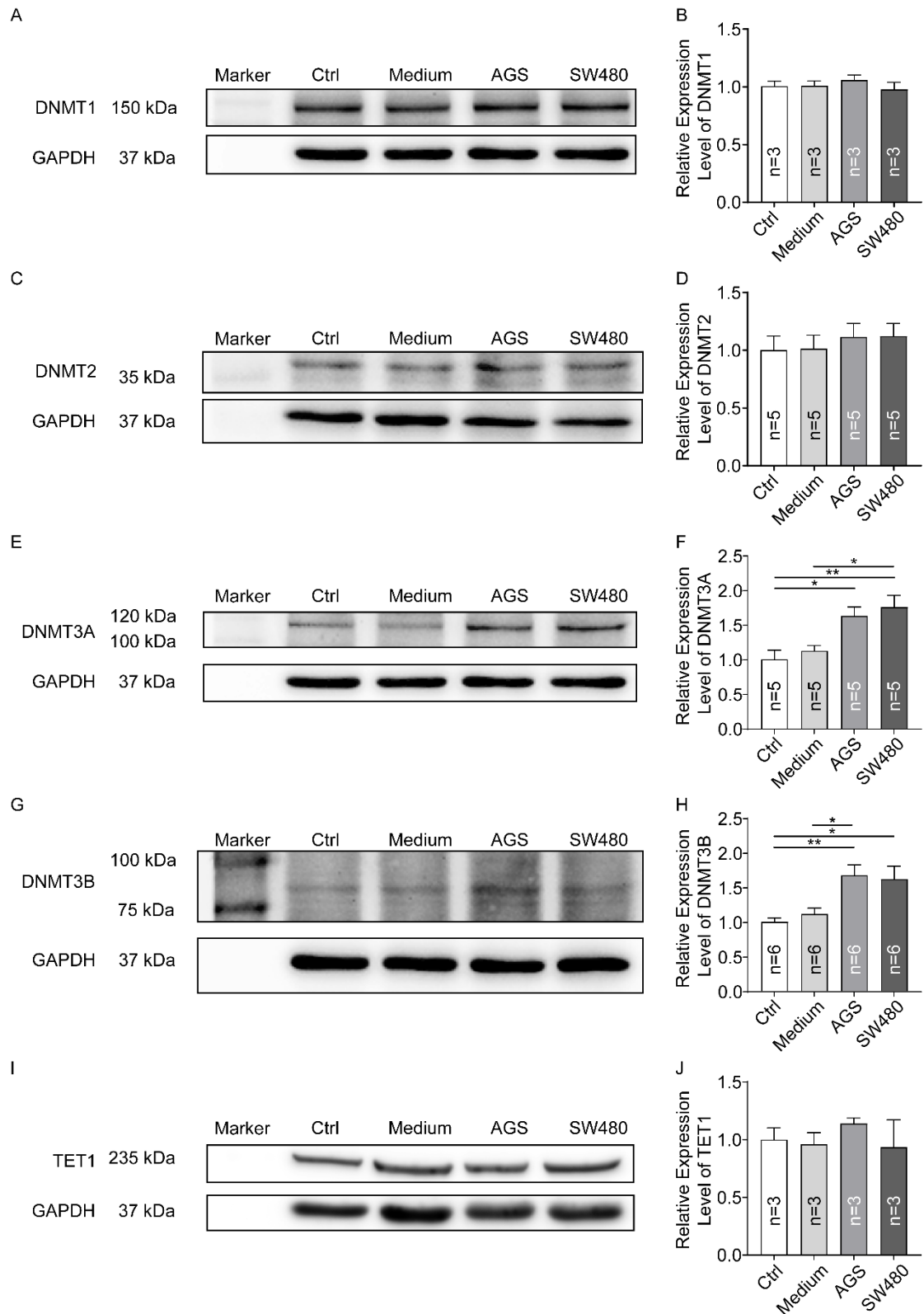


Figure 20. Protein expression levels of DNMTs and TET1 enzymes in hiPSC-CMs cultured with AGS and SW480 cancer cell media. (A) Protein bands detected with DNMT1 antibody. (B) Statistical analyses of relative expression level of DNMT1. (C) Protein

bands detected with DNMT2 antibody. (D) Statistical analyses of relative expression level of DNMT2. (E) Protein bands detected with DNMT3A antibody. (F) Statistical analyses of relative expression level of DNMT3A. (G) Protein bands detected with DNMT3B antibody. (H) Statistical analyses of relative expression level of DNMT3B. (I) Protein bands detected with TET1 antibody. (J) Statistical analyses of relative expression level of TET1. “Ctr” represents data from hiPSC-CMs without medium for cancer cells. “Medium” represents data from hiPSC-CMs with addition of un-cultured medium for cancer cells. “AGS” represents data from hiPSC-CMs with addition of cultured medium of AGS cancer cells. “SW480” represents data from hiPSC-CMs with addition of cultured medium of SW480 cancer cells. Data are presented as mean \pm SEM and analyzed by one-way ANOVA. The number of every experiment group is marketed as “n”. * P <0.05, ** P <0.01.

5.7 Overexpression of TET1 attenuated the enhancement of DNA methylation by cancer cell secretion

To prove that the observed changes of ion channel expression induced by cancer cell secretion are related to the enhanced DNA methylation, we intended to reduce the methylation by overexpression of TET1. For selecting a better concentration of plasmid DNA for transfection, different amounts of plasmid FH-TET1-pEF were tested, western blotting and dot blotting were adopted to detect the expression levels. The protein level of TET1 (Figure 21) was similar when 0.4 μ g and 1 μ g plasmid were applied, but the 5-hydroxymethylcytosine level (5-hmc) (Figure 22) was higher when the added plasmid DNA was 1 μ g. Therefore, 1 μ g was applied in following experiments.

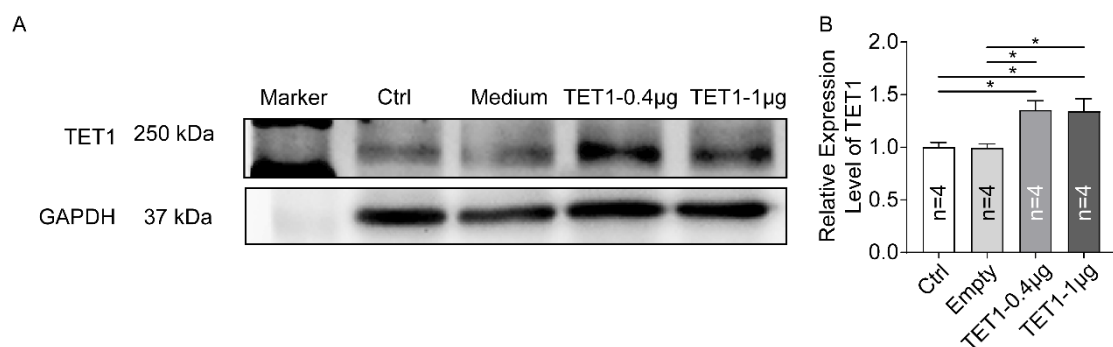


Figure 21. Protein expression levels of TET1 enzymes in hiPSC-CMs transfected with different amount of TET1 plasmid. (A) Protein bands detected with TET1 antibody. (B) Statistical analyses of relative expression level of TET1. “Ctr” represents data from hiPSC-CMs without transfection. “Empty” represents data from hiPSC-CMs transfected with empty plasmid. “TET1-0.4 μ g” represents data from hiPSC-CMs transfected with 0.4 μ g TET1 plasmid DNA. “TET1-1 μ g” represents data from hiPSC-CMs transfected with 1 μ g TET1 plasmid DNA. Data are presented as mean \pm SEM and analyzed by one-way ANOVA. The experimental number of every experiment group is marketed as “n”. * P <0.05.

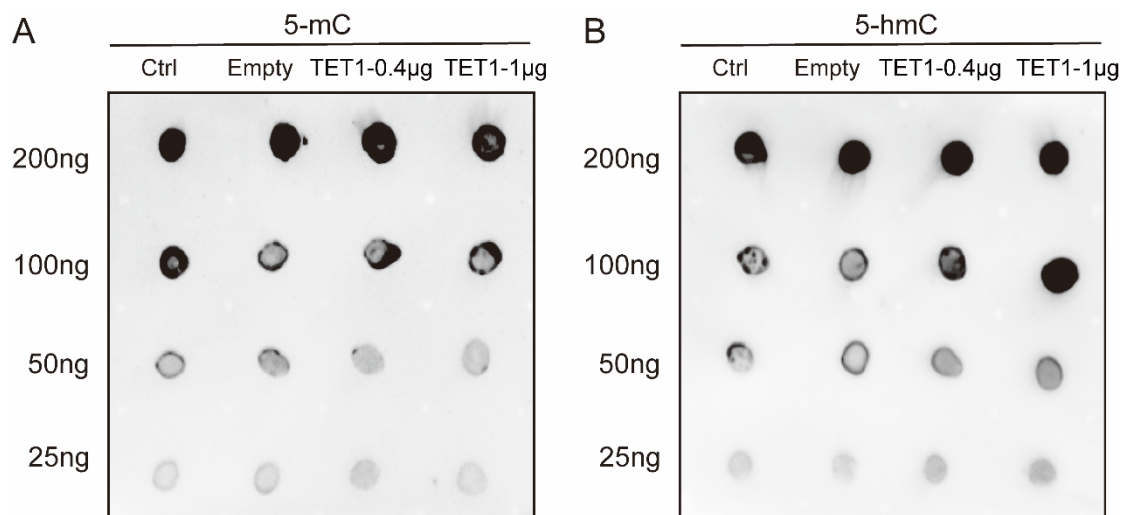


Figure 22. The level of whole genome DNA methylation after overexpression of TET1. (A) 5-mC levels detected by dot blotting. (B) 5-hmC levels detected by dot blotting. “Ctr” represents data from hiPSC-CMs without transfection. “Empty” represents data from hiPSC-CMs transfected with empty plasmid. “TET1-0.4 μ g” represents data from hiPSC-CMs transfected with 0.4 μ g TET1 plasmid DNA. “TET1-1 μ g” represents data from hiPSC-CMs transfected with 1 μ g TET1 plasmid DNA.

After transfection, the TET1 plasmid but not the empty plasmid increased the protein level of TET1 in hiPSC-CMs, independent of cancer secretions (Figure 23). Under this condition, the levels of 5-methylcytosine (5-mc) and the 5-hydroxymethylcytosine (5-hmc) were again measured by dot blotting. The results illustrated that the expression of 5-mc but not 5-hmc was decreased

after overexpression of TET1 in hiPSC-CMs treated with cancer secretions (figure 24).

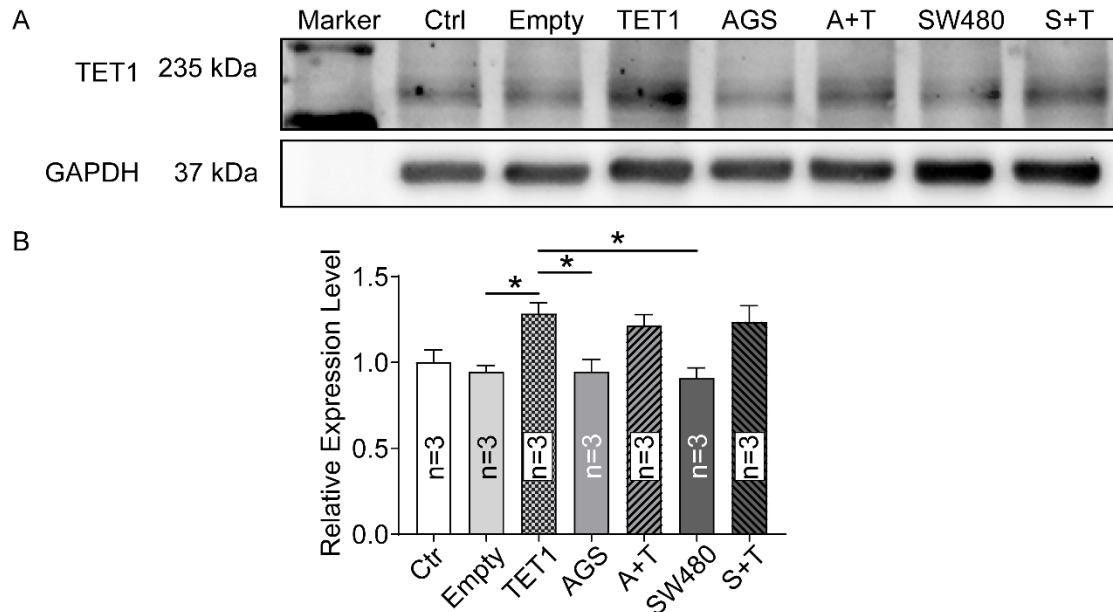


Figure 23. Protein expression levels of TET1 enzymes in hiPSC-CMs after overexpression of TET1. HiPSC-CMs were transfected with 1 μ g TET1 plasmid DNA or the empty plasmid. The protein level of TET1 was analyzed by western blotting. (A) Protein bands detected with TET1 antibody. (B) Statistical analyses of relative expression level of TET1. “Ctr” represents data from hiPSC-CMs without transfection. “Empty” represents data from hiPSC-CMs transfected with empty plasmid. “TET1” represents data from hiPSC-CMs transfected with 1 μ g TET1 plasmid DNA. “AGS” represents data from hiPSC-CMs with addition of cultured medium of AGS cancer cells without transfection. “A+T” represents data from hiPSC-CMs with addition of cultured medium of AGS cancer cells and transfected with 1 μ g TET1 plasmid DNA. “SW480” represents data from hiPSC-CMs with addition of cultured medium of SW480 cancer cells without transfection. “S+T” represents data from hiPSC-CMs with addition of cultured medium of SW480 cancer cells and transfected with 1 μ g TET1 plasmid DNA. Data are presented as mean \pm SEM and analyzed by one-way ANOVA. The number of every experiment group is marketed as “n”.

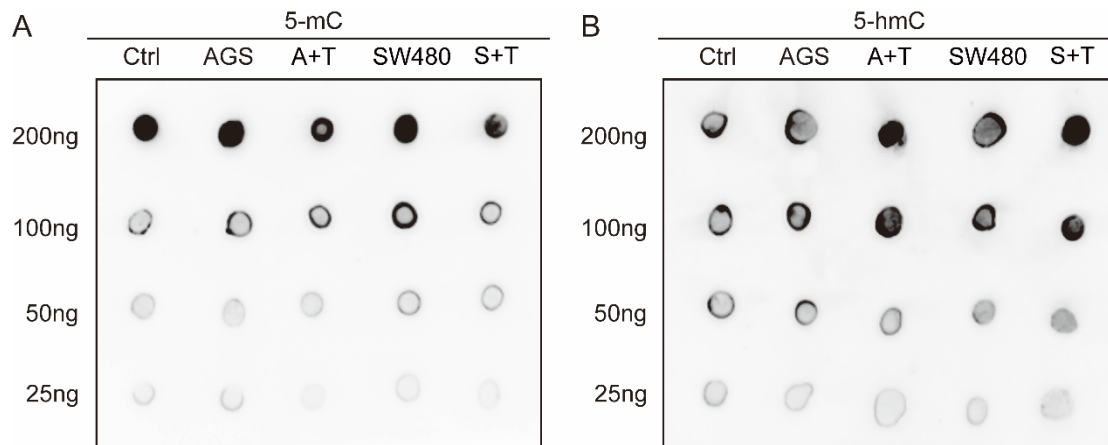


Figure 24. The level of whole genome DNA methylation in hiPSC-CMs treated with cancer cell secretion was attenuated after overexpression of TET1. HiPSC-CMs were transfected with 1 μ g TET1 plasmid DNA or the empty plasmid. The DNA methylation level of was analyzed by dot blotting. (A) 5-mC levels detected by dot blotting. (B) 5-hmC levels detected by dot blotting. “Ctrl” represents data from hiPSC-CMs without transfection. “AGS” represents data from hiPSC-CMs with addition of cultured medium of AGS cancer cells, but without transfection. “A+T” represents data from hiPSC-CMs with addition of cultured medium of AGS cancer cells and transfected with 1 μ g TET1DNA. “SW480” represents data from hiPSC-CMs with addition of cultured medium of SW480 cancer cells but without transfection. “S+T” represents data from hiPSC-CMs with addition of cultured medium of SW480 cancer cells and transfected with 1 μ g TET1 DNA.

5.8 Reduction of DNA methylation reversed the effects of cancer cell secretion on expression levels of ion channels

To assess whether the changes in DNA methylation level induced by cancer cell secretion are responsible for ion channel dysfunctions, the protein expression levels of KCND3, KCNQ1, SCN5A, SCN10A were evaluated in cells transfected with TET1 reducing the DNA methylation level. The western blotting analysis displayed that the transient outward current (KCND3) and the slowly activating delayed rectifier K⁺ channel (KCNQ1) were rescued after overexpression of TET1, while the Na⁺ channels (SCN5A and SCN10A) expression were not changed (figure 25).

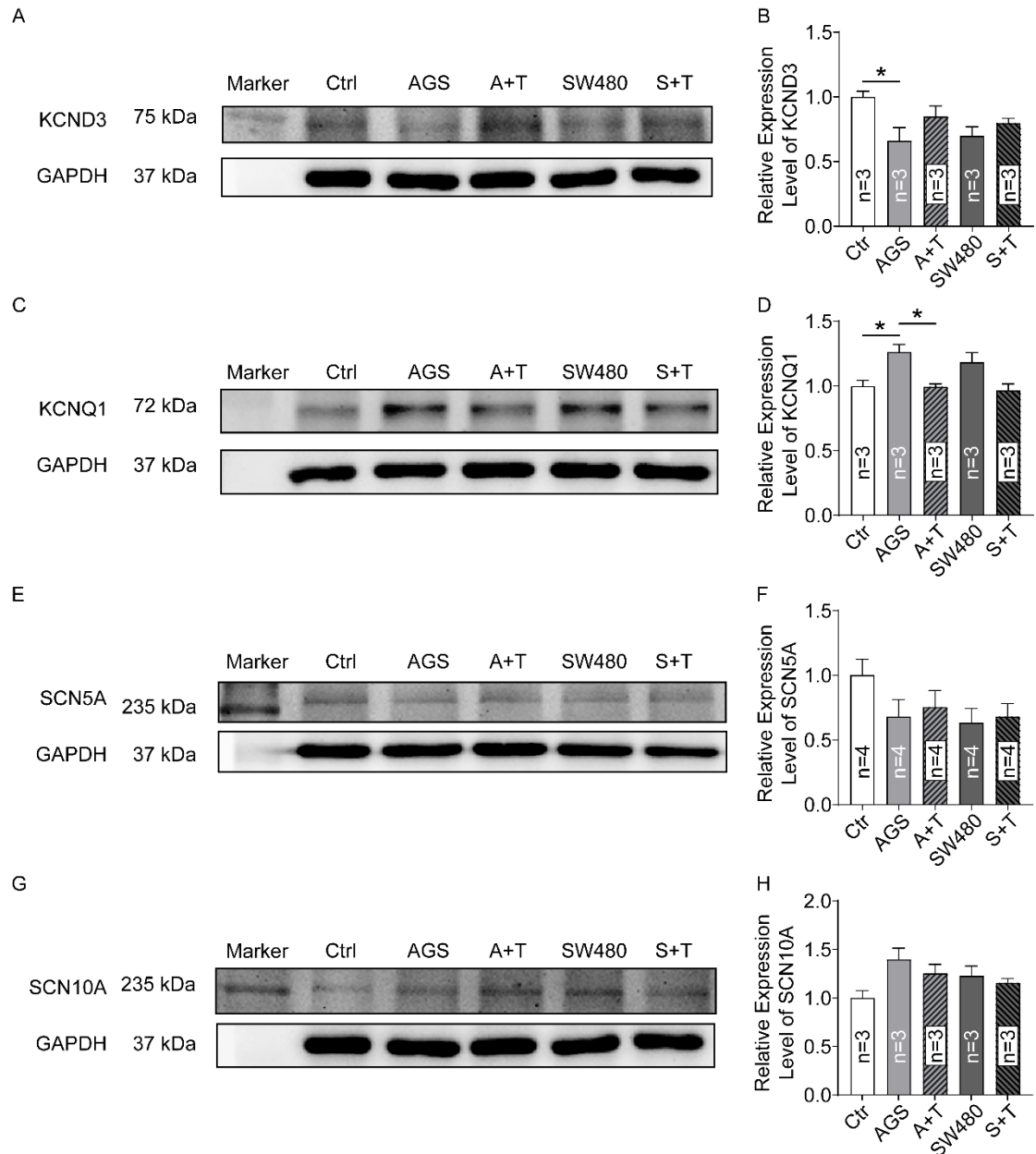


Figure 25. Protein expression levels of KCND3, KCNQ1, SCN5A, SCN10A in hiPSC-CMs after overexpression of TET1. HiPSC-CMs were transfected with 1 μ g TET1 plasmid DNA or the empty plasmid. The protein level of ion channels was analyzed by western blotting. (A) Protein bands detected with KCND3 antibody. (B) Statistical analyses of relative expression level of KCND3. (C) Protein bands detected with KCNQ1 antibody. (D) Statistical analyses of relative expression level of KCNQ1. (E) Protein bands detected with SCN5A antibody. (F) Statistical analyses of relative expression level of SCN5A. (G) Protein bands detected with SCN10A antibody. (H) Statistical analyses of relative expression level of SCN10A. Ctr⁺ represents data from hiPSC-CMs without transfection and cancer medium.

“AGS” represents data from hiPSC-CMs with addition of cultured medium of AGS cancer cells. “A+T” represents data from hiPSC-CMs with addition of cultured medium of AGS cancer cells and transfected with 1 μ g TET1 plasmid DNA. “SW480” represents data from hiPSC-CMs with addition of cultured medium of SW480 cancer cells. “S+T” represents data from hiPSC-CMs with addition of cultured medium of SW480 cancer cells and transfected with 1 μ g TET1 plasmid DNA. Data are presented as mean \pm SEM and analyzed by one-way ANOVA. The experimental number of every experiment group is marketed as “n”. *P<0.05.

5.9 Overexpression of TET1 changed ion channel currents

Finally, we examined the influences of DNA methylation level on ion channel functions. When TET1 was overexpressed (DNA methylation level was reduced) in hiPSC-CMs treated with cancer cell secretion, the transient outward current (I_{to}) currents were rescued to an extent similar to the control group (Figure 26). Similarly, the slowly activating delayed rectifier K⁺ current (I_{Ks}) was also corrected after overexpression of TET1 (Figure 27). However, the peak I_{Na} and late I_{Na} were not changed by the overexpression of TET1 (Figure 28).

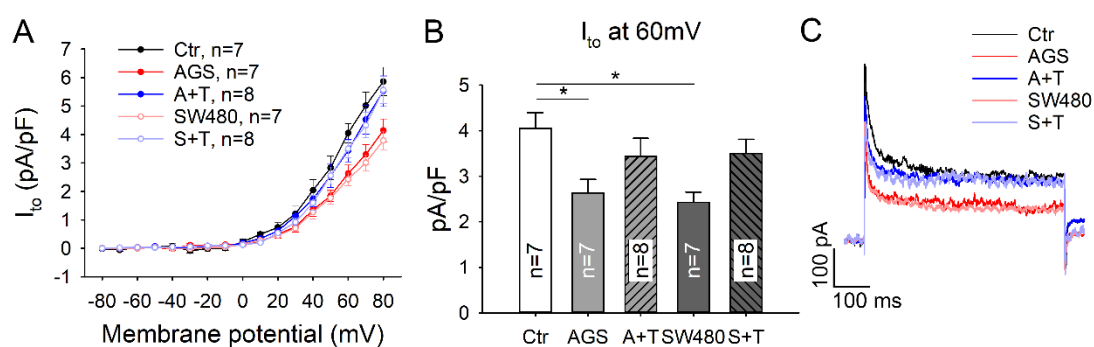


Figure 26. The transient outward current (I_{to}) of hiPSC-CMs after overexpression of TET1. HiPSC-CMs were transfected with 1 μ g TET1 plasmid DNA or the empty plasmid. The I_{to} channel currents were analyzed by patch clamp measurements. (A) I-V curves of I_{to} . (B) Mean values of peak I_{to} at 60mV. (C) Representative traces of I_{to} in Ctrl, AGS, AGS+TET1, SW480 and SW480+TET1 groups. “Ctrl” represents data from hiPSC-CMs without transfection and cancer medium. “AGS” represents data from hiPSC-CMs with

addition of cultured medium of AGS cancer cells. “A+T” represents data from hiPSC-CMs with addition of cultured medium of AGS cancer cells and transfected with 1 μ g TET1 plasmid DNA. “SW480” represents data from hiPSC-CMs with addition of cultured medium of SW480 cancer cells. “S+T” represents data from hiPSC-CMs with addition of cultured medium of SW480 cancer cells and transfected with 1 μ g TET1 plasmid DNA. Data are presented as mean \pm SEM and analyzed by one-way ANOVA. The cell number of every experiment group is marketed as “n”. *P<0.05.

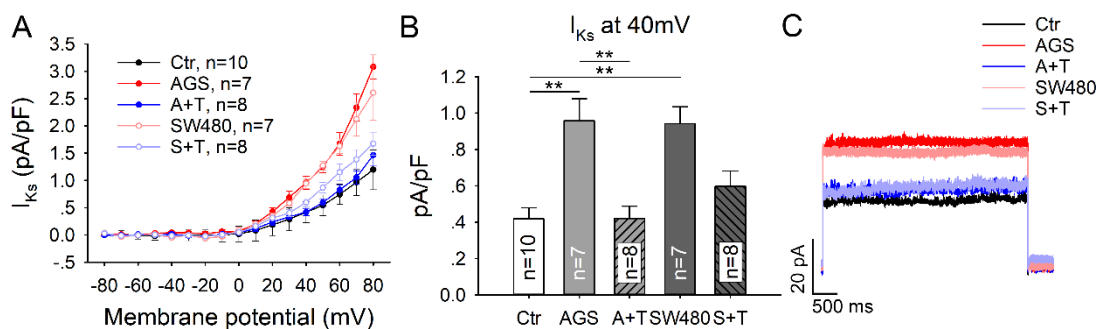


Figure 27. The slowly activating delayed rectifier K⁺ current (I_{Ks}) of hiPSC-CMs after overexpression of TET1. HiPSC-CMs were transfected with 1 μ g TET1 plasmid DNA or the empty plasmid. I_{Ks} was analyzed by patch clamp measurements. (A) I-V curves of I_{Ks} . (B) Mean values of peak I_{Ks} at 40mV. (C) Representative traces of I_{Ks} in Ctrl, AGS, AGS+TET, SW480 and SW480+TET groups. “Ctrl” represents data from hiPSC-CMs without transfection and cancer medium. “AGS” represents data from hiPSC-CMs with addition of cultured medium of AGS cancer cells. “A+T” represents data from hiPSC-CMs with addition of cultured medium of AGS cancer cells and transfected with 1 μ g TET1 plasmid DNA. “SW480” represents data from hiPSC-CMs with addition of cultured medium of SW480 cancer cells. “S+T” represents data from hiPSC-CMs with addition of cultured medium of SW480 cancer cells and transfected with 1 μ g TET1 plasmid DNA. Data are presented as mean \pm SEM and analyzed by one-way ANOVA. The cell number of every experiment group is marketed as “n”. *P<0.05.

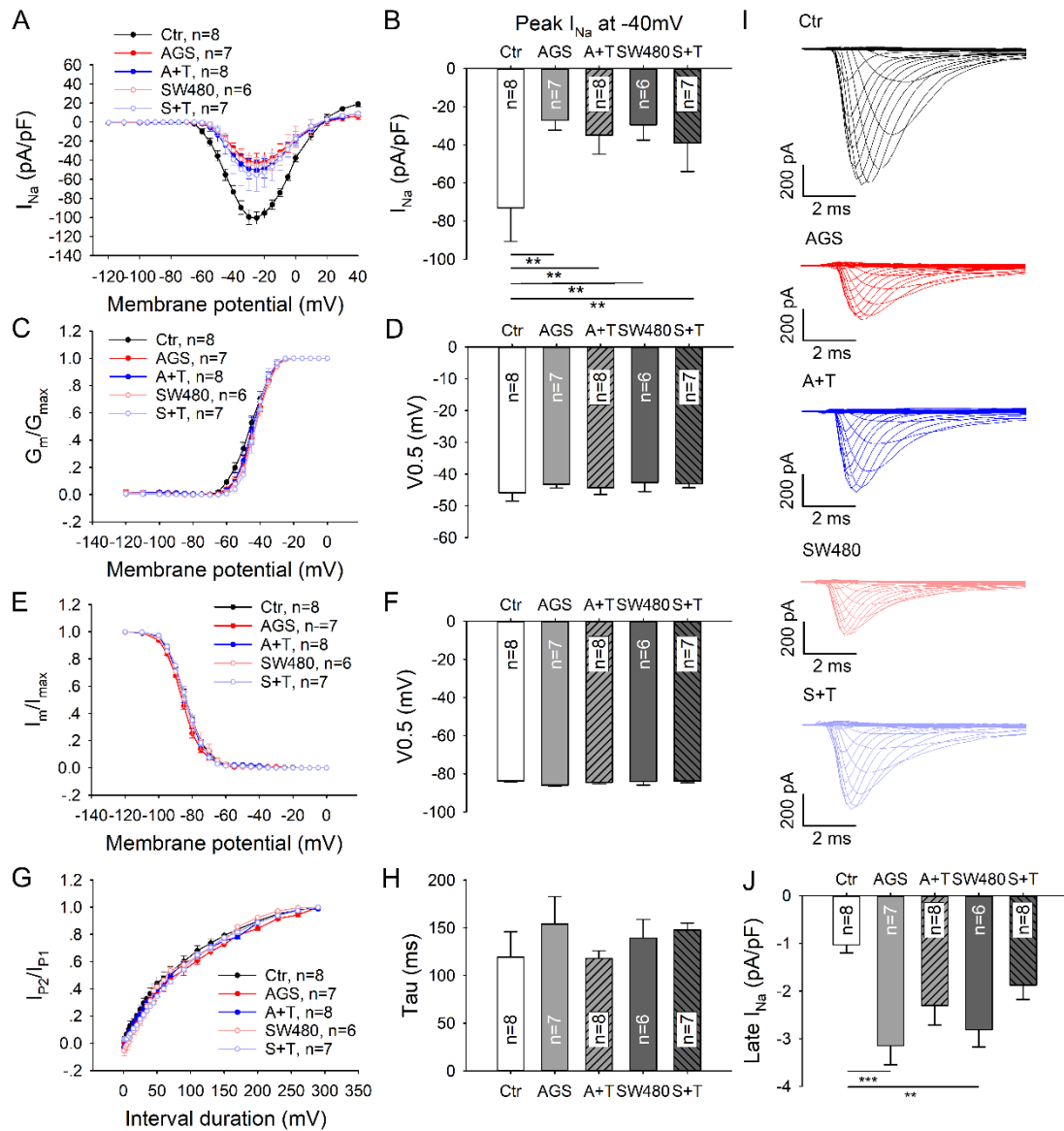


Figure 28. The sodium current of hiPSC-CMs after overexpression of TET1. HiPSC-CMs were transfected with 1 μ g TET1 plasmid DNA or the empty plasmid. The peak Na⁺ currents were analyzed by patch clamp measurements. (A) I-V curves of peak I_{Na} . (B) Mean values of peak I_{Na} at -40mV. (C) Activation curves of peak I_{Na} . (D) Mean values of $V_{0.5}$ (the voltage at half maximum) of activation. (E) Inactivation curves of peak I_{Na} . (F) Mean values of $V_{0.5}$ of inactivation. (G) Time course curves of recovery from inactivation of peak I_{Na} . (H) Mean values of time constants (tau) of recovery from inactivation. (H) Mean values of late I_{Na} at -40mV. (I) Representative traces of I_{Na} in Ctrl, AGS, AGS+TET1, SW480 and SW480+TET1 groups. “Ctrl” represents data from hiPSC-CMs without transfection and cancer medium. “AGS” represents data from hiPSC-CMs with addition of

cultured medium of AGS cancer cells. "A+T" represents data from hiPSC-CMs with addition of cultured medium of AGS cancer cells and transfected with 1 μ g TET1 plasmid DNA. "SW480" represents data from hiPSC-CMs with addition of cultured medium of SW480 cancer cells. "S+T" represents data from hiPSC-CMs with addition of cultured medium of SW480 cancer cells and transfected with 1 μ g TET1 plasmid DNA. Data are presented as mean \pm SEM and analyzed by one-way ANOVA. The cell number of every experiment group is marketed as "n". *P<0.05.

6. DISCUSSION

In the present study, we investigated for the first time the effects of cancer cell secretion on ion channel functions and the underlying mechanism using hiPSC-CMs. The novel findings of the study are: 1) the cancer cell secretion suppressed V_{max} and APA of APs; 2) the cancer cell secretion prolonged APD; 3) the cancer cell secretion down-regulated Na ($Na_v1.5$) channels and up-regulated I_{to} and I_{Ks} channels; 4) the cancer cell secretion up-regulated DNMT3A and DNMT3B, enhancing DNA methylation and leading to ion channel dysfunctions.

To examine possible effects of cancer cell secretion (secreted components in culture medium) on APs and ion channel currents that contributed to the AP, we first measured the cell growth curve of the two cancer cell lines (AGS and SW40 cell lines) to determine the time point of media harvest. A typical growth curve for cultured cells is defined as 4 phases: (1) Lag phase. During this period, the cells adapt to the culture conditions. The length of this phase differs from different cell lines and is dependent on the seeding density. (2) Logarithmic growth phase. In this phase, cells proliferate actively, and the cell density arises exponentially. The cells are most viable at this period. (3) Plateau phase. The cell proliferation slows down at this phase and cells become confluent. (4) Decline phase. Cells die and viable cells decrease at this stage. After generation of the growth curve of AGS and SW480 cell lines by cell counting and MTT assay, we found that these two cancer cell lines reached plateau phase at day 8-9. So, we determined to harvest the cancer cell media at day 8 in the end of the logarithmic growth phase with stable cancer cell number and secretion.

Since the cancer cells and hiPSC-CMs were cultured in different media, we examined the potential effects of cancer cell media on the hiPSC-CM viability. The results showed that different concentrations (10%, 20%, 40%, 80%) of the cancer cell media had no obvious effect on cell viability of hiPSC-CMs,

indicating that the cancer cell secretion has no relevant effects on the growth of hiPSC-CMs. Then, we further examined the effects of different concentrations (10%, 20%, 40%, 80%) of cancer cell media without cancer cells (the medium control group) on the ion channel gene expression. The results showed that different concentrations of cancer cell media without cancer cells had no significant effects on the ion channel gene expression. This excluded the concern that the medium (for cancer cell culture) may influence hiPSC-CMs and also supported the interpretation of the results from hiPSC-CMs treated with cancer cell medium from the flask culturing cancer cells as effects of cancer cell secretion. In hiPSC-CMs treated by medium cultured with AGS and SW40 for 8 days, expressions of different ion channel genes including SCN5A, SCN10A, KCNQ1, KCND3 and KCNJ2 were changed, with an upregulation of SCN10A and KCNQ1, a downregulation of SCN5A and KCND3, which are indicative of influences of cancer cell secretion on ion channel regulation in cardiomyocytes. In high concentrations (40% and 80%) of cancer cell media, all these gene expressions seemed to be suppressed, indicating that high concentrations (40% and 80%) of cancer cell media might have detrimental effects on hiPSC-CMs. 20% of the cancer cell media from AGS and SW480 cell lines could cause significant changes of ion channel gene expression and had less effects on cell viability. Thus, we choose the concentration of 20% of the AGS and SW480 cancer cell media for the further experiments.

Next, we measured APs paced at different frequencies and analyzed its characteristics in the hiPSC-CMs after 2-day treatment of AGS and SW480 cancer cell media. We found that the V_{max} of slope and the APA were decreased significantly, whereas the APD₁₀ was prolonged at all frequencies (0.5Hz to 3Hz). We further analyzed the ion channel currents that contributed to the AP and found that the peak I_{Na} was decreased significantly in the AGS and SW480 group cardiomyocytes when compared with control and medium group. However, the gating kinetics of Na channels including the activation,

inactivation, and recovery from inactivation were not changed, suggesting that the reduction of peak I_{Na} resulted from reduced the channel proteins rather than gating changes. This is consistent with the PCR and western blot data showing reductions of both mRNA and protein level. The peak I_{Na} predominantly contributes to the phase 1 of AP. The decrease of V_{max} and APA in cardiomyocytes treated with AGS and SW480 secretion can be explained by the decreased peak I_{Na} . The late I_{Na} was increased significantly by the AGS and SW480 secretion, which may prolong APD. The I_{to} current showed a significant decrease but the I_{Ks} current exhibited a significant increase in the AGS and SW480 group when compared with control and medium group. We also measured the I_{Ca-L} and I_{K1} but failed to detect any significant differences among these groups. The decrease in I_{to} may be the cause for the prolongation of APD10 since this phase is mainly determined by I_{to} . The increase in I_{Ks} should shorten APD, especially APD90. However, in the current study, APD50 and APD90 were not changed by AGS and SW40 cell secretion. This probably resulted from the counteraction of increased late I_{Na} and I_{Ks} , both of which can influence APD, but in opposite directions. I_{Ca-L} and I_{K1} as well as I_{Kr} are also important for determining APD. Given that these three currents were not significantly changed by cancer cell secretion, their contributions to the changes of APs are negligible.

Since the mRNA and protein levels of the ion channels were changed after AGS and SW480 cancer cell media treatment, we further checked the whole genome DNA methylation level by dot blotting and the results showed that the 5-mC but not 5-hmc level was increased significantly in AGS and SW480 group cardiomyocytes, indicating that the whole genome DNA methylation was increased after AGS and SW480 media treatment. The DNMTs are responsible for the establishment and maintenance of DNA methylation. We further checked the protein levels of DNMTs. The western blot showed that DNMT3a and DNMT3b were increased in the AGS and SW480 group cardiomyocytes

when compared with control and medium group, whereas DNMT1 and DNMT2 seemed unchanged, indicating the hypermethylation in hiPSC-CMs treated with cancer cell secretion resulted from the upregulation of DNMT3a and DNMT3b. DNMTs dysregulation has been reported in gastrointestinal cancers.⁶⁶ A measurement of DNMTs levels in different cancer cell lines and tissues showed that the mRNA levels of DNMT3a and 3b were significantly higher in colorectal cancers, and the protein level of DNMT1 was increased in colon tumors from patients compared to non-malignant mucosa from the same patients.⁶⁷ In cancer cells, overexpressed DNMTs may be linked to the hypermethylation of tumor-suppressor genes.⁶⁶ Many factors such as hypoxia or hypoglycemia may contribute to the dysregulation of DNMTs in colorectal cancer cells.⁶⁸ In our study, the cancer cell secretion changed the DNMT3a and 3b levels in the hiPSC-CMs and further affected the DNA methylation in CpG islands of the promoters of different ion channel genes. This suggested that DNMTs were important intracellular regulators for gene expression not only in cancer cells but also in cardiomyocytes.

Bisulfite sequencing is a method to determine the pattern of methylation in specific DNA sequence by using bisulfite treatment of DNA before normal sequence. Bisulfite treatment converts the unmethylated cytosine residues in DNA sequence into uracil and leaves the 5-mC unaffected. After PCR reaction with the specific primers targeting the CpG island in promoter regions of specific genes, the DNA sequences are amplified, and the uracil residues are replaced by thymine according to the rules of base pairing. Then the DNA sequences are purified and inserted into cloning vector and amplified in *Escherichia coli*. Comparison of the sequences after Sanger sequence shows the methylation patterns in the CpG island in the promoter regions. In our study, after Sanger sequence, we found that the DNA methylation was increased in the CpG island in promoter region of KCND3 gene in the AGS and SW480 group cardiomyocytes when compared with control and medium group, which was

consistent with the decreased expression of KCND3 and increased levels of DNMT3a and 3b in cardiomyocytes in AGS and SW480 media treated groups since DNA methylation usually mediates an inhibitory effect on gene expression. The DNA methylation in the CpG island in promoter region of KCNQ1 gene was decreased after AGS and SW480 media treatment, which is in line with the increased expression of KCNQ1. But the reason why the methylation of CpGs was decreased in KCNQ1 promoter region when the DNMT3a and 3b were upregulated needed to be clarified by further investigations. The DNA methylation level in the CpG island in promoter region of SCN5A gene was similar among these groups, indicating DNA methylation might not be the main regulation of SCN5A expression after cancer cell secretion treatment.

Since iPSC-CMs are highly differentiated cells, commonly used DNA methylation inhibitor 5-Azacytidine or 5-aza-2'-deoxycytidine cannot be used to inhibit the DNA methylation after treatment of cancer cell media. We overexpressed the TET1 in hiPSC-CMs to confirm the epigenetic mechanism of ion channel changes. As described above, TET1 is one of the enzymes that are responsible for the demethylation of DNA by catalyzing the conversion of the modified DNA base 5-mC to 5-hmC. We evaluated the TET1 protein level in TET1-overexpressed hiPSC-CMs. The protein level of TET1 was increased in the TET1-overexpressed cardiomyocytes indicating the overexpression model was established successfully. Then, we treated these TET1-overexpressed cardiomyocytes with AGS and SW480 cancer cell media and detected the whole genome DNA methylation by dot blotting. We found that the 5-mC level was reduced but the 5-hmC level was elevated after TET1 overexpression, indicative of a reduction of methylation and an enhancement of demethylation. Under this condition, we further analyzed the protein levels of KCND3, KCNQ1, SCN5A and SCN10A. Protein levels of KCND3 and KCNQ1 were also rescued after TET1 overexpression. However, TET1 overexpression failed to rescue the protein levels of SCN5A and SCN10A, implying that there

might be other mechanisms for the regulation of SCN5A and SCN10A gene expression.

To date, it is still unclear how the expression of DNMTs is changed in cancer cells. Firstly, mutation of the DNMTs genes may happen in some cancer cells. Emerging evidences suggested that epigenetic disruptions caused by DNMTs mutations were associated with tumorigenesis. DNMT1 mutations in coding exons were found in colorectal cancers and might potentially cause a genome-wide alteration of DNA methylation.⁶⁹ Mutations in DNMT3a were highly recurrent in patients with acute myeloid leukemia and were associated with poor event-free and overall survival.⁷⁰ DNMT3A was also frequently mutated in acute and chronic myelomonocytic leukemia, and was associated with aggressiveness and drug resistance as well.^{71, 72} Secondly, infection of viruses can also change the expression of DNMTs. For gastrointestinal cancer, it is well-accepted that infection of *Helicobacter pylori* or Epstein-Barr virus (EBV) is one of the carcinogenic risk factors. *H. pylori* is reported to change DNMTs levels and total enzymatic activity in gastric cancer cells through activation of nuclear factor- κ B (NF- κ B) pathway via interleukin-1 β (IL-1 β) stimulation which led to the up-regulation of inducible nitric oxide synthase (iNOS) and increase of NO production.⁷³ Another study also reported that IL-1 β might play a crucial role in *H. pylori*-induced gastric inflammation and DNA methylation.⁷⁴ On the other hand, EBV can induce DNA methylation by up-regulation of DNMT1 or DNMT3b through EBV latent membrane protein 2A (LMP2A).^{75, 76} EBV is also reported to induce DNMT1 expression through LMP1 via c-Jun N-terminal kinase (JNK)/activator protein-1 (AP1) signaling.⁷⁷ Taking together, either genetic or environmental factors may regulate DNMTs. In our present study, the cancer cell secretion from two different GI cancer cell lines changed the level of DNMTs and further caused changes of expressions of the ion channel genes in hiPSC-CMs. This connected cancer with cardiac disorders. But the underlying mechanism by which the level of DNMTs was regulated was still

unclear. It is believed that cancer cells could interact with the host cells and regulate their gene expression.¹⁷ Cancer cells might contribute to the DNMTs dysregulation in cardiomyocytes by secretion of cytokines or extracellular vesicles. Firstly, GI cancer cells can secrete cytokines such as IL-1 β , IL-6, IL-8, IL-11, etc.^{78, 79} These cytokines especially IL-1 β can activate NF- κ B pathway and lead to changes in expression levels of DNMTs as described above.^{73, 74} Secondly, the extracellular vesicles including exosomes containing mRNAs, microRNAs (miRNAs) and proteins may regulate the expression of DNMTs in cancer cell media treated cardiomyocytes.

Our present study is the first study to elucidate the effect of cancer cell secretion on cardiac ion channels expression and function and its potential mechanism in the hiPSC-CMs (Figure 29). We found that cancer cell secretion from two GI cancer cell lines could change the expression of DNMTs, which could further lead to the expression changes of the ion channel genes and cause electrophysiological abnormalities. However, further investigations are needed to clarify which components of cancer secretion changed the levels of DNMTs. Many components such as inflammatory factors and exosomes can be possible candidate factors that contribute to the regulation of DNMTs in cardiomyocytes and are to be investigated in future. Our findings in this study identified one potential mechanism for cancer-induced cardiophysiological changes. But there might be other mechanisms. On one hand, secretions from cancer cells including cytokines and exosomes that containing RNAs and proteins might also directly affect the expression or trafficking or gating of ion channels. On the other hand, the cancer cell could indirectly affect the ion channel gene expressions through other proteins or genes, which are needed to be investigated in future.

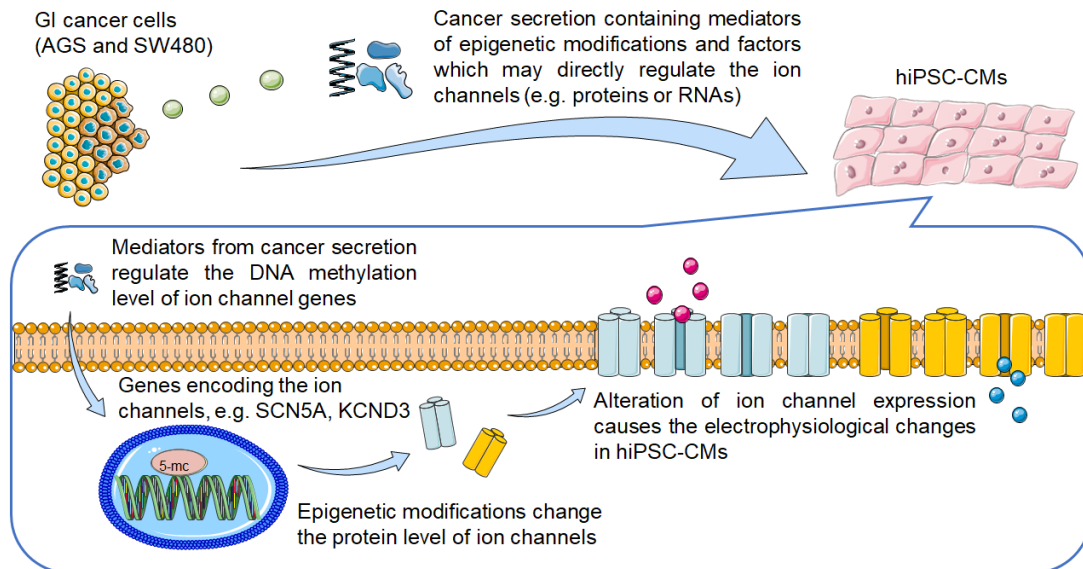


Figure 29. Potential mechanisms of effects of cancer cell secretion on hiPSC-CMs.

Cancer secretion from GI cancer cells, AGS and SW480, containing mediators of epigenetic modification regulates the level of DNMTs and changes DNA methylation in promoter regions of ion channel genes. Epigenetic changes further cause changes in expression of these ion channels, which results in alteration of electrophysiology in hiPSC-CMs.

7. SUMMARY

In summary, our results showed that GI cancer cell secretion could change the electrophysiology of human cardiac cells, especially the peak Na⁺ channel, the transient outward K⁺ channel, the slowly activating delayed rectifier K⁺ channel.

The mechanism behind the electrophysiological changes caused by GI cancer cell secretion was at least partially through epigenetic modifications of ion channel genes by upregulating DNMTs.

The ion channel dysfunctions caused by cancer cell secretion may contribute to arrhythmogenesis in cancer patients. Investigating the regulatory signaling, especially the epigenetic modifications of ion channels, may provide opportunities for discovering new therapeutic targets for treating arrhythmias in cancer patients.

8. REFERENCES

1. Pudil, R: The Future Role of Cardio-oncologists. *Cardiac failure review*, 3: 140-142, 2017.
2. Mortality, GBD, Causes of Death, C: Global, regional, and national life expectancy, all-cause mortality, and cause-specific mortality for 249 causes of death, 1980-2015: a systematic analysis for the Global Burden of Disease Study 2015. *Lancet*, 388: 1459-1544, 2016.
3. Organization—WHO, WH: Available online: http://www.who.int/cardiovascular_diseases/en/ (accessed on 20 November 2018).
4. Bray, F, Ferlay, J, Soerjomataram, I, Siegel, RL, Torre, LA, Jemal, A: Global cancer statistics 2018: GLOBOCAN estimates of incidence and mortality worldwide for 36 cancers in 185 countries. *CA: a cancer journal for clinicians*, 68: 394-424, 2018.
5. Miller, KD, Siegel, RL, Lin, CC, Mariotto, AB, Kramer, JL, Rowland, JH, Stein, KD, Alteri, R, Jemal, A: Cancer treatment and survivorship statistics, 2016. *CA: a cancer journal for clinicians*, 66: 271-289, 2016.
6. Vejpongsa, P, Yeh, ET: Prevention of anthracycline-induced cardiotoxicity: challenges and opportunities. *Journal of the American College of Cardiology*, 64: 938-945, 2014.
7. Daher, IN, Daigle, TR, Bhatia, N, Durand, JB: The prevention of cardiovascular disease in cancer survivors. *Tex Heart Inst J*, 39: 190-198, 2012.
8. Fradley, MG, Brown, AC, Shields, B, Viganego, F, Damrongwatanasuk, R, Patel, AA, Hartlage, G, Roper, N, Jaunese, J, Roy, L, Ismail-Khan, R: Developing a Comprehensive Cardio-Oncology Program at a Cancer Institute: The Moffitt Cancer Center Experience. *Oncology reviews*, 11: 340, 2017.

9. Liu, D, Ma, Z, Yang, J, Zhao, M, Ao, H, Zheng, X, Wen, Q, Yang, Y, You, J, Qiao, S, Yuan, J: Prevalence and prognosis significance of cardiovascular disease in cancer patients: a population-based study. *Aging (Albany NY)*, 11: 7948-7960, 2019.
10. Onaitis, M, D'Amico, T, Zhao, Y, O'Brien, S, Harpole, D: Risk factors for atrial fibrillation after lung cancer surgery: analysis of the Society of Thoracic Surgeons general thoracic surgery database. *Ann Thorac Surg*, 90: 368-374, 2010.
11. Chu, G, Versteeg, HH, Verschoor, AJ, Trines, SA, Hemels, MEW, Ay, C, Huisman, MV, Klok, FA: Atrial fibrillation and cancer - An unexplored field in cardiovascular oncology. *Blood Rev*, 35: 59-67, 2019.
12. Timp, JF, Braekkan, SK, Versteeg, HH, Cannegieter, SC: Epidemiology of cancer-associated venous thrombosis. *Blood*, 122: 1712-1723, 2013.
13. Prandoni, P, Lensing, AW, Piccioli, A, Bernardi, E, Simioni, P, Girolami, B, Marchiori, A, Sabbion, P, Prins, MH, Noventa, F, Girolami, A: Recurrent venous thromboembolism and bleeding complications during anticoagulant treatment in patients with cancer and venous thrombosis. *Blood*, 100: 3484-3488, 2002.
14. Coppola, C, Rienzo, A, Piscopo, G, Barbieri, A, Arra, C, Maurea, N: Management of QT prolongation induced by anti-cancer drugs: Target therapy and old agents. Different algorithms for different drugs. *Cancer treatment reviews*, 63: 135-143, 2017.
15. Korzeniowska, K, Jankowski, J, Cieslewicz, A, Jablecka, A: Is it possible to prevent chemotherapy-induced heart failure with cardiovascular drugs - the review of the current clinical evidence. *Ther Clin Risk Manag*, 15: 1095-1110, 2019.
16. Sun, Y, Wang, R, Qiao, M, Xu, Y, Guan, W, Wang, L: Cancer associated fibroblasts tailored tumor microenvironment of therapy resistance in gastrointestinal cancers. *Journal of cellular physiology*, 2018.

17. McAllister, SS, Weinberg, RA: Tumor-host interactions: a far-reaching relationship. *J Clin Oncol*, 28: 4022-4028, 2010.
18. Menna, P, Salvatorelli, E, Minotti, G: Cardiotoxicity of antitumor drugs. *Chem Res Toxicol*, 21: 978-989, 2008.
19. Cardinale, D, Bacchiani, G, Beggiano, M, Colombo, A, Cipolla, CM: Strategies to prevent and treat cardiovascular risk in cancer patients. *Semin Oncol*, 40: 186-198, 2013.
20. Chang, HM, Okwuosa, TM, Scarabelli, T, Moudgil, R, Yeh, ETH: Cardiovascular Complications of Cancer Therapy: Best Practices in Diagnosis, Prevention, and Management: Part 2. *Journal of the American College of Cardiology*, 70: 2552-2565, 2017.
21. Bettermann, H, Kroz, M, Girke, M, Heckmann, C: Heart rate dynamics and cardiorespiratory coordination in diabetic and breast cancer patients. *Clin Physiol*, 21: 411-420, 2001.
22. Nevruz, O, Yokusoglu, M, Uzun, M, Demirkol, S, Avcu, F, Baysan, O, Koz, C, Cetin, T, Sag, C, Ural, AU, Isik, E: Cardiac autonomic functions are altered in patients with acute leukemia, assessed by heart rate variability. *Tohoku J Exp Med*, 211: 121-126, 2007.
23. Hu, YF, Liu, CJ, Chang, PM, Tsao, HM, Lin, YJ, Chang, SL, Lo, LW, Tuan, TC, Li, CH, Chao, TF, Chung, FP, Liao, JN, Chen, TJ, Chen, SA: Incident thromboembolism and heart failure associated with new-onset atrial fibrillation in cancer patients. *Int J Cardiol*, 165: 355-357, 2013.
24. Venneri, L, Calicchio, F, Manivarmane, R, Pareek, N, Bakshi, J, Rosen, S, Senior, R, Lyon, A, Khattar, R: Subclinical myocardial dysfunction in cancer patients: is there a direct effect of tumour growth? *Eur Heart J Cardiovasc Imaging Abstracts Supplement*, 16 (Supplement 2): ii127, 2015.
25. Muhlfeld, C, Das, SK, Heinzl, FR, Schmidt, A, Post, H, Schauer, S, Papadakis, T, Kummer, W, Hoefler, G: Cancer induces cardiomyocyte

- remodeling and hypoinnervation in the left ventricle of the mouse heart. *PloS one*, 6: e20424, 2011.
26. Hu, S, Lou, J, Zhang, Y, Chen, P: Low heart rate variability relates to the progression of gastric cancer. *World J Surg Oncol*, 16: 49, 2018.
 27. Guzzetti, S, Costantino, G, Vernocchi, A, Sada, S, Fundaro, C: First diagnosis of colorectal or breast cancer and prevalence of atrial fibrillation. *Intern Emerg Med*, 3: 227-231, 2008.
 28. Reyes, HD, Devor, EJ, Warriar, A, Newtonson, AM, Mattson, J, Wagner, V, Duncan, GN, Leslie, KK, Gonzalez-Bosquet, J: Differential DNA methylation in high-grade serous ovarian cancer (HGSOC) is associated with tumor behavior. *Scientific reports*, 9: 17996, 2019.
 29. Jaenisch, R, Bird, A: Epigenetic regulation of gene expression: how the genome integrates intrinsic and environmental signals. *Nat Genet*, 33 Suppl: 245-254, 2003.
 30. Moore, LD, Le, T, Fan, G: DNA methylation and its basic function. *Neuropsychopharmacology*, 38: 23-38, 2013.
 31. Gu, T, Lin, X, Cullen, SM, Luo, M, Jeong, M, Estecio, M, Shen, J, Hardikar, S, Sun, D, Su, J, Rux, D, Guzman, A, Lee, M, Qi, LS, Chen, JJ, Kyba, M, Huang, Y, Chen, T, Li, W, Goodell, MA: DNMT3A and TET1 cooperate to regulate promoter epigenetic landscapes in mouse embryonic stem cells. *Genome Biol*, 19: 88, 2018.
 32. Ehrlich, M, Lacey, M: DNA methylation and differentiation: silencing, upregulation and modulation of gene expression. *Epigenomics*, 5: 553-568, 2013.
 33. Jones, PA: Functions of DNA methylation: islands, start sites, gene bodies and beyond. *Nat Rev Genet*, 13: 484-492, 2012.
 34. Jeltsch, A, Ehrenhofer-Murray, A, Jurkowski, TP, Lyko, F, Reuter, G, Ankri, S, Nellen, W, Schaefer, M, Helm, M: Mechanism and biological role of Dnmt2 in Nucleic Acid Methylation. *RNA Biol*, 14: 1108-1123, 2017.

35. Suetake, I, Shinozaki, F, Miyagawa, J, Takeshima, H, Tajima, S: DNMT3L stimulates the DNA methylation activity of Dnmt3a and Dnmt3b through a direct interaction. *J Biol Chem*, 279: 27816-27823, 2004.
36. Jin, B, Robertson, KD: DNA methyltransferases, DNA damage repair, and cancer. *Adv Exp Med Biol*, 754: 3-29, 2013.
37. He, YF, Li, BZ, Li, Z, Liu, P, Wang, Y, Tang, Q, Ding, J, Jia, Y, Chen, Z, Li, L, Sun, Y, Li, X, Dai, Q, Song, CX, Zhang, K, He, C, Xu, GL: Tet-mediated formation of 5-carboxylcytosine and its excision by TDG in mammalian DNA. *Science*, 333: 1303-1307, 2011.
38. Greco, CM, Kunderfranco, P, Rubino, M, Larcher, V, Carullo, P, Anselmo, A, Kurz, K, Carell, T, Angius, A, Latronico, MV, Papait, R, Condorelli, G: DNA hydroxymethylation controls cardiomyocyte gene expression in development and hypertrophy. *Nat Commun*, 7: 12418, 2016.
39. Whayne, TF: Epigenetics in the development, modification, and prevention of cardiovascular disease. *Mol Biol Rep*, 42: 765-776, 2015.
40. Huang, YS, Zhi, YF, Wang, SR: Hypermethylation of estrogen receptor-alpha gene in atheromatosis patients and its correlation with homocysteine. *Pathophysiology*, 16: 259-265, 2009.
41. Stenzig, J, Hirt, MN, Loser, A, Bartholdt, LM, Hensel, JT, Werner, TR, Riemenschneider, M, Indenbirken, D, Guenther, T, Muller, C, Hubner, N, Stoll, M, Eschenhagen, T: DNA methylation in an engineered heart tissue model of cardiac hypertrophy: common signatures and effects of DNA methylation inhibitors. *Basic Res Cardiol*, 111: 9, 2016.
42. Zhao, G, Zhou, J, Gao, J, Liu, Y, Gu, S, Zhang, X, Su, P: Genome-wide DNA methylation analysis in permanent atrial fibrillation. *Mol Med Rep*, 16: 5505-5514, 2017.
43. Smolarek, I, Wyszko, E, Barciszewska, AM, Nowak, S, Gawronska, I, Jablecka, A, Barciszewska, MZ: Global DNA methylation changes in

- blood of patients with essential hypertension. *Med Sci Monit*, 16: CR149-155, 2010.
44. Baccarelli, A, Wright, R, Bollati, V, Litonjua, A, Zanobetti, A, Tarantini, L, Sparrow, D, Vokonas, P, Schwartz, J: Ischemic heart disease and stroke in relation to blood DNA methylation. *Epidemiology*, 21: 819-828, 2010.
45. Castro, R, Rivera, I, Struys, EA, Jansen, EE, Ravasco, P, Camilo, ME, Blom, HJ, Jakobs, C, Tavares de Almeida, I: Increased homocysteine and S-adenosylhomocysteine concentrations and DNA hypomethylation in vascular disease. *Clin Chem*, 49: 1292-1296, 2003.
46. Kulis, M, Esteller, M: DNA methylation and cancer. *Adv Genet*, 70: 27-56, 2010.
47. Saridaki, Z, Tzardi, M, Sfakianaki, M, Papadaki, C, Voutsina, A, Kalykaki, A, Messaritakis, I, Mpananis, K, Mavroudis, D, Stathopoulos, E, Georgoulas, V, Souglakos, J: BRAFV600E mutation analysis in patients with metastatic colorectal cancer (mCRC) in daily clinical practice: correlations with clinical characteristics, and its impact on patients' outcome. *PloS one*, 8: e84604, 2013.
48. Weisenberger, DJ, Siegmund, KD, Campan, M, Young, J, Long, TI, Faasse, MA, Kang, GH, Widschwendter, M, Weener, D, Buchanan, D, Koh, H, Simms, L, Barker, M, Leggett, B, Levine, J, Kim, M, French, AJ, Thibodeau, SN, Jass, J, Haile, R, Laird, PW: CpG island methylator phenotype underlies sporadic microsatellite instability and is tightly associated with BRAF mutation in colorectal cancer. *Nat Genet*, 38: 787-793, 2006.
49. Sato, N, Matsubayashi, H, Fukushima, N, Goggins, M: The chemokine receptor CXCR4 is regulated by DNA methylation in pancreatic cancer. *Cancer Biol Ther*, 4: 70-76, 2005.
50. Han, L, Witmer, PD, Casey, E, Valle, D, Sukumar, S: DNA methylation regulates MicroRNA expression. *Cancer Biol Ther*, 6: 1284-1288, 2007.

51. Shih, HT: Anatomy of the action potential in the heart. *Tex Heart Inst J*, 21: 30-41, 1994.
52. Cubeddu, LX: Drug-induced Inhibition and Trafficking Disruption of ion Channels: Pathogenesis of QT Abnormalities and Drug-induced Fatal Arrhythmias. *Curr Cardiol Rev*, 12: 141-154, 2016.
53. Santana, LF, Cheng, EP, Lederer, WJ: How does the shape of the cardiac action potential control calcium signaling and contraction in the heart? *J Mol Cell Cardiol*, 49: 901-903, 2010.
54. Grunnet, M: Repolarization of the cardiac action potential. Does an increase in repolarization capacity constitute a new anti-arrhythmic principle? *Acta Physiol (Oxf)*, 198 Suppl 676: 1-48, 2010.
55. Kubo, Y, Adelman, JP, Clapham, DE, Jan, LY, Karschin, A, Kurachi, Y, Lazdunski, M, Nichols, CG, Seino, S, Vandenberg, CA: International Union of Pharmacology. LIV. Nomenclature and molecular relationships of inwardly rectifying potassium channels. *Pharmacol Rev*, 57: 509-526, 2005.
56. Plociennikowska, A, Hromada-Judycka, A, Dembinska, J, Roszczenko, P, Ciesielska, A, Kwiatkowska, K: Contribution of CD14 and TLR4 to changes of the PI(4,5)P2 level in LPS-stimulated cells. *Journal of leukocyte biology*, 100: 1363-1373, 2016.
57. Lu, Y, Liu, J, Liu, Y, Qin, Y, Luo, Q, Wang, Q, Duan, H: TLR4 plays a crucial role in MSC-induced inhibition of NK cell function. *Biochemical and biophysical research communications*, 464: 541-547, 2015.
58. Takahashi, K, Yamanaka, S: Induction of pluripotent stem cells from mouse embryonic and adult fibroblast cultures by defined factors. *Cell*, 126: 663-676, 2006.
59. Takahashi, K, Tanabe, K, Ohnuki, M, Narita, M, Ichisaka, T, Tomoda, K, Yamanaka, S: Induction of pluripotent stem cells from adult human fibroblasts by defined factors. *Cell*, 131: 861-872, 2007.

60. Yu, J, Vodyanik, MA, Smuga-Otto, K, Antosiewicz-Bourget, J, Frane, JL, Tian, S, Nie, J, Jonsdottir, GA, Ruotti, V, Stewart, R, Slukvin, II, Thomson, JA: Induced pluripotent stem cell lines derived from human somatic cells. *Science*, 318: 1917-1920, 2007.
61. Zhang, J, Wilson, GF, Soerens, AG, Koonce, CH, Yu, J, Palecek, SP, Thomson, JA, Kamp, TJ: Functional cardiomyocytes derived from human induced pluripotent stem cells. *Circulation research*, 104: e30-41, 2009.
62. Germanguz, I, Sedan, O, Zeevi-Levin, N, Shtrichman, R, Barak, E, Ziskind, A, Eliyahu, S, Meiry, G, Amit, M, Itskovitz-Eldor, J, Binah, O: Molecular characterization and functional properties of cardiomyocytes derived from human inducible pluripotent stem cells. *Journal of cellular and molecular medicine*, 15: 38-51, 2011.
63. Ma, J, Guo, L, Fiene, SJ, Anson, BD, Thomson, JA, Kamp, TJ, Kolaja, KL, Swanson, BJ, January, CT: High purity human-induced pluripotent stem cell-derived cardiomyocytes: electrophysiological properties of action potentials and ionic currents. *American journal of physiology Heart and circulatory physiology*, 301: H2006-2017, 2011.
64. Tahiliani, M, Koh, KP, Shen, Y, Pastor, WA, Bandukwala, H, Brudno, Y, Agarwal, S, Iyer, LM, Liu, DR, Aravind, L, Rao, A: Conversion of 5-methylcytosine to 5-hydroxymethylcytosine in mammalian DNA by MLL partner TET1. *Science*, 324: 930-935, 2009.
65. Dejosez, M, Levine, SS, Frampton, GM, Whyte, WA, Stratton, SA, Barton, MC, Gunaratne, PH, Young, RA, Zwaka, TP: Ronin/Hcf-1 binds to a hyperconserved enhancer element and regulates genes involved in the growth of embryonic stem cells. *Genes Dev*, 24: 1479-1484, 2010.
66. Fattahi, S, Golpour, M, Amjadi-Moheb, F, Sharifi-Pasandi, M, Khodadadi, P, Pilehchian-Langroudi, M, Ashrafi, GH, Akhavan-Niaki, H: DNA

- methyltransferases and gastric cancer: insight into targeted therapy. *Epigenomics*, 10: 1477-1497, 2018.
67. Honeywell, RJ, Sarkisjan, D, Kristensen, MH, de Klerk, DJ, Peters, GJ: DNA methyltransferases expression in normal tissues and various human cancer cell lines, xenografts and tumors. *Nucleosides Nucleotides Nucleic Acids*, 37: 696-708, 2018.
68. Skowronski, K, Dubey, S, Rodenhiser, D, Coomber, B: Ischemia dysregulates DNA methyltransferases and p16INK4a methylation in human colorectal cancer cells. *Epigenetics*, 5: 547-556, 2010.
69. Kanai, Y, Ushijima, S, Nakanishi, Y, Sakamoto, M, Hirohashi, S: Mutation of the DNA methyltransferase (DNMT) 1 gene in human colorectal cancers. *Cancer Lett*, 192: 75-82, 2003.
70. Ley, TJ, Ding, L, Walter, MJ, McLellan, MD, Lamprecht, T, Larson, DE, Kandoth, C, Payton, JE, Baty, J, Welch, J, Harris, CC, Lichti, CF, Townsend, RR, Fulton, RS, Dooling, DJ, Koboldt, DC, Schmidt, H, Zhang, Q, Osborne, JR, Lin, L, O'Laughlin, M, McMichael, JF, Delehaunty, KD, McGrath, SD, Fulton, LA, Magrini, VJ, Vickery, TL, Hundal, J, Cook, LL, Conyers, JJ, Swift, GW, Reed, JP, Alldredge, PA, Wylie, T, Walker, J, Kalicki, J, Watson, MA, Heath, S, Shannon, WD, Varghese, N, Nagarajan, R, Westervelt, P, Tomasson, MH, Link, DC, Graubert, TA, DiPersio, JF, Mardis, ER, Wilson, RK: DNMT3A mutations in acute myeloid leukemia. *The New England journal of medicine*, 363: 2424-2433, 2010.
71. Xu, J, Wang, YY, Dai, YJ, Zhang, W, Zhang, WN, Xiong, SM, Gu, ZH, Wang, KK, Zeng, R, Chen, Z, Chen, SJ: DNMT3A Arg882 mutation drives chronic myelomonocytic leukemia through disturbing gene expression/DNA methylation in hematopoietic cells. *Proc Natl Acad Sci U S A*, 111: 2620-2625, 2014.

72. Yan, XJ, Xu, J, Gu, ZH, Pan, CM, Lu, G, Shen, Y, Shi, JY, Zhu, YM, Tang, L, Zhang, XW, Liang, WX, Mi, JQ, Song, HD, Li, KQ, Chen, Z, Chen, SJ: Exome sequencing identifies somatic mutations of DNA methyltransferase gene DNMT3A in acute monocytic leukemia. *Nat Genet*, 43: 309-315, 2011.
73. Huang, FY, Chan, AO, Rashid, A, Wong, DK, Cho, CH, Yuen, MF: Helicobacter pylori induces promoter methylation of E-cadherin via interleukin-1beta activation of nitric oxide production in gastric cancer cells. *Cancer*, 118: 4969-4980, 2012.
74. Huang, FY, Chan, AO, Lo, RC, Rashid, A, Wong, DK, Cho, CH, Lai, CL, Yuen, MF: Characterization of interleukin-1beta in Helicobacter pylori-induced gastric inflammation and DNA methylation in interleukin-1 receptor type 1 knockout (IL-1R1(-/-)) mice. *Eur J Cancer*, 49: 2760-2770, 2013.
75. Hino, R, Uozaki, H, Murakami, N, Ushiku, T, Shinozaki, A, Ishikawa, S, Morikawa, T, Nakaya, T, Sakatani, T, Takada, K, Fukayama, M: Activation of DNA methyltransferase 1 by EBV latent membrane protein 2A leads to promoter hypermethylation of PTEN gene in gastric carcinoma. *Cancer Res*, 69: 2766-2774, 2009.
76. Zhao, J, Liang, Q, Cheung, KF, Kang, W, Lung, RW, Tong, JH, To, KF, Sung, JJ, Yu, J: Genome-wide identification of Epstein-Barr virus-driven promoter methylation profiles of human genes in gastric cancer cells. *Cancer*, 119: 304-312, 2013.
77. Tsai, CL, Li, HP, Lu, YJ, Hsueh, C, Liang, Y, Chen, CL, Tsao, SW, Tse, KP, Yu, JS, Chang, YS: Activation of DNA methyltransferase 1 by EBV LMP1 involves c-Jun NH(2)-terminal kinase signaling. *Cancer Res*, 66: 11668-11676, 2006.

78. Voronov, E, Apte, RN: IL-1 in Colon Inflammation, Colon Carcinogenesis and Invasiveness of Colon Cancer. *Cancer Microenviron*, 8: 187-200, 2015.
79. West, NR, McCuaig, S, Franchini, F, Powrie, F: Emerging cytokine networks in colorectal cancer. *Nat Rev Immunol*, 15: 615-629, 2015.

9. CURRICULUM VITAE

PERSONALIEN INFORMATION

Family name, first name:	Zhong, Rujia
Birthday:	14.05.1990
Place of birth:	Liaoning, China
Father:	Zhong, Sheng
Mather:	Li, Suwen
Spouse:	Zhang, Feng

SCHOOL EDUCATION

09.2005-07.2008	Kaifaqu No.1 Middle School, Dalian, Liaoning, China
-----------------	--

UNIVERSITY EDUCATION

09.2008-07.2013	Dalian Medical University, Dalian, Liaoning, China Bachelor of Medicine
09.2014-07.2017	Dalian Medical University, Dalian, Liaoning, China Master of Medicine
11.2017-Now	First Department of Medicine, Medical Faculty Mannheim, University of Heidelberg

10. PUBLICATIONS

1. Fanis Buljubasic, Ibrahim El-Battrawy, Huan Lan, Santosh K Lomada, Anupriya Chatterjee, Zhihan Zhao, Xin Li, **Rujia Zhong**, Qiang Xu, Mengying Huang, Zhenxing Liao, Siegfried Lang, Lukas Cyganek, Xiaobo Zhou, Thomas Wieland, Martin Borggreffe, Ibrahim Akin. Nucleoside Diphosphate Kinase B Contributes to Arrhythmogenesis in Human-Induced Pluripotent Stem Cell-Derived Cardiomyocytes from a Patient with Arrhythmogenic Right Ventricular Cardiomyopathy. **Journal of Clinical Medicine**,9(2), 2020.doi: 10.3390/jcm9020486
2. Ibrahim El-Battrawy, Jonas Müller, Zhihan Zhao, Lukas Cyganek, **Rujia Zhong**, Feng Zhang, Mandy Kleinsorge, Huan Lan, Xin Li, Qiang Xu, Mengying Huang, Zhenxing Liao, Alexander Moscu-Gregor, Sebastian Albers, Hendrik Dinkel, Siegfried Lang, Sebastian Diecke, Wolfram-Hubertus Zimmermann, Jochen Utikal, Thomas Wieland, Martin Borggreffe, Xiaobo Zhou, Ibrahim Akin. Studying Brugada Syndrome with an SCN1B Variants in Human-Induced Pluripotent Stem Cell-Derived Cardiomyocytes. **Frontiers in Cell and Developmental Biology**,11: 261, 2019. doi 10.3389/fcell.2019.00261
3. Zhihan Zhao, Xin Li, Ibrahim El-Battrawy, Huan Lan, **Rujia Zhong**, Qiang Xu, Mengying Huang, Zhenxing Liao, Siegfried Lang, Wolfram-Hubertus Zimmermann, Lukas Cyganek, Thomas Wieland, Ibrahim Akin, Xiao-Bo Zhou and Martin Borggreffe. Drug Testing in Human-Induced Pluripotent Stem Cell-Derived Cardiomyocytes From a Patient With Short QT Syndrome Type 1. **Clinical Pharmacology & Therapeutics**, 106 (3): 642-651,2019. doi: 10.1002 /cpt.1449
4. Ibrahim El-Battrawy, Sebastian Albers, Lukas Cyganek, Zhihan Zhao, Huan Lan, Xin Li, Qiang Xu, Mandy Kleinsorge, Mengying Huang, Zhenxing Liao, **Rujia Zhong**, Boris Rudic, Jonas Mueller, Hendrik Dinkel, Siegfried Lang, Sebastian Diecke, Wolfram-Hubertus Zimmermann, Jochen Utikal, Thomas Wieland, Martin Borggreffe, Xiaobo Zhou, and Ibrahim Akin. A cellular model of

Brugada syndrome with SCN10A variants using human-induced pluripotent stem cell-derived cardiomyocytes. **Europace**, 21: 1410–1421,2019.
doi:10.1093/europace/euz122

11. ACKNOWLEDGEMENT

The completion of my thesis is attributed to all who love me around. So, I would like to express my gratitude to all who helped me during my study in Faculty of Medicine, University Medical Centre Mannheim, University of Heidelberg as a doctoral student.

First, I would like to extend my sincere thanks to my supervisor, Prof. Martin Borggreffe, who gave me the chance to study here as a doctoral student and helped me with my graduate thesis.

Second, I would like to express my deepest gratitude to my second supervisor, Dr. Xiaobo Zhou, whose guidance and help led to perfect execution and the finish of my experimental researches and the writing of this thesis. He gave me a lot of help and advice during my whole process of writing and motivated me to move on during my study.

Furthermore, I'd like to thank my experimental partner and husband, Feng Zhang, for accompanying me through the unforgettable period of my life and helping me be better.

Besides, I am deeply grateful to my parents and my family. Without their love and support, I could not complete my study successfully. Many thanks to their care and support.

What's more, I would like to thank my colleagues, Huan Lan, Qiang Xu, Zhen Yang, Yingrui Li, Zhihan Zhao, Xin Li, Zhenxing Liao, Mengying Huang, Lin Qiao, Siegfried Lang, Claudia Liebetrau, Ibrahim El-Batrawy, who kindly and warmly helped me a lot during my studying here.